A high-order discontinuous Galerkin solver and exact solutions for helically invariant flows

Am Fachbereich Maschinenbau
an der Technischen Universität Darmstadt
zur Erlangung des akademischen Grades
eines Doktor-Ingenieurs (Dr.-Ing.)
genehmigte

D i s s e r t a t i o n

von

Dominik Dierkes
aus Bad Soden - Salmünster

Berichterstatter:	Prof. Dr.-Ing. M. Oberlack
Mitberichterstatter:	Prof. Dr. rer. nat. A. Sadiki
Tag der Einreichung:	11.11.2019
Tag der mündlichen Prüfung:	15.01.2020

Darmstadt, 2019
D17

Erklärung

Hiermit versichere ich, die vorliegende Dissertation ohne Hilfe Dritter nur mit den angegebenen Quellen und Hilfsmitteln angefertigt zu haben. Alle Stellen, die aus Quellen entnommen wurden, sind als solche kenntlich gemacht. Diese Arbeit hat in gleicher oder ähnlicher Form noch keiner Prüfungsbehörde vorgelegen.

Darmstadt, den 11. November 2019

Dominik Dierkes

Dierkes, Dominik: A high-order discontinuous Galerkin solver and exact solutions for helically invariant flows
Darmstadt, Technische Universität Darmstadt,
Jahr der Veröffentlichung der Dissertation auf TUprints: 2020
URN: urn:nbn:de:tuda-tuprints-118416
Tag der mündlichen Prüfung: 15.01.2020

Abstract

In this thesis helical flows are investigated, in which the fluid particles simultaneously perform a rotational as well as a translational motion and, thus, move along a helix. The special feature of such flows is that they are based on a dimensional reduction, i.e. the number of coordinates, used to describe the flow is reduced. Such a reduction is referred to as dimensional reduction, since each coordinate represents one spatial dimension.

The present work is divided into an analytical and a numerical part. In the analytical part, a new time-dependent coordinate system is derived from the symmetries of the incompressible Navier-Stokes equations. New conservation laws for viscous and non-viscous helical flows could be found for this coordinate system, which are shown in this thesis and have been published in the article Dierkes and Oberlack (2017). Furthermore, we consider the classical, temporally constant helical coordinate system and derive two classes of new exact solutions of the helical symmetric, full time-dependent Navier-Stokes equations. The first class of solutions is based on the symmetries of the Navier-Stokes equations and hence are denoted as invariant solutions. The second class of solutions is based on a linearization of the Navier-Stokes equations using the so-called Beltrami condition, whereby the velocity and vorticity vectors are assumed to be parallel to each other.

In the numerical part of the work, a solver for the simulation of helically symmetrical flows is developed using the discontinuous Galerkin (DG) method, in which the solution is approximated by high-order polynomials. Due to the fact that helical flows in most cases are periodically in the direction of the central axis of the helix, a periodicity condition for the helical coordinates is derived. A condition for the velocity and the pressure is formulated analogously to the procedure known from the literature for axisymmetric flows (cf. Khorrami et al., 1989). This ensures the uniqueness of these physical quantities at the central axis of the helix. In addition, we introduce a suitable function space and formulate the spatial and temporal discretization of the helically symmetric Navier-Stokes equations. For the temporal discretization, we use a third order semi-explicit method in which the spatial operator is split into an explicit and an implicit part. Using this, the computational effort for transient simulations has been reduced significantly. The correct implementation is verified by various test cases including the exact solutions which have been found before. It is further shown that the convergence rates that we expect from theory are achieved. Finally, the results of direct numerical simulations at high Reynolds numbers are performed which reveal the formation of vortices, Kelvin-Helmholtz instabilities and the temporal development of energy spectra for helically invariant flows.

Zusammenfassung

Dominik Dierkes - Ein hochgenauer Discontinuous-Galerkin-Löser und exate Lösungen für helikal invariante Strömungen

In dieser Arbeit werden helikale Strömungen untersucht, bei der die Fluidteilchen gleichzeitig eine rotatorische und translatorische Bewegung ausführen und sich somit entlang einer Helix bewegen. Das Besondere solcher Strömungen ist, dass ihnen eine Dimensionsreduktion zugrunde liegt. Das bedeutet, dass die Anzahl der Koordinaten, die zur Beschreibung der Strömung dienen, verringert wird. Eine solche Reduktion wird als Dimensionsreduktion bezeichnet, da jede der Koordinaten eine Raumdimension darstellt.

Die vorliegende Arbeit ist in einen analytischen und einen numerischen Teil gegliedert. Im analytischen Teil wird zunächst, ausgehend von den Symmetrien der inkompressiblen Navier-Stokes Gleichungen, ein neues, zeitabhängiges Koordinatensystem hergeleitet. Für dieses konnten neue Erhaltungssätze für viskose sowie nicht-viskose helikale Strömungen gefunden werden, die in der vorliegenden Arbeit betrachtet und im Artikel Dierkes and Oberlack (2017) veröffentlicht wurden. Im weiteren Verlauf der Arbeit betrachten wir klassische, d. h. zeitlich konstante, helikale Koordinaten und leiten zwei Klassen von neuen exakten Lösungen der helikal-symmetrischen, instationären Navier-Stokes Gleichungen her. Die erste Klasse der Lösungen basiert auf den Symmetrien der helikal reduzierten Navier-Stokes Gleichungen und werden auch als invariante Lösungen bezeichnet. Die zweite Klasse von Lösungen beruht auf einer Linearisierung der Navier-Stokes Gleichungen durch die sogenannte Beltrami-Bedingung. Hierbei wird angenommen, dass der Geschwindigkeits- und Wirbelvektor des Strömungsfeldes parallel zueinander stehen.

Im numerischen Teil der Arbeit wird ein Löser zur Simulation helikal symmetrischer Strömungen mit dem diskontinuierlichen Galerkin (DG) Verfahren entwickelt, bei dem die Lösung durch Polynome höherer Ordnung approximiert wird. Aufgrund der Tatsache, dass helikale Strömungen periodisch in Richtung der zentralen Achse der Helix verlaufen, wird zunächst eine Periodizitätsbedingung für die helikalen Koordinaten hergeleitet. Analog zu dem aus der Literatur bekannten Vorgehen für achsensymmetrische Strömungen (vgl. Khorrami et al., 1989) wird eine Bedingung für die Geschwindigkeit und den Druck formuliert, wodurch die Eindeutigkeit dieser physikalischen Größen auf der zentralen Achse sichergestellt ist. Nach der Einführung eines geeigneten Funktionenraums wird die räumliche und zeitliche Diskretisierung der helikal symmetrischen Navier-Stokes Gleichungen formuliert. Für die zeitliche Diskretisierung verwenden wir ein semi-explizites Verfahren dritter Ordnung, bei dem der räumliche Operator in einen expliziten und einen impliziten Teil aufgespalten wird. Hierdurch konnte der Rechenaufwand für instationäre Simulationen deutlich reduziert werden. Es wird die korrekte Implementierung anhand von verschiedenen

Tests, einschließlich den zuvor gefundenen exakten Lösungen verifiziert. Zudem sind die aus der Theorie erwarteten Konvergenzraten erreicht worden. Schließlich werden die Ergebnisse von numerischen Simulationen für hohe Reynolds-Zahlen gezeigt, welche die Entstehung von Wirbeln, Kelvin-Helmholtz Instabilitäten und die zeitliche Entwicklung von Energiespektren für helikal invariante Strömungen darstellen.

Acknowledgments

I want to thank the German Research Foundation (DFG) for the financial support under the grant number OB 96/41-1 and the Graduate school of Computational Engineering of the TU Darmstadt.

I further would like to thank Prof. Dr. Martin Oberlack for the opportunity to do this PhD thesis at the Chair of Fluid dynamics and his support during the last years. I additionally want to thank him for the possibility to participate in many workshops and to complete the "Zertifikat Hochschullehre" which was provided at the TU Darmstadt as an additional education for PhD students. I am also very grateful for the excellent cooperation with Prof. Dr. Alexei Cheviakov and his great hospitality during my residence in Canada. Furthermore, I want to thank Prof. Dr. Suad Jakirlić for beeing my second supervisor.

Furthermore, I am very thankful to Dr. Florian Kummer and Dr. Björn Müller for their great patience and endless support for the development of my numerical code in the BoSSS framework and the very fruitful exchange of ideas concerning mathematical or software issues. In addition, I am deeply grateful to all my colleagues at the Chair of Fluid dynamics, in particular Markus Geisenhofer, Anne Kikker, Dominik Plümacher and Martin Smuda for the many helpful discussions about helical flows and the numerical implementation. Special thanks also goes to Stefanie Kraheberger for the great time in the office and her support in various difficult situations.

Furthermore, I want to thank all of my friends for having a fantastic time doing sports or many other funny and exciting activities. Finally, I want to thank my family for their encouragement and support in all my decisions.

Contents

List of Figures

List of Tables

Nomenclature

B	helical geometric function
D_i	total derivative
E	total energy
E_h	helical kinetic energy
E_{U^j}	Euler operator
G^i	Lie symmetry groups
H_c	confluent Heun function
I	invariants
J_c	global conserved quantity
K	cell of the numerical grid
$L^2(\Omega)$	Lebesgue space of qudratic integrable functions
N_k	maximal polynomial degree
P	modified pressure
R^σ	system of PDE's
T	total time
T_R	rotation group
X	infinitesimal generator
X_G	infinitesimal generator of generalized galilean group
X_R	infinitesimal generator of rotation group
Y	solution of the confluent Heun equation
Δt	time step
Γ	set of all edges of the grid
Γ_D	dirichlet boundary
Γ_P	periodic boundary
Γ_{int}	set of internal edges
Λ_σ	conservation law multiplier
Ω	fluid dmain

Ω_j	single finite element
Φ^i, Ψ^i	fluxes of a conservation law
Θ	density of a conservation law
$\alpha(t)$	time-dependent helical parameter
$\bar{\xi}, \bar{\eta}$	infinitesimals
$\beta_0 \dots \beta_3$	coefficients of BDF scheme
$\boldsymbol{B}$	matrix of basis functions, evaluated at the centerline
$\boldsymbol{I}$	identity matrix
$\boldsymbol{J}$	Jacobi matrix
$\boldsymbol{K}$	stiffness matrix
$\boldsymbol{M}$	mass matrix
$\boldsymbol{U}$	arbitrary functions
$\boldsymbol{\Phi_G}$	group transformation
$\boldsymbol{\Phi}$, $\boldsymbol{\Psi}$	DG basis
$\boldsymbol{\omega}$	vorticity
$\tilde{\boldsymbol{f}}$	numerical flux
$\boldsymbol{e}$	unit vector
$\boldsymbol{n}$	normal vector
$\boldsymbol{u}$	velocity
η	helical invariant coordinate, used in the present work
η^*	helical invariant coordinate in time-dependent system
η_{SIP}	wighting function for penalty term
$\gamma_1 \dots \gamma_3$	coefficients of third order extrapolation
κ	condition number
λ_{Stab}	stabilization term
$\mathbb{P}_k$	space of polynomial functions
$\mathbb{R}^d$	d-dimensional space of real numbers
$\mathbb{V}_k$	function space of broken polynomials
$\mathcal{A}$	discretization of viscous terms of Navier-Stokes equations
$\mathcal{C}$	discretization of continuity equation
$\mathcal{F}^\sigma$	general form of a differential equation
$\mathcal{K}$	numerical grid
$\mathcal{N}$	discretization of nonlinear terms of Navier-Stokes equations

$\mathrm{d}A$	infinitesimal surface
$\mathrm{d}S$	surface element
$\mathrm{d}V$	volume element
ν	viscosity
$\partial\Omega$	boundary of the fluid domain
$\tau_x i$	period of helically invariant solution
$\tilde{K}$	kinetic energy density
$\tilde{\eta}$	helical invariant coordinate, used in KCO
$\tilde{h}$	helicity density
$\tilde{u}_i$	DG coefficient
$\tilde{v}$	test function
ε	group parameter
$\xi_{p_c}, \xi_l, \eta_{p_c}$	periodic lengths
ζ	conserved quantity
a, b	constant helical parameters
e_p	L^2-norm error for pressure
e_u	L^2-norm error for velocity
f_{sw}	super weak formulation
f_{upw}	upwind formulation
h	cell size
k	polynomial order
k_h	wave number
m	slope
n_F	number of points for FFT
n_s	number of time steps
p	pressure
p_c	periodic length at the centerline
r, φ, z	cylindrical coordinates
s_p	penalty scaling
u_h	approximation function
ξ	helical coordinate

Abbreviations

2D two-dimensional

3D three-dimensional

BC boundary condition

BDF backward differencing formula

BDF-3 backward differencing formula of third order

BoSSS Bounded Support Spectral Solver

CFD computational fluid dynamics

CL conservation law

DG discontinuous Galerkin

DNS direct numerical simulation

DoF degrees of freedom

EOC experimental order of convergence

EP conservation law for Euler equations in primitive variables

EV conservation law for Euler equations in vorticity formulation

FFT fast Fourier transformation

KCO Kelbin, Cheviakov, Oberlack: publication Kelbin et al. (2013)

MPI message passing interface

NSP conservation law for Navier-Stokes equations in primitive variables

NSV conservation law for Navier-Stokes equations in vorticity formulation

ODE ordinary differential equation

PDE partial differential equation

Re Reynolds number

RHS right-hand side

SIP symmetric interior penalty

TU Technische Universität

XDG extended discontinuous Galerkin

1 Introduction

In this thesis helically invariant flows are investigated analytically and numerically. It is a continuation of the exploration of helical flows that was published in Kelbin et al. (2013) and Kelbin (2015) and hence is based on the equations and denominations that were introduced therein.

The starting point of continuing the research towards helically invariant flows was the author's master's thesis (Dierkes, 2015), where I extended the work of Kelbin et al. (2013) significantly by developing a new time-dependent helical coordinate system that is based on the Lie point symmetries of the incompressible Navier-Stokes equations. In this chapter we introduce helical flows, the DG method and list a few other numerical techniques of discretizing the Navier-Stokes equations in non-cartesian coordinates. After that, the BoSSS framework is described. We further show the goal of this work as well as the motivation for the investigations. Finally, we present the outline of this thesis.

Helical flow structures appear in various natural phenomena and technological devices, for example, in the wake of windmills (Vermeer et al., 2003), as wing tip vortices (Mitchell et al., 1997), in astrophysical plasmas (Bogoyavlenskij, 2000a) and in laboratory applications, including "straight tokamak" plasma flow approximations, (see e.g. Schnack et al., 1985; Johnson et al., 1958) and other experiments. In particular, helical vortex structures were observed by Sarpkaya (1971) in experiments with swirling flows in a cylindrical tube, and as such, they are part of the various flow structures observed in the known vortex breakdown.
Various groups have worked on the theoretical description of helical flows in recent decades. The simplest approach here is to introduce a helical coordinate $\xi = az + b\varphi$, $a, b = \text{const.} \neq 0$ and to assume that all physical quantities depend on the cylinder radius r and the helical coordinate ξ. Helically invariant flows include translationally and axially invariant ones as special cases. For both steady Euler equations describing incompressible fluid flows and for plasma equilibrium equations in the magnetohydrodynamics (MHD) framework, the helical invariance requirement allows to reduce the governing equations to a single partial differential equation (PDE) known as the JFKO equation (Johnson et al., 1958). This important equation generalizes the famous Bragg-Hawthorne-Grad-Rubin-Shafranov equation (Bragg and Hawthorne, 1950; Grad and Rubin, 1958; Shafranov, 1958) describing steady axisymmetric inviscid flows onto the helically invariant case. Families of exact solutions of JFKO equations are known, including those derived by Bogoyavlenskij (2000c) (see also Bogoyavlenskij, 2000b; Cheviakov and Bogoyavlenskij, 2004). In the more general context of helical geometry, several works focused on twisted pipes following a given spatial curve (Wang, 1981; Germano, 1982, 1989; Tuttle, 1990). Using non-orthogonal and local-orthogonal coordi-

nate systems, the effects of pipe curvature and torsion on the flow were investigated. Special analytical solutions of steady flows in helically symmetric pipes were found by Zabielski and Mestel (1998). Delbende et al. (2012) has developed a DNS code for the helical invariant Navier-Stokes equations in a generalized vorticity-streamfunction formulation. Dritschel (1991) reduced the three-dimensional Euler equations to a linear equation, assuming that the flow has helical symmetry and consists of a rigidly rotating basic part and a Beltrami disturbance part. Further, he derived exact solutions for flows in a straight pipe of circular cross section. Exact solutions for helical flows of a Maxwell fluid constrained between two infinite coaxial circular cylinders were derived by Jamil and Fetecau (2010).

The DG method is a modern numerical method used today to solve PDE's in fluid mechanics. As mentioned in Cockburn (2003), in the past decades it has found application for compressible (Bassi and Rebay, 1997) and incompressible (Baumann and Oden, 1998) flows as well as in turbomachinery (Bassi et al., 1997). In particular, a DG solver for incompressible unsteady two-dimensional flows has been developed by Ferrer and Willden (2011), whereas in three dimensions a DG solver is presented in Shahbazi et al. (2007), in which a semi explicit temporal discretization with explicit treatment of the nonlinear term and implicit treatment of the Stokes operator is used. Both solvers use the Interior Penalty (IP) Galerkin formulation (cf. Arnold, 1982a). In addition, an extended DG method has been developed for solving multiphase problems (see e.g. Kummer, 2017). The DG method has also been applied to PDE's given in non-cartesian coordinates, e.g., in Nair et al. (2005) the shallow water equations are discretized on a cubic sphere. There are also numerous works concerning a numerical discretization of the incompressible Navier-Stokes equations in polar and cylindrical coordinates, most applying spectral elements (Lopez and Shen, 1998) and finite difference schemes (Verzicco and Orlandi, 1996; Barbosa and Daube, 2005; Griffin et al., 1979) for the spatial discretization. They all have in common that due to the singularities in the equations a special treatment at the centerline axis, where the radial coordinate r is zero, needs to be taken into account. For example, in Lopez and Shen (1998) so-called *essential* and *natural* pole conditions are discussed, which are necessary for the well-posedness and the reglarity of the solutions at the centerline, respectively. In Constantinescu and Lele (2002) governing equations for the flow at the centerline are derived using series expansions near $r = 0$, whereas in Khorrami et al. (1989) the authors demand smoothness of all physical variables along the centerline which results in constraints for the velocity and the pressure.

In the present thesis, in order to ensure well-posedness, smoothness and regularity of the numerical solutions along the centerline, we will present a formulation of the helically invariant Navier-Stokes equations which can also be seen as a discontinuous Petrov-Galerkin (DPG) formulation. In a DPG formulation the trial and test functions may differ and correspond to different function spaces (cf. Roberts et al., 2014). For some convection-diffusion type problems the DPG method has been developed in Ellis et al. (2014). Furthermore, a DPG formulation for elliptic problems is proposed in Bottasso et al. (2002) and the method is used to solve the Poisson equation in Demkowicz and Gopalakrishnan (2011). Moreover, a framework for the analysis of the

DPG method is developed in Roberts et al. (2014) and applied to the Stokes problem to show its well-posedness.

1.1 The BoSSS framework

The CFD framework BoSSS (Bounded Support Spectral Solver) was originally founded by Kummer (Kummer et al., 2009; Kummer, 2012) and since then has been continuously developed at the Chair of Fluid Dynamics at TU Darmstadt. It is based on the DG method and offers the possibility to calculate numerical solutions of various types of partial differential equation systems. In recent years the framework has been used for numerous simulations of subsonic and supersonic compressible flows using immersed boundary methods (IBM) (Müller et al., 2017; Geisenhofer et al., 2019), incompressible flows (Klein et al., 2015; Utz et al., 2017; Utz, 2018) as well as moving body flows (Krause and Kummer, 2017). Beside this, within the BoSSS framework the extended discontinuous Galerkin method (XDG) (Kummer, 2017) can be used for multiphase flows with a sharp interface approach. The framework is written in the programming language C#. It can be used for MPI parallel computations and hence offers the possibility to perform direct numerical simulations of, e.g., turbulent flows with high resolving computational grids. The latest versions of BoSSS are open source and can be found on the website `https://github.com/FDYdarmstadt/BoSSS` for download.

1.2 Goal of this work and Motivation

The goal of this thesis is the development of three basic milestones which enhance the understanding of helically invariant flows and thus form the basis for an application in turbulence theory. These three milestones are firstly the derivation of new conservation laws, secondly the construction of exact solutions of the helically invariant Navier-Stokes equations and thirdly the development of a numerical code to perform direct numerical simulations of helically invariant flows at high Reynolds numbers.

The motivation for these milestones is to generate a deeper understanding of the behaviour of such turbulent flows, which are based on a reduction in dimensions, i.e. on a certain symmetry within the flow. The physical processes in the turbulence of two-dimensional (2D) flows differ significantly from those of three-dimensional (3D) flows. The main difference is that in 3D turbulence the central mechanism of vortex stretching occurs, which is responsible for the generation of turbulence in general and for the energy cascade characteristic of 3D turbulence in particular. In this case a so-called forward energy cascade exists, i.e. energy is transferred from large eddies to smaller ones and finally dissipates into heat on the smallest eddies. In contrast, the vortex stretching term disappears in 2D flows and the energy cascade changes direction in the way that the energy is now transferred from small eddies to larger ones.

Examples of well-known, classical dimensional reductions of 3D flows are plane and axisymmetric flows. In the case of plane flows, it is assumed that all velocity components

and the pressure are independent of the z-coordinate and that the velocity component vanishes in the z-direction, i.e. $u^z = 0$. In the same way, for axisymmetric flows one assumes that all physical quantities are independent of the angular coordinate φ and that the corresponding velocity component also disappears, i.e. $u^\varphi = 0$.

For the investigations of helically symmetric flows Lie Symmetry methods are employed in a first step as such, that the spatial dependence of the originally three independent variables is reduced by one and the remaining variables are: the cylindrical radius r, the time-dependent helical variable $\xi = \frac{z}{\alpha(t)} + b\varphi$, $b = \text{const.}$, and time t. Assuming $\alpha = \text{const.}$, the classical helically symmetric case is retained. As in the classical examples, independence of all physical quantities from the third coordinate is required, whereas no reduction of the velocity components is assumed. Hence, in contrast to 2D flows, a full 3D velocity field is considered for the investigation of helical turbulence, where all velocity components are different from zero. Due to the discrepancy in the number of dependent and independent variables, i.e. especially two independent variables r, ξ and three dependent u^r, u^ξ, u^η the description of helical flows is often referred to as "2 1/2"-dimensional flows.

The central question to be answered by future research is to what extent helical turbulence has a two- or three-dimensional character. The simulations using the DG code developed in this thesis can contribute to answer this question. For example, by means of simulations with high Reynolds numbers, it can be decided on the basis of the energy cascade whether energy is transferred to small scales like in 3D turbulence or vice versa which is the case in 2D.

1.3 Outline of this thesis

The present work is divided into two parts. In the analytical part, symmetries, conservation laws and exact solutions of the helically invariant Navier-Stokes equations are derived and investigated. In the numerical part, the system is discretized and a numerical code for simulations of helically symmetric flows is developed.

In the analytical part in chapter 3 the symmetries of the incompressible 3D Navier-Stokes equations, which represent the starting point of the dimensional reduction, are considered. Classical reductions such as plane and axisymmetric flows are shown and a helical coordinate system is derived in which the incompressible Navier-Stokes equations are formulated under the assumption of helical invariance. For the reduced equations in the classical helical frame the Lie-point symmetries are finally calculated and discussed.

Starting from the helically invariant Navier-Stokes equations derived in chapter 3, the corresponding conservation laws are determined and discussed in chapter 4. Furthermore, in chapter 5 two different exact solutions for the helically invariant Navier-Stokes equations are derived, which result from two different solution approaches. The first solution is based on an invariant solution approach which could be found from the symmetries determined in chapter 3. The second solution is based on the assumption of a Beltrami flow in which velocity and vortex vectors are parallel to each other.

The numerical part of this thesis starts with the discretization of the helically invariant system of the Navier-Stokes equations using the DG method in chapter 6. In the following chapter 7 different test cases are introduced to verify the numerical code. In addition to artificially generated solutions for benchmark tests, the exact solution found in chapter 5 is also used for verification. The results of simulations for flows in a cylindrical shell are presented.

In chapter 8 the periodicity conditions on the centerline axis of the helix at $r = 0$ that were derived in chapter 6 are used to reduce the number of degrees of freedom by a change of the DG basis. The numerical results are discussed and the good performance of the numerical discretization is shown by spatial and temporal convergence studies.

In chapter 9 the newly developed code is used for simulations of helically invariant flows at high Reynolds numbers, which show the evolution of vortices and the generation of Kelvin-Helmholtz instabilities. Furthermore the temporal development of energy cascades is discussed.

Finally, in chapter 10 the conclusions are presented and an outlook is provided that shows to which extent the results of this thesis may be used in future research of helically invariant flows.

2 Mathematical Basics

In the present chapter the basics of one-parameter Lie Group symmetries, conservation laws and the discontinuous Galerkin method are introduced. These three mathematical tools represent the fundamental basis for the investigations of helically invariant flows in an analytical and a numerical way. Lie point symmetries and conservation laws of the helical flow are used in the first part, whereas the DG method is applied in the second part of this thesis. A short summary of the most important literature references concerning these mathematical basics is presented at the beginning of each section in this chapter.

2.1 Lie point symmetries

Lie point symmetries and in particular their application for differential equations are extremely useful in many situations. One of these great benefits is that one may achieve simplifications of the considered equations. For ordinary differential equations (ODEs) the order of the equation can be reduced whereas for partial differential equations (PDEs) it is frequently possible to find a combination of the independent variables which results in a dimensional reduction of the considered problem. Furthermore, symmetries can be used to directly construct exact solutions of the governing differential equation (e.g. Cantwell, 2002). In the present thesis we use both of these strengths. The symmetries of the Navier-Stokes equations lead to an appropriate combination of the independent variables and hence, under the assumption of helical invariance, to a dimensional reduction. From a further symmetry analysis of the helically invariant Navier-Stokes equations (3.19) new invariant quantities are constructed which are used to derive new exact solutions of this system of equations.

Since in this thesis only one-parameter Lie Groups are used, we will not introduce multi-parameter Lie groups. Details of the multi-parameter Lie group theory may be found for instance in Cantwell (2002) or Kilmister and Hydon (2001). As a starting point, we consider the symmetry properties of functions. In Cantwell (2002, p. 121) a definition of the symmetry of a mathematical object is given:

> **Definition 1.** *"A mathematical relationship between variables is said to possess a symmetry property if one can subject the variables to a group of transformations and the resulting expression reads the same in the new variables as the original expression. The relationship is said to be invariant under the transformation group."*

In other words, we define $F(x)$ to be an invariant function with respect to the transformation

$$\tilde{\boldsymbol{x}} = \boldsymbol{\Phi}_G\left(\boldsymbol{x};\varepsilon\right), \tag{2.1}$$

if the relation

$$F\left(\boldsymbol{x}\right) = F\left(\tilde{\boldsymbol{x}}\right) \tag{2.2}$$

holds. Here, the parameter ε is the group transformation parameter, which is subjected to Group properties. For details of Group properties in general and in particular for the Group properties of Lie groups we refer to Bluman et al. (2010), Cantwell (2002) and Kilmister and Hydon (2001). As a simple example, we consider the function $F(x,y) = x^2 + y^2$ which is invariant under a rotational transformation. The transformation of the independent variables (x,y) is given by

$$\tilde{x} = \cos(\varepsilon)x - \sin(\varepsilon)y, \tag{2.3a}$$
$$\tilde{y} = \sin(\varepsilon)x + \cos(\varepsilon)y, \tag{2.3b}$$

such that $F(x,y) = x^2 + y^2 = \tilde{x}^2 + \tilde{y}^2 = F(\tilde{x},\tilde{y})$ (cf. Stephani, 1994). That means the form of the function $F(x,y)$ has not changed and, hence, $F(x,y)$ is invariant under the rotational symmetry. The idea and definition of symmetries can be transferred to differential equations in a similar way. First, we define a point transformation as follows:

Definition 2. *A point transformation is a transformation of the independent variables* $\boldsymbol{x} = \left(x^1,\ldots,x^n\right)$ *and dependent variables* $\boldsymbol{u} = \left(u^1,\ldots,u^m\right)$*, given by*

$$\tilde{\boldsymbol{x}} = \boldsymbol{f}\left(\boldsymbol{x},\boldsymbol{u}\right), \qquad \tilde{\boldsymbol{u}} = \boldsymbol{g}\left(\boldsymbol{x},\boldsymbol{u}\right). \tag{2.4}$$

The symmetry transformations of partial differential equations can depend on several parameters and functions, but it is always possible to choose a set of transformations

$$\tilde{\boldsymbol{x}} = \tilde{\boldsymbol{x}}\left(\boldsymbol{x},\boldsymbol{u};\varepsilon\right), \qquad \tilde{\boldsymbol{u}} = \tilde{\boldsymbol{u}}\left(\boldsymbol{x},\boldsymbol{u};\varepsilon\right) \tag{2.5}$$

that only depends on one single parameter ε (cf. Stephani, 1994). In the case where $\varepsilon = 0$, (2.5) is the identity transformation, i.e.

$$\tilde{\boldsymbol{x}} = \tilde{\boldsymbol{x}}\left(\boldsymbol{x},\boldsymbol{u};0\right) = \boldsymbol{x}, \qquad \tilde{\boldsymbol{u}} = \tilde{\boldsymbol{u}}\left(\boldsymbol{x},\boldsymbol{u};0\right) = \boldsymbol{u} \tag{2.6}$$

which ensures that the transformation is a group transformation. A Taylor expansion of (2.5) around $\varepsilon = 0$ is given by

$$\tilde{\boldsymbol{x}} = \boldsymbol{x} + \varepsilon\bar{\boldsymbol{\xi}}\left(\boldsymbol{x},\boldsymbol{u}\right) + \mathcal{O}\left(\varepsilon^2\right), \qquad \bar{\boldsymbol{\xi}} := \left.\frac{\partial\tilde{\boldsymbol{x}}}{\partial\varepsilon}\right|_{\varepsilon=0}, \tag{2.7a}$$

$$\tilde{\boldsymbol{u}} = \boldsymbol{u} + \varepsilon\bar{\boldsymbol{\eta}}\left(\boldsymbol{x},\boldsymbol{u}\right) + \mathcal{O}\left(\varepsilon^2\right), \qquad \bar{\boldsymbol{\eta}} := \left.\frac{\partial\tilde{\boldsymbol{u}}}{\partial\varepsilon}\right|_{\varepsilon=0}, \tag{2.7b}$$

where $\bar{\boldsymbol{\xi}}$ and $\bar{\boldsymbol{\eta}}$ are the infinitesimals. The infinitesimal Generator is given by

$$X = \bar{\xi}^i(\boldsymbol{x}, \boldsymbol{u}) \frac{\partial}{\partial x^i} + \bar{\eta}^j(\boldsymbol{x}, \boldsymbol{u}) \frac{\partial}{\partial u^j}, \tag{2.8}$$

which can be extended up to the k-th order as follows (see Bluman et al., 2010)

$$\begin{aligned} X^{(k)} = \bar{\xi}^i(\boldsymbol{x}, \boldsymbol{u}) \frac{\partial}{\partial x^i} + \bar{\eta}^j(\boldsymbol{x}, \boldsymbol{u}) \frac{\partial}{\partial u^j} + \bar{\eta}_i^{(1)\,j}(\boldsymbol{x}, \boldsymbol{u}, \partial \boldsymbol{u}) \frac{\partial}{\partial \boldsymbol{u}_i^j} \\ + \ldots + \bar{\eta}_{i_1 \ldots i_k}^{(k)\,j} \left(\boldsymbol{x}, \boldsymbol{u}, \partial u, \ldots \partial^k \boldsymbol{u}\right) \frac{\partial}{\partial u^j_{i_1 \ldots i_k}}. \end{aligned} \tag{2.9}$$

The extended infinitesimals are given by

$$\bar{\eta}_i^{(1)\,j} = D_i \bar{\eta}^j - \left(D_i \bar{\xi}^\alpha\right) u_\alpha^j \tag{2.10}$$

and

$$\bar{\eta}_{i_1 \ldots i_k}^{(k)\,j} = D_{i_k} \bar{\eta}_{i_1 \ldots i_k}^{(k-1)\,j} - \left(D_{i_k} \bar{\xi}^\alpha\right) u^j_{i_1 \ldots i_k\,\alpha}, \tag{2.11}$$

where $j = 1 \ldots m$, $i, i_s = 1, \ldots, n$ for $s = 1, \ldots, k$ with $k = 2, 3, \ldots$. For brevity, in this thesis partial derivatives are denoted by $u_i^j := \frac{\partial u^j}{\partial x^i}$. Furthermore, the total derivative operator is given by

$$D_i = \frac{\partial}{\partial x^i} + u_i^j \frac{\partial}{\partial u^j} + u_{ii_1}^j \frac{\partial}{\partial u_{i_1}^j} + u_{ii_1i_2}^j \frac{\partial}{\partial u_{i_1i_2}^j} + \ldots, \qquad i = 1, \ldots n. \tag{2.12}$$

Following Bluman et al. (2010) we define a point symmetry of a system of PDEs as follows:

Definition 3. *The transformation* (2.4) *is a point symmetry of the PDE system* $\boldsymbol{\mathcal{F}}(\boldsymbol{x}, \boldsymbol{u})$ *consisting of N PDEs of order k if and only if for each* $\alpha = 1, \ldots, N$

$$X^{(k)} \mathcal{F}^\alpha \left(\boldsymbol{x}, \boldsymbol{u}, \partial u, \ldots \partial^k \boldsymbol{u}\right) = 0 \tag{2.13}$$

when

$$\mathcal{F}^\sigma \left(\boldsymbol{x}, \boldsymbol{u}, \partial u, \ldots \partial^k \boldsymbol{u}\right) = 0, \qquad \sigma = 1, \ldots, N. \tag{2.14}$$

In this definition, in (2.13) $X^{(k)}$ is the $k-$th extension of the infinitesimal generator, given by (2.9).

In other words, a point symmetry of a differential equation is a local transformation of the independent and the dependent variables such that the form of the differential equation remains unchanged. A general form of a scalar differential equation is given by

$$\mathcal{F}\left(\boldsymbol{x}, \boldsymbol{y}, \boldsymbol{y}^1, \ldots, \boldsymbol{x}^n\right) = 0, \tag{2.15}$$

where, as before, $\boldsymbol{x}$ are the independent variables, $\boldsymbol{y}$ the dependent variables and $\boldsymbol{y}^1, \ldots, \boldsymbol{y}^n$ the derivatives up to n-th order. The transformation

$$\boldsymbol{x} = f(\tilde{\boldsymbol{x}}, \tilde{\boldsymbol{y}}), \qquad \boldsymbol{y} = g(\tilde{\boldsymbol{x}}, \tilde{\boldsymbol{y}}) \tag{2.16}$$

is a symmetry transformation if the form of differential equation (2.15) is not changed by the transformation (2.16), i.e.

$$\mathcal{F}\left(\boldsymbol{x}, \boldsymbol{y}, \boldsymbol{y}^1, \ldots, \boldsymbol{x}^n\right) = \mathcal{F}\left(\tilde{\boldsymbol{x}}, \tilde{\boldsymbol{y}}, \tilde{\boldsymbol{y}}^1, \ldots, \tilde{\boldsymbol{x}}^n\right) = 0. \tag{2.17}$$

2.2 Invariant solutions

One of the central results of this thesis are invariant solutions of the helically symmetric Navier-Stokes equations. For that reason we briefly introduce the idea of invariant solutions in the present section.

Following Bluman et al. (2010), an *invariant solution* is defined as follows:

Definition 4. *Let $\boldsymbol{F}(\boldsymbol{x}, \boldsymbol{u})$ be a system of PDEs, given by* (2.14)*. The function $\boldsymbol{u} = \boldsymbol{\theta}(\boldsymbol{x})$, consisting of components $u^\mu = \theta^\mu(\boldsymbol{x})$, $\mu = 1, \ldots, m$ is an invariant solution of* (2.14) *resulting from the point symmetry* (2.8) *if and only if the following statements hold:*

(i) For each component $\mu = 1, \ldots, m$ the function $u^\mu = \theta^\mu(\boldsymbol{x})$ is an invariant surface of the point symmetry (2.8)*.*

(ii) The function $\boldsymbol{u} = \boldsymbol{\theta}(\boldsymbol{x})$ is a solution of the PDE system (2.14)

To determine invariant solutions one demands that the condition

$$X\left(\boldsymbol{u} - \boldsymbol{\theta}(\boldsymbol{x})\right)\big|_{\boldsymbol{u}=\boldsymbol{\theta}(\boldsymbol{x})} = 0 \tag{2.18}$$

is satisfied by the function $\boldsymbol{u} = \boldsymbol{\theta}(\boldsymbol{x})$. Invariant quantities of the point symmetry (2.8) can be found which are solutions of the characteristic ODE system emerging from (2.18). As it will be shown in chapter 5, the invariants can still depend on unknown functions. These are finally determined by employing the invariants into the PDE system (2.14). Thus, particular solutions of the PDE system (2.14) are obtained.

2.3 Conservation Laws

The following introduction of conservation laws is heavily based on Dierkes and Oberlack (2017), which is a publication of mine.

In mathematical physics, symmetries and conservation laws (CL) are considered to be one of the most fundamental objects. For example, in fluid mechanics CL describe physical quantities such as the conservation of mass, energy, momentum or angular momentum. In practice, local conservation laws are of fundamental importance for several reasons. They are essential for numerical simulations with modern numerical methods, where the equations are assumed to be in divergence form, e.g. for DG

methods (see Zienkiewicz and Taylor, 2002). Additionally, they give the possibility to easily find potential variables (see Bluman et al., 2010), which in turn leads to a reduction of the dependent variables and new analytical solutions. Further, CL are used to establish existence and uniqueness of solutions as well as in the analysis of stability and global behavior of solutions (Bluman et al., 2010).

For 3D time-dependent fluid flows, CLs were studied in very much detail in Cheviakov and Oberlack (2014). Therein, they considered higher-order conservation law multipliers and obtained an infinite family of vorticity conservation laws. Further, Rosenhaus and Shankar (2019) considered the correspondence between symmetries and conservation laws of a differential system. They introduced sub-symmetries to find further infinite sets of conservation laws of the Euler equations, involving arbitrary functions of the dependent variables.

Most important, additional CLs appear to exist in reduced dimensions such as in plane or axis-symmetric flows. Recently new CLs for Euler and Navier-Stokes equations were found for helically invariant flows (see Kelbin et al., 2013). Therein they considered a helical coordinate system, given by the radius r and a helical variable $\xi = az + b\varphi$, arising from a linear combination of the cylindrical coordinates z and φ. The parameters a and b, involved in this coordinate, were assumed to be constant. Further, the authors expressed the three dimensional, incompressible Euler and Navier-Stokes equations in a helical symmetric setting and finally obtained new conservation laws for primitive variables as well as for the vorticity formulation. Interesting enough, they also derived new conservation laws for plane and axisymmetric flows. Due to many citations the publication of Kelbin et al. (2013) is subsequently denoted as KCO.

In a fluid dynamical context, divergence-type local conservation laws usually have the form

$$\partial_t \Theta + \nabla \cdot \mathbf{\Phi} = 0, \tag{2.19}$$

where $\nabla \cdot \mathbf{\Phi} = \partial_i \Phi^i = \partial_1 \Phi^1 + \partial_2 \Phi^2 + \ldots + \partial_{n-1} \Phi^{n-1}$ denotes the spatial divergence. The quantity Θ is called density, whereas Φ^i are the spatial fluxes of the conservation law.

In order to compute a globally conserved quantity one may integrate (2.19) over a fluid domain Ω and apply Gauss's theorem

$$\int_\Omega \partial_t \Theta \, \mathrm{d}^n x + \int_{\partial\Omega} \mathbf{\Phi} \cdot \boldsymbol{n} \, \mathrm{d}S = 0, \tag{2.20}$$

where $\mathrm{d}^n x$ defines the volume element while $\mathrm{d}S$ corresponds to a surface element on $\partial\Omega$. Assuming that the fluxes Φ^i vanish on the boundary $\partial\Omega$ or if periodicity is assumed and the domain Ω is time-independent $(\Omega \neq \Omega(t))$, one obtains the global conserved quantity given by

$$\frac{\partial}{\partial t} \int_\Omega \Theta \, \mathrm{d}V = 0 \quad \Leftrightarrow \quad J_c = \int_\Omega \Theta \, \mathrm{d}V = \text{const.} \tag{2.21}$$

In practice, one is interested in finding non-trivial conservation laws (2.19) since trivial conservation laws usually do not carry a physical or mathematical meaning. To distinguish between trivial and non-trivial conservation laws, we first explicate the meaning of trivial conservation laws.

Following Bluman et al. (2010), a trivial conservation law of first type arises, when each of its fluxes Φ vanish identically on the solutions of a given PDE system. A conservation law, vanishing identically as a differential identity is denoted as a trivial conservation law, e.g. $(div(curl(\cdot)) \equiv 0)$.

The equivalence and linear dependence of conservation laws is defined as follows: Two conservation laws $\partial_i \Phi^i = 0$ and $\partial_i \Psi^i = 0$ are equivalent, if $\partial_i \left(\Phi^i - \Psi^i\right) = 0$ is a trivial conservation law. All conservation laws that can be reduced to a class of non-trivial conservation laws build an equivalence class of conservation laws.

A definition for linearly dependent conservation laws is presented in Bluman et al. (2010, p. 43): "A set of l conservation laws $\left\{\partial_i \Phi^i_j = 0\right\}_{j=1}^{l}$ is linearly dependent if there exists a set of constants $\left\{c^{(j)}\right\}_{j=1}^{l}$ not all zero such that the linear combination

$$\partial_i \left(c^{(j)} \Phi^i_{(j)}\right) = 0 \tag{2.22}$$

is a trivial conservation law." The direct method (see e.g. Anco and B., 2002), described and employed in the following, seeks nontrivial sets of local conservation laws of a given PDE system in non-conservative form.

The direct method is based on two key ideas. The first idea can be explained as follows: Consider an arbitrary and non-conservative PDE system given by

$$R^\sigma \left(\boldsymbol{x}, \boldsymbol{u}, \partial_i \boldsymbol{u}\right) = 0, \quad \sigma = 1, \ldots, N, \quad i = 1, \ldots, k. \tag{2.23}$$

It is proven in Anco and Bluman (2002) that a PDE system only admits non-trivial conservation laws arising from linear combinations of these equations with multipliers of k-th order given by

$$\left\{\Lambda_\sigma \left(\boldsymbol{x}, \boldsymbol{U}, \partial_1 \boldsymbol{U}, \ldots, \partial_k \boldsymbol{U}\right)\right\}_{\sigma=1}^{N}. \tag{2.24}$$

If the multipliers (2.24) are known they yield divergence expressions of the form

$$\Lambda_\sigma R^\sigma \equiv D_i \Gamma^i \tag{2.25}$$

for arbitrary functions $\boldsymbol{U}(\boldsymbol{x})$ and $D_i = \frac{\partial}{\partial x_i}$. The multipliers Λ_σ are of the form (2.24) and can be chosen to depend on all dependent and independent variables $\boldsymbol{x}$ and $\boldsymbol{U}$ as well as on derivatives $\partial_k \boldsymbol{U}$ up to a certain order k. A priori it is not known up to which order one may choose the multipliers. On solutions $\boldsymbol{U}\left(\boldsymbol{x}\right) = \boldsymbol{u}\left(\boldsymbol{x}\right)$ of the PDE system (2.23) one obtains the conservation law

$$D_i \Gamma^i = 0. \tag{2.26}$$

To calculate the multipliers Λ_σ, the second key idea is to apply the Euler operator E_{U^j} with respect to U^j to equation (2.25). The Euler operator has the property to annihilate an expression if, and only if it is a divergence expression $D_i\Gamma^i$, and is given by

$$\mathrm{E}_{U^j} = \frac{\partial}{\partial U^j} - D_i \frac{\partial}{\partial U^j_i} + \ldots + (-1)^s D_{i_1} \ldots D_{i_s} \frac{\partial}{\partial U^j_{i_1 \ldots i_s}} + \ldots \tag{2.27}$$

for each $j = 1 \ldots m$, while D_i is defined above.

In order to derive the multipliers Λ_σ, we apply the Euler operator (2.27) to equation (2.25). Based on the above, the right-hand side vanishes identically and one obtains

$$\mathrm{E}_{U^j} \left(\Lambda_\sigma R^\sigma \right) = 0, \quad j = 1 \ldots m, \tag{2.28}$$

which holds for arbitrary functions $\boldsymbol{U}\left(\boldsymbol{x}\right)$. Expending all derivatives in (2.28), a set of linear determining equations for all multipliers Λ_σ arises, where the quantities $\boldsymbol{x}, \boldsymbol{U}, \partial_1 \boldsymbol{U}, \ldots, \partial_k \boldsymbol{U}$ have to be treated as independent variables. Once the conservation law multipliers are derived, one may compute the density and fluxes using (2.26). For details, see e.g. Bluman et al. (2010).

2.4 The discontinuous Galerkin Method

In the following, a linear transport equation is considered to explain the spatial discretization of a PDE using the DG method. After that, we use a poisson equation to explain the discretization of a second order PDE in the DG formulation, introducing the symmetric interior penalty (SIP) method. The following explanations are linked to Cockburn (2003), Arnold et al. (2000), Li (2006), Müller (2014) and Utz (2018).

A scalar conservation law for a physical quantity u is given by

$$\frac{\partial u}{\partial t} + \nabla \cdot \boldsymbol{f}\left(u\right) = 0 \qquad \text{in } \mathbb{R}^d \times (0, T), \tag{2.29}$$

where $u = u(x,t)$ and $x \in \Omega \subset \mathbb{R}^d, t \in (0,T)$ and $\boldsymbol{f}$ beeing a $d-$dimensional vector of smooth functions. The weak form of (2.29) is obtained by multiplying this equation with a test function $\tilde{v} = \tilde{v}(x)$ and integrating over the fluid domain Ω leading to

$$\begin{aligned} &\int_\Omega \frac{\partial u}{\partial t} \tilde{v} \, \mathrm{d}V + \int_\Omega \nabla \cdot \boldsymbol{f}(u) \tilde{v} \, \mathrm{d}V \\ &= \frac{\partial}{\partial t} \int_\Omega u \tilde{v} \, \mathrm{d}V - \int_\Omega \boldsymbol{f}(u) \cdot \nabla \tilde{v} \, \mathrm{d}V + \int_{\partial\Omega} \boldsymbol{f}(u) \cdot \boldsymbol{n} \, \tilde{v} \, \mathrm{d}S = 0, \end{aligned} \tag{2.30}$$

where partial integration is used for the second term. In (2.30) the vector $\boldsymbol{n}$ is the normal vector, pointing outward of the cell. In a next step, the domain is divided into a set of non-overlapping finite elements $\Omega = \cup_{j=1}^N \Omega_j$. This set of elements is approximated by a computational grid denoted as $\mathcal{K} = \{K_1 \ldots K_N\}$. In each cell of the grid the solution is approximated by an interpolation function u_h, which can be

discontinuous across the element boundaries. Hence, it is necessary to introduce a function space of broken polynomials, given by

$$\mathbb{V}_k := \left\{ \tilde{v} \in L^2(\Omega) \mid \tilde{v}|_K \in \mathbb{P}_k \, \forall K \in \mathcal{K} \right\}, \tag{2.31}$$

where $L^2(\Omega)$ is the Lebesgue space of quadratically integrable functions over the domain Ω and $\mathbb{P}_k(K)$ a finite dimensional space of smooth functions, which are polynomials in our case (c.f. Li, 2006; Arnold et al., 2000). Following Kummer (2017), we define a set that contains all edges e of the grid, which is denoted as $\Gamma := \cup_j \partial\Omega_j$ and a set of internal edges $\Gamma_{\text{int}} = \Gamma \setminus \partial\Omega$. Using that, we define inner-values (u^-) and outer-values (u^+) of the field $u \in C^0(\Omega \setminus \Gamma_{\text{int}})$ as follows

$$u^-(\boldsymbol{x}) := \lim_{\epsilon \searrow 0} u(\boldsymbol{x} - \epsilon \boldsymbol{n}_\Gamma) \qquad \text{for } \boldsymbol{x} \in \Gamma, \tag{2.32a}$$

$$u^+(\boldsymbol{x}) := \lim_{\epsilon \searrow 0} u(\boldsymbol{x} + \epsilon \boldsymbol{n}_\Gamma) \qquad \text{for } \boldsymbol{x} \in \Gamma_{\text{int}} \tag{2.32b}$$

as well as mean and jump operators

$$\{u\} := \begin{cases} \frac{1}{2}(u^- + u^+) & \text{on } \Gamma_{\text{int}} \\ u^- & \text{on } \partial\Omega \end{cases}, \tag{2.33a}$$

$$[\![u]\!] := \begin{cases} u^- - u^+ & \text{on } \Gamma_{\text{int}} \\ u^- & \text{on } \partial\Omega \end{cases}. \tag{2.33b}$$

Due to these definitions and the assumption of the polynomial function space $\mathbb{V}_h$ a decoupling of the cells in the computational grid is obtained. That means the approximation can be made on each cell locally. Employing u and $\tilde{v}$ into the weak form leads to the following discretized problem (c.f Utz, 2018)

$$\begin{aligned} &\text{find } u \in \mathbb{V}_k, \text{such that} \\ \frac{\partial}{\partial t} \sum_{K \in \mathcal{K}} \int_{K_i} u\tilde{v} \, \mathrm{d}V + \sum_{K \in \mathcal{K}} \int_{K_i} \boldsymbol{f}(u) \cdot \nabla \tilde{v} \, \mathrm{d}V + \sum_{e \in \Gamma} \int_e \tilde{\boldsymbol{f}}(u^+, u^-, \boldsymbol{n}) \, [\![\tilde{v}]\!] \, \mathrm{d}S \\ = 0, \qquad \forall \tilde{v} \in \mathbb{V}_k(\mathcal{K}), \end{aligned} \tag{2.34}$$

where the quantity $\tilde{\boldsymbol{f}}(u^+, u^-, \boldsymbol{n})$ that couples neighboring cells needs to be defined. For that, a numerical flux $\tilde{\boldsymbol{f}}$ is introduced and chosen as such that it is conservative, i.e.

$$\tilde{\boldsymbol{f}}(u^+, u^-, \boldsymbol{n}) = -\tilde{\boldsymbol{f}}(u^+, u^-, -\boldsymbol{n}) \tag{2.35}$$

and that it fulfills the consistency condition, which means that we can replace the numerical solution u_h by the exact solution u in the weak formulation (2.30) (cf. Cockburn, 2003). That leads to the condition

$$\tilde{\boldsymbol{f}}(u^+, u^-, \boldsymbol{n}) = \boldsymbol{f}(u) \cdot \boldsymbol{n} \tag{2.36}$$

for the flux $\tilde{\boldsymbol{f}}$.
Since the function space $\mathbb{V}_k$ is polynomial, we approximate the solution u by a linear combination of polynomials, given by

$$u = \sum_i \tilde{u}_i \varphi_i, \tag{2.37}$$

where $\tilde{u}_i = \tilde{u}_i(t)$ are in general time-dependent scalar coefficients. The basis functions are orthonormal, i.e. they fulfill the condition

$$\int \varphi_i \varphi_j \mathrm{d}V = \delta_{ij}, \tag{2.38}$$

with δ_{ij} being the Kronecker Delta.
Employing (2.37) into (2.34) finally leads to a system of ODEs for the time-dependent problem (2.29), given by

$$\boldsymbol{M}\frac{\mathrm{d}\tilde{\boldsymbol{u}}}{\mathrm{d}t} + \boldsymbol{K}\tilde{\boldsymbol{u}} = \boldsymbol{b}, \tag{2.39}$$

where $\boldsymbol{b}$ is a vector consisting of boundary conditions and forcing terms if they are present in the original continuous problem. $\boldsymbol{M}$ is the mass matrix and $\boldsymbol{K}$ is the stiffness matrix.

As an example for a DG discretization of second order PDEs, we consider the Poisson equation with Dirichlet BCs, given by

$$-\Delta u = f \qquad \text{in } \Omega \tag{2.40a}$$
$$u = 0 \qquad \text{on } \partial\Omega. \tag{2.40b}$$

The weak form of (2.40a) is constructed by partial integration over all cells K_j

$$\sum_j \left(\int_{K_j} \nabla u \cdot \nabla \tilde{v} \, \mathrm{d}V - \int_{\partial K_j} (\nabla u \cdot \boldsymbol{n}) \, \tilde{v} \, \mathrm{d}S \right) = \sum_j \left(\int_{K_j} f \tilde{v} \, \mathrm{d}V \right) \qquad \forall \tilde{v} \in \mathbb{V}_k. \tag{2.41}$$

Taking the sum, one could re-formulate (see, e.g. Arnold et al., 2000)

$$\int_\Omega \nabla_h u \cdot \nabla_h \tilde{v} \, \mathrm{d}V - \int_{\Gamma_{\text{int}}} \{\nabla_h u\} \cdot \boldsymbol{n} \, [\![\tilde{v}]\!] \, \mathrm{d}S = \int_\Omega f \tilde{v} \, \mathrm{d}V \qquad \forall \tilde{v} \in \mathbb{V}_k. \tag{2.42}$$

One may write (2.41) as follows

$$\begin{aligned} \int_\Omega f \tilde{v} \, \mathrm{d}V = \int_\Omega \nabla_h u \cdot \nabla_h \tilde{v} \, \mathrm{d}V - \int_{\partial\Omega} \{\nabla_h u\} \cdot \boldsymbol{n} \, [\![\tilde{v}]\!] \, \mathrm{d}S \\ - \int_{\partial\Omega} \{\nabla_h \tilde{v}\} \cdot \boldsymbol{n} \, [\![u]\!] \, \mathrm{d}S + \int_{\partial\Omega} \eta_{\text{SIP}} \, [\![u]\!] \, [\![\tilde{v}]\!] \, \mathrm{d}S, \end{aligned} \tag{2.43}$$

where the weighting function is denoted as η_{SIP} in order to avoid confusion with the helical coordinate η and ∇_h is the broken gradient which is defined subsequently. It is known that (2.42) is not stable, i.e. the solution u is not unique. To overcome this issue, Arnold (1982b) added a so-called symmetry and a penalty term, which ensure

coercitivity of (2.43). The fourth term is added in order to obtain a symmetric discrete problem, whereas the last term in (2.43) is added to generate stability. For $\eta_{\text{SIP}} = \frac{C}{h}$, where h is the element size that can be chosen, for instance as the largest edge of the element. The constant C needs to be sufficiently large such that a convergence of the discrete solution to the exact solution is obtained (cf. Arnold et al., 2000). The DG approximation of (2.43) is given by (cf. Wihler and Rivière, 2011)

$$\begin{aligned} &\text{find } u \in \mathbb{V}_k, \text{such that} \\ &a(u, \tilde{v}) = b(\tilde{v}) \qquad \forall \tilde{v} \in \mathbb{V}_k, \end{aligned} \tag{2.44}$$

where the linear forms $a(u, \tilde{v})$ and $b(\tilde{v})$ read

$$\begin{aligned} a(u, \tilde{v}) = &\int_\Omega \nabla_h u \cdot \nabla_h \tilde{v} \, \mathrm{d}V - \int_\Gamma \{\nabla_h u\} \cdot \boldsymbol{n}_\Gamma \, [\![\tilde{v}]\!] \, \mathrm{d}S \\ &- \int_\Gamma \{\nabla_h \tilde{v}\} \cdot \boldsymbol{n}_\Gamma \, [\![u]\!] \, \mathrm{d}S + \int_\Gamma \eta_{\text{SIP}} \, [\![u]\!] \, [\![\tilde{v}]\!] \, \mathrm{d}S, \end{aligned} \tag{2.45a}$$

$$b(\tilde{v}) = \int_\Omega f \, \tilde{v} \, \mathrm{d}V. \tag{2.45b}$$

The broken gradient in (2.42), (2.43) and (2.45a) is defined as follows

$$\nabla_h f \;:=\; \begin{cases} 0 & \text{on } \cup_j \partial K_j \\ \nabla f & \text{elsewhere} \end{cases} . \tag{2.46}$$

For the DG discretization of the helically invariant Navier-Stokes equations (3.19) in each cell we use the following penalty function

$$\eta_{\text{SIP}} := c \cdot k^2 \frac{|\partial K|}{|K|}, \qquad c \approx 1, \tag{2.47}$$

where k is the polynomial degree of the DG discretization and

$$\eta_{\text{SIP}} := \max\left(\eta^-, \eta^+\right) \tag{2.48}$$

on the cell boundaries Γ (cf. Kummer and Müller, 2018).

Part I

Analysis

3 Navier-Stokes equations and symmetry reductions

The incompressible Navier-Stokes equations are a non-linear system of partial differential equations which describe viscous Newtonian fluid flows (cf. Drazin and Riley, 2006; Pope and Pope, 2000). They consist of the continuity equation (3.1a) and the momentum equations (3.1b) and are given by

$$\nabla \cdot \boldsymbol{u} = 0, \tag{3.1a}$$

$$\boldsymbol{u}_t + (\boldsymbol{u} \cdot \nabla)\boldsymbol{u} + \nabla p - \nu \nabla^2 \boldsymbol{u} = 0, \tag{3.1b}$$

where, in cartesian coordinates, $\boldsymbol{u} = u^1 \boldsymbol{e}_x + u^2 \boldsymbol{e}_y + u^3 \boldsymbol{e}_z$ is the velocity vector of the fluid and p the pressure, in which the density has already been absorbed. The velocity and the pressure are both functions of $\boldsymbol{x} = (x, y, z)$ and the time t. The viscosity ν is constant and for $\nu = 0$ the Euler equations are obtained (cf. KCO).

The vorticity, defined by

$$\boldsymbol{\omega} = \nabla \times \boldsymbol{u}, \tag{3.2}$$

is the physical quantity characterizing the rotation of fluid elements (Wu et al., 2007). By taking the curl of the Navier-Stokes equations one may easily derive the vorticity transport equations and a solenoidal condition for the vorticity, given by

$$\nabla \cdot \boldsymbol{\omega} = 0, \tag{3.3a}$$

$$\boldsymbol{\omega}_t + \nabla \times (\boldsymbol{\omega} \times \boldsymbol{u}) - \nu \Delta \boldsymbol{\omega} = 0. \tag{3.3b}$$

The vorticity transport equations (3.3b) can be written as

$$\boldsymbol{\omega}_t + (\boldsymbol{u} \cdot \nabla)\boldsymbol{\omega} - \nu \Delta \boldsymbol{\omega} = \nabla \boldsymbol{u} \cdot \boldsymbol{\omega}, \tag{3.4}$$

such that the vortex stretching terms are isolated on the right hand side of the equation.

3.1 Symmetries and reductions of the Navier-Stokes equations

The Lie point symmetries of the three-dimensional Navier-Stokes equations in cartesian coordinates (Oberlack, 2000) are given by

$$X_1 = \frac{\partial}{\partial t}, \tag{3.5a}$$

$$X_2 = 2t\frac{\partial}{\partial t} + x\frac{\partial}{\partial x} + y\frac{\partial}{\partial y} + z\frac{\partial}{\partial z} - u\frac{\partial}{\partial u} - v\frac{\partial}{\partial v} - w\frac{\partial}{\partial w} - 2p\frac{\partial}{\partial p}, \tag{3.5b}$$

$$X_3 = -y\frac{\partial}{\partial x} + x\frac{\partial}{\partial y} - v\frac{\partial}{\partial u} + u\frac{\partial}{\partial v}, \tag{3.5c}$$

$$X_4 = -z\frac{\partial}{\partial y} + y\frac{\partial}{\partial z} - w\frac{\partial}{\partial v} + v\frac{\partial}{\partial w}, \tag{3.5d}$$

$$X_5 = -z\frac{\partial}{\partial x} + x\frac{\partial}{\partial z} - w\frac{\partial}{\partial u} + u\frac{\partial}{\partial w}, \tag{3.5e}$$

$$X_6 = f_1(t)\frac{\partial}{\partial x} + f_1'(t)\frac{\partial}{\partial u} - xf_1''(t)\frac{\partial}{\partial p}, \tag{3.5f}$$

$$X_7 = f_2(t)\frac{\partial}{\partial y} + f_2'(t)\frac{\partial}{\partial v} - yf_2''(t)\frac{\partial}{\partial p}, \tag{3.5g}$$

$$X_8 = f_3(t)\frac{\partial}{\partial z} + f_3'(t)\frac{\partial}{\partial w} - zf_3''(t)\frac{\partial}{\partial p}, \tag{3.5h}$$

$$X_9 = f_4(t)\frac{\partial}{\partial p}, \tag{3.5i}$$

where $f_4(t)$ is a time-dependent parameter function and $f_1(t) \dots f_3(t)$ two-times differentiable functions of time.The symmetries of the Navier-Stokes equations (3.5) are given in the form of infinitesimal generators. The corresponding global transformations can be obtained applying Lie's theorem and are given in Oberlack (2000). The set of point symmetries (3.5) consist of a translation symmetry in time (X_1) as well as for the pressure (X_9), a scaling symmetry in space and time (X_2), the rotational symmetries about each coordinate axis $(X_3, \dots, X_5)$ and the generalized Galilean symmetries $(X_6 - X_8)$ which reduce to the classical Galilean boost assuming that $f_1(t), \dots, f_3(t)$ are linear functions in time and to a translation symmetry if $f_1(t), \dots, f_3(t)$ are constant.

The symmetries of the Navier-Stokes equations represent the basis of symmetry reductions and hence the well-known considerations of axisymmetric and plane flows. As already mentioned, for constant $f_1(t), \dots, f_3(t)$, the generalized Galilean symmetry (3.5f) - (3.5h) reduces to a translational symmetry. The fact that the Navier-Stokes equations are invariant with respect to translation represents the possibility to assume that all physical variables are independent of the z-coordinate, which is known as the two-dimensional case of plane flows. This reduction, and the additional assumption of a vanishing velocity component in z-direction leads to the set of variables, given by

$$u = u(x, y, t), \qquad v = v(x, y, t), \qquad p = p(x, y, t), \qquad w = 0. \tag{3.6}$$

The rotational symmetry (3.5c), written in cylindrical coordinates (r, φ, z) leads to a translational invariance in the angular coordinate, given by

$$X_R = \frac{\partial}{\partial \varphi}, \tag{3.7}$$

which, written as a global transformation, is given by

$$T_R: \qquad \tilde{t} = t, \qquad \tilde{\varphi} = \varphi + a_R, \qquad \tilde{\boldsymbol{u}} = \boldsymbol{u}, \tag{3.8}$$

where T_R denotes the global transformation group of the rotational symmetry and a_R the group parameter. As before for plane flows, the assumption of φ-independence of all physical variables and a vanishing circumferential velocity component u^φ leads to axisymmetric flows, consisting of the following set of variables in cylindrical coordinates

$$u^r = u^r(r,z,t), \qquad u^z = u^z(r,z,t), \qquad p = p(r,z,t), \qquad u^\varphi = 0. \tag{3.9}$$

For the axisymmetric flows various exact solutions of the Navier-Stokes equations have been found. Famous examples are the Oseen-Lamb vortex, the Taylor vortex and the Burgers vortex. A summary of these vortex solutions can be found in Wu et al. (2007). For the just described 2D flows only one non-zero vorticity component remains. Most important in turbulence theory, the vortex stretching term in the Navier-Stokes equations vanishes for 2D flows and the vorticity transport equations (3.4) reduce to

$$\boldsymbol{\omega}_t + (\boldsymbol{u} \cdot \nabla)\boldsymbol{\omega} - \nu \Delta \boldsymbol{\omega} = 0. \tag{3.10}$$

3.2 Helically symmetric flows

The present chapter is heavily based on the following publication of mine (Dierkes and Oberlack, 2017) as well as on results of my Master's thesis (Dierkes, 2015).

The main goal of the present chapter is to derive the helically reduced system of Navier-Stokes equations. The proceeding of that will be as follows: starting with the three dimensional Navier-Stokes we employ the Lie symmetry methods to derive a time-dependent helical coordinate $\xi = z/\alpha(t) + b\varphi$, where $b = \text{const.}$ and $\alpha(t)$ is an arbitrary function of time t. Assuming $\alpha = \text{const.}$, the classical helically symmetric case will be retained which is investigated extensively analytically and numerically in the chapters 5 and 6. Using the newly derived coordinate $\xi(t)$ and imposing helical invariance onto the equations of motion leads to the helically symmetric system of Euler and Navier-Stokes equations with a time-dependent pitch $\alpha(t)$, which may be varied arbitrarily and which is explicitly contained in all of the latter equations. This will be conducted for primitive variables, which consist of the velocity components and the pressure as well as for the vorticity formulation. Hence a set of helically invariant flows may be considered, which may be altered by an external time-dependent strain along the axis of the helix, which is a significant extension of the classical description of helical symmetric flows where $\alpha = \text{const.}$ is assumed. To avoid confusion, I would like to point out once again that the analytical and numerical investigations in chapters

5, 6, 7 and 8 of this thesis are essentially based on the classical description of helically invariant flows. Such investigations as the derivation of exact solutions as well as the development of a numerical code for the time-dependent helical coordinate system are, due to their complexity, contents of future scientific work.

3.2.1 Derivation of a time-dependent helical coordinate system

The three-dimensional time-dependent Navier-Stokes equations for a viscous and incompressible fluid without external forces in cylindrical coordinates are given by

$$\frac{1}{r}u^r + \frac{\partial u^r}{\partial r} + \frac{1}{r}\frac{\partial u^\varphi}{\partial \varphi} + \frac{\partial u^z}{\partial z} = 0, \tag{3.11a}$$

$$\frac{\partial u^r}{\partial t} + u^r\frac{\partial u^r}{\partial r} + \frac{1}{r}\left(u^\varphi\frac{\partial u^r}{\partial \varphi} - (u^\varphi)^2\right) + u^z\frac{\partial u^r}{\partial z} = -\frac{\partial p}{\partial r} + \nu\left[\Delta u^r - \frac{1}{r^2}\left(u^r + 2\frac{\partial u^\varphi}{\partial \varphi}\right)\right], \tag{3.11b}$$

$$\frac{\partial u^\varphi}{\partial t} + u^r\frac{\partial u^\varphi}{\partial r} + \frac{1}{r}\left(u^\varphi\frac{\partial u^\varphi}{\partial \varphi} + u^r u^\varphi\right) + u^z\frac{\partial u^\varphi}{\partial z} = -\frac{1}{r}\frac{\partial p}{\partial \varphi} + \nu\left[\Delta u^\varphi - \frac{1}{r^2}\left(u^\varphi - 2\frac{\partial u^r}{\partial \varphi}\right)\right], \tag{3.11c}$$

$$\frac{\partial u^z}{\partial t} + u^r\frac{\partial u^z}{\partial r} + \frac{1}{r}u^\varphi\frac{\partial u^z}{\partial \varphi} + u^z\frac{\partial u^z}{\partial z} = -\frac{\partial p}{\partial z} + \nu\Delta u^z, \tag{3.11d}$$

where Δ denotes the Laplacian, given by

$$\Delta = \frac{\partial}{\partial r^2} + \frac{1}{r}\frac{\partial}{\partial r} + \frac{1}{r^2}\frac{\partial}{\partial \varphi^2} + \frac{\partial}{\partial z^2}. \tag{3.12}$$

For inviscid flows, i.e. if $\nu = 0$ the system (3.11) reduces to the Euler equations. The helical Navier-Stokes equations (3.11) are invariant under the helical symmetry, which is obtained by combining the rotation group (3.5c) and the generalized Galilean invariance (3.5h). Without restricting generality, the coordinate system is chosen as such that the common symmetry lies along the z-axis. The global form of the two parameter Lie symmetry group is given by

$$\tilde{\varphi} = \varphi + c, \tag{3.13a}$$
$$\tilde{z} = z + \alpha(t), \tag{3.13b}$$
$$\tilde{u^z} = u^z + \dot{\alpha}, \tag{3.13c}$$
$$\tilde{p} = p - z\ddot{\alpha}, \tag{3.13d}$$

where the dot denotes the time derivative of the parameter function $\alpha(t)$, i.e. $\dot{\alpha} = \frac{\mathrm{d}\alpha(t)}{\mathrm{d}t}$. For $\alpha(t) = \text{const.}$ translational invariance in $z-$direction is obtained, while $\alpha(t) = at$

corresponds to the classical Galilean group in the same direction.
Using the symmetry group (3.13a)-(3.13d), a set of independent variables (i.e. the time-dependent helical coordinates) and dependent variables has been derived which is given by

$$\eta^* = b\varphi, \tag{3.14a}$$
$$\xi = b\varphi + \frac{z}{\alpha}, \tag{3.14b}$$
$$\tilde{r} = r, \tag{3.14c}$$
$$\tau = t, \tag{3.14d}$$
$$u^\xi = \left(\frac{b}{r}u^\varphi + \frac{1}{\alpha}(u^z + \dot{\alpha}b\varphi)\right) \cdot B(r,t), \tag{3.14e}$$
$$u^\eta = \left(\frac{1}{\alpha}u^\varphi - \frac{b}{r}(u^z + \dot{\alpha}b\varphi)\right) \cdot B(r,t), \tag{3.14f}$$
$$\tilde{u}^r = u^r, \tag{3.14g}$$
$$\tilde{p} = p + \frac{1}{2}\frac{\ddot{\alpha}}{\alpha}z^2. \tag{3.14h}$$

For the derivation of these variables Lie symmetry methods were employed, in particular the method of canonical coordinates. Details are presented in appendix A. The geometric function $B(r,t)$ in (3.14e) and (3.14f) is given by $B(r,t) = \frac{r\alpha}{\sqrt{r^2+b^2\alpha^2}}$. The assumption that $\alpha(t) = \text{const.} = \frac{1}{a}$ leads to the classical helical velocity components, pressure, similarity variable and form function $B(r)$ given by

$$\xi = az + b\varphi, \tag{3.15a}$$
$$u^\xi = B\left(\frac{b}{r}u^\varphi + au^z\right), \tag{3.15b}$$
$$u^\eta = B\left(au^\varphi - \frac{b}{r}u^z\right), \tag{3.15c}$$
$$\tilde{u}^r = u^r, \tag{3.15d}$$
$$\tilde{p} = p, \tag{3.15e}$$
$$B(r) = \frac{r}{\sqrt{(a^2r^2 + b^2)}}, \tag{3.15f}$$

which are found in KCO. Due to the high importance of this classical description in the second part of this thesis and for comprehensibility the essential variables for both, the time dependent and the classical case, are presented here in such a detail.

In the limiting case $b = 0$, for classical and time-dependent helical coordinates, the helical symmetry reduces to an axial symmetry. For the extended frame (3.14) the similarity variable (3.14b) becomes $\xi = \frac{z}{\alpha}$, though is still time-dependent owing to the scaling of the $z-$coordinate by the parameter function $\alpha(t)$. In the opposite case $\frac{1}{\alpha} = 0$, in which helical symmetry reduces to a planar symmetry, the time-dependence of the coordinate system vanishes and the classical planar case as discussed KCO is retained.

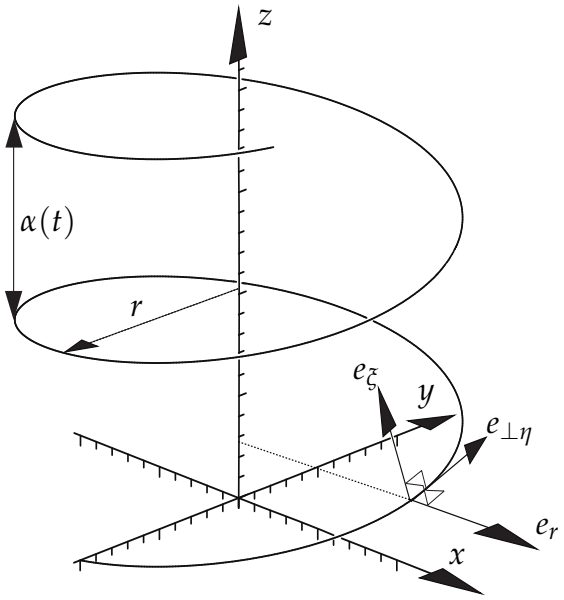

Figure 3.1: An illustration of the helix ξ=const.with parameter function $\alpha(t)$ (cf. KCO).

Inverting the equations (3.14e) - (3.14h) and replacing the cylindrical coordinates (r, φ, z) by the helical coordinates (r, ξ, η), the following relations are obtained, which are given by

$$u^{\varphi} = B(r,t) \cdot \left(\frac{b}{r} u^{\xi} + \frac{1}{\alpha} u^{\eta} \right), \tag{3.16a}$$

$$u^{z} = B(r,t) \cdot \left(\frac{1}{\alpha} u^{\xi} - \frac{b}{r} u^{\eta} \right) - \dot{\alpha}\eta^{*}, \tag{3.16b}$$

$$u^{r} = \tilde{u}^{r}, \tag{3.16c}$$

$$p = \tilde{p} - \frac{1}{2}\ddot{\alpha}\alpha \left(\xi - \eta^{*}\right)^{2}. \tag{3.16d}$$

The additional term $-\dot{\alpha}\eta^{*}$ in the z-component of the velocity (3.16b) describes a relative movement between the time-dependent and the time-independent coordinate system (see figure 3.1). In the classical helical case (α = const.), the cylindrical velocity components are related to the helical velocity components by

$$u^{\varphi} = B(r) \left(a u^{\eta} + \frac{b}{r} u^{\xi} \right), \qquad u^{z} = B(r) \left(-\frac{b}{r} u^{\eta} + a u^{\xi} \right). \tag{3.17}$$

In the following, we will write $B(r) = B$ and $\frac{\mathrm{d}B(r)}{\mathrm{d}r} = B'$.

3.2.2 Helically invariant Navier-Stokes equations in primitive variables

In order to obtain the reduced system of helically invariant Navier-Stokes equations the new variables (3.14e)-(3.14h) are introduced into the system (3.11) and helical invariance is imposed, i.e. $\frac{\partial}{\partial \eta^{*}} \equiv 0$, which eliminates η^{*} from the system. From this,

the helical invariant continuity equation and the three components of the momentum equations in r-, η^*- and ξ- direction are obtained and given by

$$\frac{u^r}{r} + u^r_r + \frac{1}{B}u^\xi_\xi = 0, \tag{3.18a}$$

$$-\frac{\dot\alpha}{\alpha}u^r_\xi\xi + u^r_\tau + u^r u^r_r + \frac{1}{B}u^\xi u^r_\xi - \frac{B^2}{r}\left(\frac{b}{r}u^\xi + \frac{1}{\alpha}u^\eta\right)^2 = -\tilde p_r + \nu\left[\frac{1}{r}\left(ru^r_r\right)_r + \frac{1}{B^2}u^r_{\xi\xi} - \frac{1}{r^2}u^r - \frac{2bB}{r^2}\left(\frac{1}{\alpha}u^\eta_\xi + \frac{b}{r}u^\xi_\xi\right)\right], \tag{3.18b}$$

$$\dot\alpha\frac{b}{r}u^\xi + \dot\alpha\frac{b^2B^2}{r^2\alpha}u^\eta - \frac{\dot\alpha}{\alpha}\xi u^\eta_\xi + u^\eta_\tau + u^r u^\eta_r + \frac{B^2}{r\alpha^2}u^r u^\eta + \frac{1}{B}u^\xi u^\eta_\xi = -B\ddot\alpha\frac{b}{r}\xi + \nu\left[\frac{1}{r}\left(ru^\eta_r\right)_r + \frac{1}{B^2}u^\eta_{\xi\xi} + \left(\frac{\frac{B^2}{\alpha^2}\left(\frac{B^2}{\alpha^2}-2\right)}{r^2}\right)u^\eta + \frac{2bB}{r^2\alpha}\left(u^r_\xi - \left(Bu^\xi\right)_r\right)\right], \tag{3.18c}$$

$$-2\dot\alpha\frac{bB^2}{r\alpha^2}u^\eta - \dot\alpha\frac{b^2B^2}{r^2\alpha}u^\xi - \frac{\dot\alpha}{\alpha}\xi u^\xi_\xi + u^\xi_\tau + u^r u^\xi_r + \frac{b^2B^2}{r^3}u^r u^\xi + \frac{1}{B}u^\xi u^\xi_\xi + \frac{2bB^2}{r^2\alpha}u^r u^\eta = -\frac{1}{B}\tilde p_\xi + B\frac{\ddot\alpha}{\alpha}\xi + \nu\left[\frac{1}{r}\left(ru^\xi_r\right)_r + \frac{1}{B^2}u^\xi_{\xi\xi} + \frac{\frac{B^4}{\alpha^4}-1}{r^2}u^\xi + \frac{2bB}{r}\left(\frac{b}{r^2}u^r_\xi + \left(\frac{B}{\alpha r}u^\eta\right)_r\right)\right]. \tag{3.18d}$$

In the case where $\alpha = \text{const.} = \frac{1}{a}$ all terms involving the first or second time-derivative of α vanish the equations describing classical helically symmetric flows with a constant pitch are retained. Due to the extensive analytical and numerical investigations of classical helical flows at a constant pitch in the following chapters of this thesis, we subsequently present the helically invariant system of Navier-Stokes equations for classical helical flows derived in KCO. The system of equations for $\alpha = \text{const.} = \frac{1}{a}$ is given by

$$\frac{1}{r}u^r + u^r_r + \frac{1}{B}u^\xi_\xi = 0, \tag{3.19a}$$

$$u^r_t + u^r u^r_r + \frac{1}{B}u^\xi u^r_\xi - \frac{B^2}{r}\left(\frac{b}{r}u^\xi + au^\eta\right)^2 = -p_r + \nu\left[\frac{1}{r}(ru^r_r)_r + \frac{1}{B^2}u^r_{\xi\xi} - \frac{1}{r^2}u^r - \frac{2bB}{r^2}\left(au^\eta_\xi + \frac{b}{r}u^\xi_\xi\right)\right], \tag{3.19b}$$

$$u_t^\eta + u^r u_r^\eta + \frac{1}{B} u^\xi u_\xi^\eta + \frac{a^2 B^2}{r} u^r u^\eta = \nu \left[\frac{1}{r} (r u_r^\eta)_r + \frac{1}{B^2} u_{\xi\xi}^\eta + \frac{a^2 B^2 (a^2 B^2 - 2)}{r^2} u^\eta + \frac{2abB}{r^2} \left(u_\xi^r - \left(B u^\xi \right)_r \right) \right], \quad (3.19c)$$

$$u_t^\xi + u^r u_r^\xi + \frac{1}{B} u^\xi u_\xi^\xi + \frac{2abB^2}{r^2} u^r u^\eta + \frac{b^2 B^2}{r^3} u^r u^\xi = -\frac{1}{B} p_\xi + \nu \left[\frac{1}{r} (r u_r^\xi)_r + \frac{1}{B^2} u_{\xi\xi}^\xi + \frac{a^4 B^4 - 1}{r^2} u^\xi + \frac{2bB}{r} \left(\frac{b}{r^2} u_\xi^r + \left(\frac{aB}{r} u^\eta \right)_r \right) \right]. \quad (3.19d)$$

where the velocity components u^r, u^η, u^ξ and the pressure p are functions of r, ξ and t and the geometric factor B is given by (3.15f). Due to the 2π-periodicity of the cylindrical polar angle φ, in order to be globally defined, every component of a helically invariant solution must be periodic in ξ with the period

$$\tau_\xi = 2\pi b. \quad (3.20)$$

3.2.3 Helically invariant Navier-Stokes equations in vorticity formulation

For the Navier-Stokes equations in vorticity formulation a local orthogonal basis system in analogy to KCO can be introduced to compute the helical vorticity components $\omega^r, \omega^\xi, \omega^\eta$. The unit vectors are given by

$$\boldsymbol{e}_r = \frac{\nabla r}{|\nabla r|}, \quad \boldsymbol{e}_\xi = \frac{\nabla \xi}{|\nabla \xi|}, \quad \boldsymbol{e}_{\perp\eta} = \boldsymbol{e}_\xi \times \boldsymbol{e}_r. \quad (3.21)$$

The vorticity vector in the helical basis is given by

$$\boldsymbol{\omega} = \omega^r \boldsymbol{e}_r + \omega^\varphi \boldsymbol{e}_\varphi + \omega^z \boldsymbol{e}_z = \omega^r \boldsymbol{e}_r + \omega^\eta \boldsymbol{e}_{\perp\eta} + \omega^\xi \boldsymbol{e}_\xi. \quad (3.22)$$

The helical vorticity components are related to the cylindrical vorticity components given by

$$\omega^\eta = \boldsymbol{\omega} \cdot \boldsymbol{e}_{\perp\eta} = B \left(\frac{1}{\alpha} \omega^\varphi - \frac{b}{r} \omega^z \right), \quad \omega^\xi = B \left(\frac{b}{r} \omega^\varphi + \frac{1}{\alpha} \omega^z \right). \quad (3.23)$$

The definition of vorticity (3.2) in cylindrical coordinates is given by

$$\boldsymbol{\omega} = \nabla \times \boldsymbol{u} = \left(\frac{1}{r} u_\varphi^z - u_z^\varphi \right) \boldsymbol{e}_r + \left(u_z^r - u_r^z \right) \boldsymbol{e}_\varphi + \left(\frac{1}{r} u^\varphi + u_r^\varphi - \frac{1}{r} u_\varphi^r \right) \boldsymbol{e}_z. \quad (3.24)$$

Replacing the expressions for the velocity components (3.16a)-(3.16c) and their derivatives and, further, assuming helical invariance $\left(\frac{\partial}{\partial\eta} \equiv 0\right)$ one obtains the respective components of $\boldsymbol{\omega}$ given by

$$\omega^r = -\frac{1}{B}u^\eta_\xi - \frac{b}{r}\dot{\alpha}, \tag{3.25a}$$

$$\omega^\eta = \frac{1}{B}u^r_\xi - \frac{1}{r}\left(ru^\xi\right)_r - \frac{2bB^2}{\alpha r^2}u^\eta + \frac{B^2}{\alpha^2 r}u^\xi, \tag{3.25b}$$

$$\omega^\xi = u^\eta_r + \frac{B^2}{\alpha^2 r}u^\eta. \tag{3.25c}$$

Employing a transformation similarly to the Navier-Stokes equations in primitive variables, one obtains the helically invariant Navier-Stokes equations in vorticity formulation given by

$$\frac{\omega^r}{r} + \omega^r_r + \frac{1}{B}\omega^\xi_\xi = 0, \tag{3.26a}$$

$$\begin{aligned} -\frac{\dot{\alpha}}{\alpha}\omega^r_\xi\xi + \omega^r_\tau + u_r\omega^r_r + \frac{1}{B}u^\xi\omega^r_\xi = \omega^r u^r_r + \frac{1}{B}\omega^\xi u^r_\xi \\ + \nu\left[\frac{1}{r}\left(r\omega^r_r\right)_r + \frac{1}{B^2}\omega^r_{\xi\xi} - \frac{1}{r^2}\omega^r - \frac{2bB}{r^2}\left(\frac{1}{\alpha}\omega^\eta_\xi + \frac{b}{r}\omega^\xi_\xi\right)\right], \end{aligned} \tag{3.26b}$$

$$\begin{aligned} \frac{b}{r}\dot{\alpha}\left(-\frac{b^2}{r^2} + \frac{1}{\alpha^2}\right)B^2\omega^\xi - \frac{\dot{\alpha}}{\alpha}\omega^\eta_\xi\xi - \frac{b^2\dot{\alpha}}{\alpha r^2}B^2\omega^\eta + \omega^\eta_\tau + u^r\omega^\eta_r + \frac{1}{B}u^\xi\omega^\eta_\xi \\ - \frac{B^2}{r\alpha^2}(u^r\omega^\eta - u^\eta\omega^r) + \frac{2bB^2}{\alpha r^2}(u^\xi\omega^r - u^r\omega^\xi) = \omega^r u^\eta_r + \frac{1}{B}\omega^\xi u^\eta_\xi \\ + \nu\left[\frac{1}{r}\left(r\omega^\eta_r\right)_r + \frac{1}{B^2}\omega^\eta_{\xi\xi} + \frac{B^2(\frac{1}{\alpha^2}B^2 - 2)}{\alpha^2 r^2}\omega^\eta + \frac{2bB}{\alpha r^2}\left(\omega^r_\xi - (B\omega^\xi)_r\right)\right], \end{aligned} \tag{3.26c}$$

$$\begin{aligned} -\frac{\dot{\alpha}}{\alpha}\omega^\xi_\xi\xi + \frac{b^2\dot{\alpha}}{r^2\alpha}B^2\omega^\xi + \omega^\xi_\tau + u^r(\omega^\xi)_r + \frac{1}{B}u^\xi\omega^\xi_\xi + \frac{1 - \frac{B^2}{\alpha^2}}{r}(u^\xi\omega^r - u^r\omega^\xi) = \omega^r u^\xi_r + \frac{1}{B}\omega^\xi u^\xi_\xi \\ + \nu\left[\frac{1}{r}\left(r\omega^\xi_r\right)_r + \frac{1}{B^2}\omega^\xi_{\xi\xi} + \frac{\frac{1}{\alpha^4}B^4 - 1}{r^2}\omega^\xi + \frac{2bB}{r}\left(\frac{b}{r^2}\omega^r_\xi + \left(\frac{B}{\alpha r}\omega^\eta\right)_r\right)\right]. \end{aligned} \tag{3.26d}$$

Likewise in KCO, the first two terms on the right-hand side of each equation in (3.26b)-(3.26d) correspond to vortex stretching. Since in this thesis the vorticity components of the classical helical case are used to derive exact solutions of the Navier-Stokes equations in chapter 5, we present the formulation in the following, which are also published in KCO. As before in the case where $\alpha = \text{const.} = \frac{1}{a}$ the vorticity components (3.25) simplify to

$$\omega^r = -\frac{1}{B}u^\eta_\xi, \tag{3.27a}$$

$$\omega^{\eta} = \frac{1}{B}u^{r}_{\xi} - \frac{1}{r}\left(ru^{\xi}\right)_{r} - \frac{2abB^2}{r^2}u^{\eta} + \frac{a^2B^2}{r}u^{\xi}, \tag{3.27b}$$

$$\omega^{\xi} = u^{\eta}_{r} + \frac{a^2B^2}{r}u^{\eta}. \tag{3.27c}$$

3.2.4 Symmetries of the helically invariant Navier-Stokes equations

In the present section, the Lie symmetry group and the invariants of the classical helically symmetric system of Navier-Stokes equations in primitive variables (3.19) are considered. The two cases of (i) a nonzero velocity component in η-direction which is the "2 1/2−dimensional" case and (ii) the assumption of a vanishing third velocity component $u^{\eta} = 0$, i.e. classical $2D$ plane flows in the helical formulation are distinguished. The central difference between both cases is that in (i) the vortex stretching is present which vanishes in case (ii). In most cases a reduction of dependent variables leads to more symmetries of the PDE system. For the helically invariant equations under the assumption of a vanishing third coordinate this seems not to be the case, but we find a slightly different and more general symmetry, given by (3.33d).

The symmetry generators of the classical helically invariant Navier-Stokes equations in primitive variables (3.19) are given by

$$X_1 = \frac{\partial}{\partial t}, \tag{3.28a}$$

$$X_2 = \frac{\partial}{\partial \xi}, \tag{3.28b}$$

$$X_3 = f(t)\frac{\partial}{\partial p}, \tag{3.28c}$$

$$X_4 = -\frac{b}{ar}B\frac{\partial}{\partial u^{\eta}} + B\frac{\partial}{\partial u^{\xi}} + t\frac{\partial}{\partial \xi}. \tag{3.28d}$$

To determine the invariants of (3.19), the symmetry (3.28d) is used to obtain the characteristic system of PDEs given by

$$\frac{\mathrm{d}u^{r}}{0} = -\frac{ar}{bB}\mathrm{d}u^{\eta} = \frac{\mathrm{d}u^{\xi}}{B} = \frac{\mathrm{d}\xi}{t} = \frac{\mathrm{d}r}{0} = \frac{\mathrm{d}t}{0} = \frac{\mathrm{d}p}{0}. \tag{3.29}$$

The solution of the system (3.29) leads to the following invariants

$$I_1 = r, \tag{3.30a}$$
$$I_2 = t, \tag{3.30b}$$
$$u^r = F_1(r,t), \tag{3.30c}$$
$$u^\xi = \frac{B}{t}\xi + F_2(r,t), \tag{3.30d}$$
$$u^\eta = -\frac{b}{ar}\frac{B}{t}\xi + F_3(r,t), \tag{3.30e}$$
$$p = F_4(r,t). \tag{3.30f}$$

In the case of two-dimensional flows, i.e. when the velocity component u^η is zero ($u^\eta = 0$), the momentum equation in invariant direction reduces to

$$(u^r)_\xi = \left(Bu^\xi\right)_r. \tag{3.31}$$

Employing (3.31) into (3.19) leads to the system of equations in $2D$ written in a helical frame, given by

$$\frac{1}{r}u^r + u^r_r + \frac{1}{B}u^\xi_\xi = 0, \tag{3.32a}$$

$$u^r_t + u^r u^r_r + \frac{1}{B}u^\xi\left(Bu^\xi\right)_r - \frac{B^2b^2}{r^3}\left(u^\xi\right)^2 = -p_r + \nu\left[\frac{1}{r}(ru^r_r)_r + \frac{1}{B^2}\left(Bu^\xi\right)_{r\xi} - \frac{1}{r^2}u^r - \frac{2bB}{r^2}\left(au^\eta_\xi + \frac{b}{r}u^\xi_\xi\right)\right], \tag{3.32b}$$

$$u^\xi_t + u^r u^\xi_r + \frac{1}{B}u^\xi u^\xi_\xi + \frac{b^2B^2}{r^3}u^r u^\xi = -\frac{1}{B}p_\xi + \nu\left[\frac{1}{r}(ru^\xi_r)_r + \frac{1}{B^2}u^\xi_{\xi\xi} + \frac{a^4B^4-1}{r^2}u^\xi + \frac{2bB}{r}\left(\frac{b}{r^2}u^r_\xi\right)\right]. \tag{3.32c}$$

The Lie point symmetries $\tilde{X}_1$-$\tilde{X}_4$ of the system (3.32) as infinitesimal generators read

$$\tilde{X}_1 = \frac{\partial}{\partial t}, \tag{3.33a}$$
$$\tilde{X}_2 = \frac{\partial}{\partial \xi}, \tag{3.33b}$$
$$\tilde{X}_3 = f_1(t)\frac{\partial}{\partial p}, \tag{3.33c}$$
$$\tilde{X}_4 = -\left(\frac{f_2(t)}{B}\,u^\xi + \frac{\mathrm{d}f_2(t)}{\mathrm{d}t}\,\xi\right)\frac{\partial}{\partial p} + \frac{f_2(t)}{B}\frac{\partial}{\partial u^\xi}. \tag{3.33d}$$

Comparing (3.28) with (3.33) a more general symmetry has been found, which contains the time-derivative $\frac{\mathrm{d}f_2(t)}{\mathrm{d}t}$ of the arbitrary parameter function $f_2(t)$. This result is obtained by comparison of X_4 and $\tilde{X}_4$.

4 Conservation laws of helically invariant Navier-Stokes equations

In this chapter we present new CLs of the helically invariant Navier-Stokes equations in the time-dependent helical frame (3.18). It is heavily based on Dierkes and Oberlack (2017), which is a publication of mine.
In section 4.1 we present the newly derived conservation laws of the helically invariant Euler system (3.18), where the assumption of vanishing viscosity ($\nu = 0$) holds. In both common formulations, i.e. in (i) the velocity-pressure formulation and (ii) the vorticity formulation new conservation laws have been discovered. In section 4.2 new conservation laws of the helically invariant Navier-Stokes equations with a nonzero viscosity ($\nu \neq 0$) are shown, for the velocity-pressure and the vorticity formulation. Finally in sections 4.3 and 4.4 we prove that the kinetic energy and the helicity is not conserved in time-dependent helical coordinates.

4.1 CLs of the helically invariant Euler system in time-dependent helical coordinates

In order to seek local conservation laws, we subsequently apply the direct construction method (Bluman et al., 2010) to the Euler system (3.18) with $\nu = 0$ in primitive variables as well as in vorticity formulation (3.26) with $\nu = 0$. In both cases, the conservation law multipliers Λ_σ are chosen to be of zeroth order and, thus, only depend on the dependent and independent variables

$$\Lambda_\sigma = \Lambda_\sigma \left(t, r, \xi, u^r, u^\eta, u^\xi, \tilde{p} \right). \tag{4.1}$$

Computations with conservation law multipliers of first order, i.e. Λ_σ in (4.1) containing first derivatives of $\boldsymbol{u}$ and $\tilde{p}$, have also been done. However, no additional multipliers exist and, hence, also no extended set of CL.

All computations to derive local conservation laws were conducted with the aid of the symbolic software package GEM for MAPLE (Cheviakov, 2007) and the MAPLE RIFSIMP-tool. Further, with these tools we also obtained the corresponding fluxes of the general form Γ^i in equation (2.26). The relation between the fluxes Γ^i and the density Θ and the spatial fluxes Φ^i in equation (2.19) can be derived as follows:

In the helical setting any divergence form reads

$$\frac{\partial \Gamma^t}{\partial t} + \frac{\partial \Gamma^r}{\partial r} + \frac{\partial \Gamma^\xi}{\partial \xi} = 0, \tag{4.2a}$$

while a divergence expression of an evolution process in helically symmetric form reads

$$\frac{\partial \Theta}{\partial t} + \nabla \cdot \mathbf{\Phi} = \frac{\partial \Theta}{\partial t} + \frac{1}{r}\frac{\partial}{\partial r}\left(r\Phi^r\right) + \frac{1}{B}\frac{\partial \Phi^\xi}{\partial \xi} = 0, \tag{4.2b}$$

which is apparently not identical to (4.2a) due to metric terms. However, multiplying (4.2b) by r and using (4.2a) leads to

$$\frac{\partial \Gamma^t}{\partial t} + \frac{\partial \Gamma^r}{\partial r} + \frac{\partial \Gamma^\xi}{\partial \xi} = \frac{\partial}{\partial t}\left(r\Theta\right) + \frac{\partial}{\partial r}\left(r\Phi^r\right) + \frac{\partial}{\partial \xi}\left(\frac{r}{B}\Phi^\xi\right). \tag{4.3}$$

Comparing the left- and right-hand side of (4.3) one obtains

$$\Gamma^t = r\Theta, \quad \Gamma^r = r\Phi^r, \quad \Gamma^\xi = \frac{r}{B}\Phi^\xi. \tag{4.4}$$

Subsequently, we always list the density Θ and the spatial fluxes $\mathbf{\Phi}$ for each conservation law. The obvious conservation laws like the continuity equations $\nabla \cdot \boldsymbol{u} = 0$, $\nabla \cdot \boldsymbol{\omega} = 0$ and the scaling of these equations with a time-dependent function leading to $\nabla \cdot (G(t)\boldsymbol{u}) = 0$, $\nabla \cdot (G(t)\boldsymbol{\omega}) = 0$ will not be listed explicitly.

In the next section we seek local conservation laws that arise from the helically invariant Euler equations in primitive variables, given by (3.19) with $\nu = 0$. These conservation laws will be denoted by the prefix 'EP'. The conservation laws obtained from the helically invariant Euler system in vorticity formulation will be denoted by the prefix 'EV'.

4.1.1 Primitive variables

EP1. Extension of the Conservation of the z-projection of momentum. The first conservation law is given by

$$\Theta = \alpha^2 B\left(\frac{1}{\alpha}u^\xi - \frac{b}{r}u^\eta\right), \tag{4.5a}$$

$$\Phi^r = \alpha^2\left(u^r B\left(\frac{1}{\alpha}u^\xi - \frac{b}{r}u^\eta\right) - \dot{\alpha}\xi u^r - \frac{1}{2}\ddot{\alpha}r\xi\right), \tag{4.5b}$$

$$\begin{aligned}\Phi^\xi = {} & \alpha^2\left(u^\xi B\left(\frac{1}{\alpha}u^\xi - \frac{b}{r}u^\eta\right) + \frac{B}{\alpha}p\right) \\ & - \alpha^2\dot{\alpha}\xi u^\xi - \alpha\dot{\alpha}\xi B^2\left(\frac{1}{\alpha}u^\xi - \frac{b}{r}u^\eta\right).\end{aligned} \tag{4.5c}$$

Compared to the classical conservation of the z-projection of momentum, one determines that the density and the spatial fluxes are multiplied by the square of the arbitrary function $\alpha(t)$. It may further be noted, that Θ in (4.5a) is linked to u^z in cylindrical coordinates by $\Theta = \alpha^2\left(u^z + \dot{\alpha}\eta^*\right)$. Moreover, the spatial fluxes are extended by terms involving first and second time-derivatives of the arbitrary function. ($\alpha = \text{const.}$ corresponds to EP2 in KCO)

EP2. Extension of the Conservation of the z-projection of angular momentum. The second conservation law is given by

$$\Theta = \alpha r B \left(\frac{1}{\alpha} u^{\eta} + \frac{b}{r} u^{\xi} \right) = \alpha r u^{\varphi}, \tag{4.6a}$$

$$\Phi^{r} = \alpha r u^{r} u^{\varphi}, \tag{4.6b}$$

$$\Phi^{\xi} = \alpha \left(r u^{\xi} u^{\varphi} + bBp \right) - \dot{\alpha} r \xi B u^{\varphi}. \tag{4.6c}$$

In contrast to the velocity component in z-direction, the component in the angular direction has no relative movement. Therefore, we are able to express the density and the fluxes in terms of cylindrical velocities. ($\alpha = \text{const.}$ corresponds to EP3 in KCO)

EP3. Extension of the conservation of the generalized momenta/angular momenta. Here we obtain an infinite family of conservation laws

$$\Theta = \alpha F \left(\frac{\alpha r}{B} u^{\eta} + b \alpha \dot{\alpha} \xi \right) - b \alpha^{2} \dot{\alpha} \xi, \tag{4.7a}$$

$$\Phi^{r} = \alpha F \left(\frac{\alpha r}{B} u^{\eta} + b \alpha \dot{\alpha} \xi \right) u^{r} + \frac{1}{2} \alpha^{2} \ddot{\alpha} b r \xi, \tag{4.7b}$$

$$\begin{aligned} \Phi^{\xi} = {} & \alpha F \left(\frac{\alpha r}{B} u^{\eta} + b \alpha \dot{\alpha} \xi \right) u^{\xi} - B \dot{\alpha} \xi F \left(\frac{\alpha r}{B} u^{\eta} + b \alpha \dot{\alpha} \xi \right) \\ & + B b \alpha \dot{\alpha}^{2} \xi^{2}, \end{aligned} \tag{4.7c}$$

where $F(\cdot)$ is a once differentiable arbitrary function.

The density and the spatial fluxes contain the first and second time derivative of α. Referring to KCO, the quantity

$$\zeta = \frac{\alpha r}{B} u^{\eta} + b \alpha \dot{\alpha} \xi \tag{4.8}$$

can be physically interpreted as a 'blend' of momentum and angular momentum density in the η^{*}-direction since with the use of (3.14e) and $z = \alpha \left(\xi - \eta^{*} \right)$ the quantity reads

$$\zeta = \frac{\alpha r}{B} u^{\eta} + b \alpha \dot{\alpha} \xi = r u^{\varphi} - \alpha b u^{z} + b \dot{\alpha} z \tag{4.9}$$

$$= \alpha \left(\frac{r}{\alpha} u^{\varphi} - b u^{z} + \frac{b}{\alpha} \dot{\alpha} z \right), \tag{4.10}$$

where the term $\frac{b}{\alpha} \dot{\alpha} z$ describes the relative movement. For the special cases $b = 0$ the quantity is proportional to the angular momentum density in z-direction $\tilde{\zeta} \sim \frac{r}{\alpha} u^{\varphi}$ in equation (4.10) while for $\frac{1}{\alpha} = 0$ it is proportional to the linear momentum density in z-direction $\tilde{\zeta} \sim u^{z}$ in equation (4.10). ($\alpha = \text{const.}$ corresponds to EP4 in KCO)

Comparing the above results to the classical cases one observes, that the only quantity, which is not conserved, is kinetic energy. In the next section we will see that also helicity is not conserved. In order to ensure that this proposition is appropriate in

any helical, time-dependent coordinate system, we will prove the non-existence of conservation of energy and helicity in the sections 4.3 and 4.4.

4.1.2 The vorticity formulation

The following conservation laws are derived from the helically invariant Euler equations in vorticity formulation, consisting of the continuity equation for velocity as well as for vorticity, equations (3.18a) and (3.26a), the equations defining the vorticity components (3.25) and the vorticity dynamics equations (3.26b)-(3.26d) with $\nu = 0$. Similar to the multipliers (4.1) for the primitive variables we assume the present multipliers to be of the form

$$\Lambda_\sigma = \Lambda_\sigma \left(t, r, \xi, u^r, u^\eta, u^\xi, \tilde{p}, \omega^r, \omega^\eta, \omega^\xi \right), \tag{4.11}$$

i.e. we limit ourselfs again to zeroth order multipliers.

EV1. Extended family of conservation laws involving ω^φ. The family of conservation laws is given by

$$\Theta = \frac{q(t)}{r}\omega^\varphi, \tag{4.12a}$$

$$\Phi^r = \frac{1}{r}\left(q(t)\left[u^r\omega^\varphi - \omega^r u^\varphi\right] + \dot{q}(t)B\left(\frac{1}{\alpha}u^\xi - \frac{b}{r}u^\eta\right) - \dot{\alpha}q(t)B\left(\frac{1}{\alpha^2}u^\xi - \frac{b}{r\alpha}u^\eta\right)\right), \tag{4.12b}$$

$$\Phi^\xi = -\frac{B}{r\alpha}\left(q(t)\left(u^\eta\omega^\xi - u^\xi\omega^\eta\right) + \dot{q}(t)u^r + q(t)\dot{\alpha}\xi\omega^\varphi - q(t)\frac{\dot{\alpha}}{\alpha}u^r\right), \tag{4.12c}$$

where $q(t)$ and $\dot{q}(t)$ is an arbitrary function and its time-derivative, respectively. ($\alpha =$ const. corresponds to EV3 in KCO)

EV2. Vorticity conservation law. The conservation law is given by the density and fluxes

$$\Theta = -\alpha^4 rB\left(\frac{1}{\alpha^3}\omega^\eta - \frac{b^3}{r^3}\omega^\xi\right), \tag{4.13a}$$

$$\begin{aligned}\Phi^r = \alpha^4\Bigg(&-\frac{B}{r^2}\left(\frac{r^3}{\alpha^3}\left(u^r\omega^\eta - u^\eta\omega^r\right) - b^3\left(u^r\omega^\xi - u^\xi\omega^r\right)\right) - \frac{2B}{\alpha^2}u^r\left(-\frac{b}{r}u^\eta + \frac{1}{\alpha}u^\xi\right)\Bigg)\\ &+ \frac{B}{r^2}\dot{\alpha}\left(-r^3u^\xi - 2\alpha^3b^3u^\eta - \alpha r^2bu^\eta + \frac{2}{B}\alpha^2r^2\xi u^r\right),\end{aligned} \tag{4.13b}$$

$$\begin{aligned}\Phi^\xi = \alpha^4\Bigg(&\frac{B}{\alpha^3}\left((u^r)^2 + (u^\eta)^2 - \left(u^\xi\right)^2 + r\left(u^\eta\omega^\xi - u^\xi\omega^\eta\right)\right) + \frac{2bB}{\alpha^2 r}u^\eta u^\xi\Bigg)\\ &- \frac{B^2}{r^2}\dot{\alpha}\left(b^3\alpha^3\xi\omega^\xi - 2b^2\alpha^2\xi u^\xi - r^3\xi\omega^\eta - 2r^2\xi u^\xi - \frac{r^3}{B}u^r\right).\end{aligned} \tag{4.13c}$$

The assumption $b = 0$ leads to $\Theta = -\alpha^2 r\omega^\varphi$. Corresponding to KCO, for problems, where the velocity vanishes on the boundary of the time-independent flow domain

$\Omega \neq \Omega(t)$, the quantity $\alpha^2 r\omega^\varphi$ corresponds to the conservation of linear momentum in z-direction since

$$\frac{1}{2}\alpha^2 \int\int_\Omega r\omega^\varphi \mathrm{d}A = \alpha^2 \int\int_\Omega u^z \mathrm{d}A, \tag{4.14}$$

where $\alpha(t)$ is the parameter function. ($\alpha = $ const. corresponds to EV4 in KCO)

EV3. Vorticity conservation law. The conservation law is given by

$$\begin{aligned}
\Theta &= -\alpha^4 \frac{B}{r^2}\left(\frac{r^2b^2}{B^2}\omega^\xi + \frac{r^4}{\alpha^3}\left(-\frac{b}{r}\omega^\eta + \frac{1}{\alpha}\omega^\xi\right)\right) \\
&= -\alpha^4 \frac{B}{r^2}\left(\frac{r^2b^2}{B^2}\omega^\xi + \frac{r^4}{\alpha^3 B}\omega^z\right), && \text{(4.15a)} \\
\Phi^r &= \alpha^4 \frac{rB}{\alpha^3}\Bigg(2u^r\left(\frac{1}{\alpha}u^\eta + \frac{b}{r}u^\xi\right) + b\left(u^r\omega^\eta - u^\eta\omega^r\right) \\
&\quad - \frac{r^4 + r^2\alpha^2b^2 + b^4\alpha^4}{r^3\alpha}\left(u^r\omega^\xi - u^\xi\omega^r\right) + \dot\alpha\left(\frac{b}{\alpha}u^\xi + 2\alpha^2\frac{b^4}{r^3}u^\eta + \frac{b^2}{r}u^\eta\right)\Bigg), && \text{(4.15b)} \\
\Phi^\xi &= \alpha^4\left(-\frac{1}{\alpha^3}bB\right)\Bigg((u^r)^2 + (u^\eta)^2 - \left(u^\xi\right)^2 + r\left(u^\eta\omega^\xi - u^\xi\omega^\eta\right) \\
&\quad - 2\frac{r}{\alpha b}u^\eta u^\xi + \dot\alpha\left(B\frac{r}{\alpha}\xi\omega^\eta + \frac{r}{\alpha}u^r - \frac{r^4 + r^2\alpha^2b^2 + b^4\alpha^4}{r^2\alpha^2 b}B\xi\omega^\xi\right)\Bigg). && \text{(4.15c)}
\end{aligned}$$

As already seen before, the vorticity component ω^z has no relative movement. Hence, the helical vorticity components ω^ξ, ω^η were replaced by ω^z in the density (4.15a). For rotationally symmetric flows, $b = 0$, the density reduces to $-\frac{1}{2}\alpha r^2\omega^z$. In a similar way to (4.14), for problems with vanishing flow velocities on the boundary and $\Omega \neq \Omega(t)$, it corresponds to the conservation of angular momentum in z-direction. As before, the time-dependent parameter function $\alpha(t)$ is still involved. ($\alpha = $ const. corresponds to EV5 in KCO)

EV4. Vorticity conservation law. We further obtain a family of conservation laws, given by the density and fluxes

$$\begin{aligned}
\Theta &= 0, && \text{(4.16a)} \\
\Phi^r &= N\omega^r - \frac{1}{B}N_\xi u^\eta + \frac{b}{r}\dot\alpha N, && \text{(4.16b)} \\
\Phi^\xi &= N\omega^\xi + N_r u^\eta. && \text{(4.16c)}
\end{aligned}$$

where $N = N(r, \xi, t)$. This conservation law is a linear combination of the continuity equation for the vorticity (3.26a) and the equations defining the vorticity components (3.25). For $\alpha = $ const. we obtain an additional CL of the classical case that has not been listed in KCO. In KCO only a dimensionally reduced form of (4.16b)/(4.16c) was found, where the function only depended on ξ and t, i.e. $N = N(\xi, t)$ (EV6 in KCO).

EV5. Vorticity conservation law. In this case the conservation law multipliers again depend on an arbitrary function $M = M(\xi, r, t)$ and one obtains the following family of conservation laws, given by its density and fluxes

$$\Theta = M_r \omega^r + \frac{M_\xi}{B}\omega^\xi, \tag{4.17a}$$

$$\Phi^r = \frac{M_\xi}{B}\left(u^r\omega^\xi - u^\xi\omega^r\right) - M_t\omega^r + \frac{\dot\alpha}{\alpha}\omega^r\left(M + \xi M_\xi\right), \tag{4.17b}$$

$$\Phi^\xi = M_r\left(u^\xi\omega^r - u^r\omega^\xi\right) - M_t\omega^\xi + \frac{\dot\alpha}{\alpha}\left(M\omega^\xi - B\xi M_r\omega^r\right). \tag{4.17c}$$

This conservation law is a subset of the infinite family of vorticity conservation laws for helical flows presented in Cheviakov and Oberlack (2014) for arbitrary time-dependent 3D flows and closely linked to Ertel's theorem.

4.2 CLs of the helically invariant Navier-Stokes system in time-dependent coordinates

Presently, the application of the direct method to the reduced Navier-Stokes system (3.18) in primitive variables leads to two new conservation laws. For the related vorticity formulation (3.26) five new conservation laws will be derived. For the present calculations all multipliers (4.1) have been chosen to be of zeroth order. Similarly to the classical case, all new present conservation laws are subsets of those admitted by the helically symmetric Euler equations in the previous chapter, whereas the densities are the same, the fluxes are extended by additional viscous terms.

4.2.1 Primitive variables

NSP1. Extension of the conservation of the z-projection of momentum. The conservation law is respectively defined by the density and fluxes

$$\Theta = \alpha^2 B\left(\frac{1}{\alpha}u^\xi - \frac{b}{r}u^\eta\right), \tag{4.18a}$$

$$\begin{aligned}\Phi^r = {}& \alpha^2\left(u^r B\left(\frac{1}{\alpha}u^\xi - \frac{b}{r}u^\eta\right) - \dot\alpha\xi u^r - \frac{1}{2}\ddot\alpha r\xi\right)\\ & - \alpha^2\nu\left(B\left(\frac{1}{\alpha}u^\xi - \frac{b}{r}u^\eta\right)\right)_r,\end{aligned} \tag{4.18b}$$

$$\begin{aligned}\Phi^\xi = {}& \alpha^2\left(u^\xi B\left(\frac{1}{\alpha}u^\xi - \frac{b}{r}u^\eta\right) + \frac{B}{\alpha}p\right)\\ & - \alpha^2\dot\alpha\xi u^\xi - \alpha\dot\alpha\xi B^2\left(\frac{1}{\alpha}u^\xi - \frac{b}{r}u^\eta\right) - \nu\frac{\alpha^2}{B}\left(B\left(\frac{1}{\alpha}u^\xi - \frac{b}{r}u^\eta\right)\right)_\xi.\end{aligned} \tag{4.18c}$$

(4.18) is a viscous extension of the conservation law (4.5). In order to clearly see the momentum conservation we may write the density Θ in terms of a cylindrical coordinate system to obtain

$$\Theta = \alpha^2\left(u^z + \dot\alpha\eta^*\right). \tag{4.19}$$

(α = const. corresponds to NSP1 in KCO)

NSP2. Extension of the conservation of generalized momentum. For the present viscous case, the family of conservation laws for the helical Euler system (4.7) reduces to one single conservation law, given by the density and fluxes

$$\Theta = \alpha^2 \frac{r}{B} u^\eta, \tag{4.20a}$$

$$\begin{aligned}\Phi^r &= \alpha^2 \left(\frac{r}{B} u^\eta u^r + \dot{\alpha}\xi b u^r + \frac{1}{2}\ddot{\alpha} b r \xi \right) \\ &\quad - \alpha^2 \nu \left[-2\frac{B}{\alpha} \left(\frac{1}{\alpha} u^\eta + \frac{b}{r} u^\xi \right) + \left(\frac{r}{B} u^\eta \right)_r \right] \\ &= \alpha^2 \left(\frac{r}{B} u^\eta u^r + \dot{\alpha}\xi b u^r + \frac{1}{2}\ddot{\alpha} b r \xi \right) \\ &\quad - \alpha^2 \nu \left[-\frac{2}{\alpha} u^\varphi + \left(\frac{r}{B} u^\eta \right)_r \right],\end{aligned} \tag{4.20b}$$

$$\begin{aligned}\Phi^\xi &= \alpha^2 \left(\frac{r}{B} u^\eta u^\xi + \alpha^2 \dot{\alpha}\xi b u^\xi \right) - \alpha\dot{\alpha} r \xi u^\eta \\ &\quad - \alpha^2 \nu \frac{1}{B} \left[\frac{2bB^2}{\alpha r} u^r + \left(\frac{r}{B} u^\eta \right)_\xi \right].\end{aligned} \tag{4.20c}$$

Presently, the analysis and interpretation below (4.7) also holds true, namely that (4.20a)-(4.20c) refers to a blend of momentum and angular momentum. (α = const. corresponds to NSP2 in KCO)

4.2.2 The vorticity formulation

In case of conservation laws in vorticity formulation we obtained five distinct cases all of which are one-to-one extensions of the five cases in KCO.

NSV1. Extension of an infinite family of vorticity conservation laws. The family of conservation laws (4.12) is extended by the viscous terms and the density and fluxes are given by

$$\Theta = \frac{q(t)}{r} B \left(\frac{1}{\alpha} \omega^\eta + \frac{b}{r} \omega^\xi \right) = \frac{q(t)}{r} \omega^\varphi, \tag{4.21a}$$

$$\begin{aligned}\Phi^r &= \frac{1}{r} \left(q(t) \left[u^r \omega^\varphi - \omega^r u^\varphi \right] + \dot{q}(t) B \left(\frac{1}{\alpha} u^\xi - \frac{b}{r} u^\eta \right) - \dot{\alpha} q(t) B \left(\frac{1}{\alpha^2} u^\xi - \frac{b}{r\alpha} u^\eta \right) \right) \\ &\quad - \frac{q(t)}{r} \nu \left[\frac{B}{r\alpha} \omega^\eta + \frac{b^2}{r\left(\frac{r^2}{\alpha^2} + b^2 \right)} \omega^\varphi + B \left(\frac{1}{\alpha} \omega_r^\eta + \frac{b}{r} \omega_r^\xi \right) \right],\end{aligned} \tag{4.21b}$$

$$\begin{aligned}\Phi^\xi &= -\frac{B}{r\alpha} \left(q(t) \left(u^\eta \omega^\xi - u^\xi \omega^\eta \right) + \dot{q}(t) u^r + q(t) \dot{\alpha} \xi \omega^\varphi - q(t) \frac{\dot{\alpha}}{\alpha} u^r \right) \\ &\quad - \frac{q(t)}{r^4} B \nu \left[\frac{r^3}{B} \left(\frac{1}{\alpha} \omega_\xi^\eta + \frac{b}{r} \omega_\xi^\xi \right) + 2br\omega^r \right].\end{aligned} \tag{4.21c}$$

where $q(t)$ is an arbitrary function of time. ($\alpha =$ const. corresponds to NSV1 in KCO)

NSV2. Extension of the vorticity conservation law. This conservation law is given by

$$\Theta = -\alpha^4 rB\left(\frac{1}{\alpha^3}\omega^\eta - \frac{b^3}{r^3}\omega^\xi\right), \tag{4.22a}$$

$$\begin{aligned}\Phi^r = {}& \alpha^4\left(-\frac{B}{r^2}\left(\frac{r^3}{\alpha^3}\left(u^r\omega^\eta - u^\eta\omega^r\right) - b^3\left(u^r\omega^\xi - u^\xi\omega^r\right)\right) - \frac{2B}{\alpha^2}u^r\left(-\frac{b}{r}u^\eta + \frac{1}{\alpha}u^\xi\right)\right)\\ &+ \frac{B}{r^2}\dot\alpha\left(-r^3u^\xi - 2\alpha^3b^3u^\eta - \alpha r^2bu^\eta + \frac{2}{B}\alpha^2r^2\xi u^r\right)\\ &- \alpha^4\frac{B}{r^2}\nu\left[\frac{r^2}{B^2}\left(\frac{1}{\alpha}\omega^\eta + \frac{b}{r}\omega^\xi\right) - r^3\left(\frac{1}{\alpha^3}\omega^\eta_r - \frac{b^3}{r^3}\omega^\xi_r\right) + \frac{b}{\alpha}B^2r\left(\frac{b^3}{r^3}\omega^\eta + \frac{1}{\alpha^3}\omega^\xi\right)\right],\end{aligned} \tag{4.22b}$$

$$\begin{aligned}\Phi^\xi = {}& \alpha^4\left(\frac{B}{\alpha^3}\left((u^r)^2 + (u^\eta)^2 - \left(u^\xi\right)^2 + r\left(u^\eta\omega^\xi - u^\xi\omega^\eta\right)\right) + \frac{2bB}{\alpha^2r}u^\eta u^\xi\right)\\ &- \frac{B^2}{r^2}\dot\alpha\left(b^3\alpha^3\xi\omega^\xi - 2b\alpha^2\xi u^\xi - r^3\xi\omega^\eta - 2r^2\xi u^\xi - \frac{r^3}{B}u^r\right)\\ &+ \alpha^4\frac{2bB}{\alpha^2r}\nu\left[\left(1 - \frac{b^2\alpha^2}{r^2}\right)\omega^r + \frac{r^2\alpha^2}{2bB}\left(\frac{1}{\alpha^3}\omega^\eta_\xi - \frac{b^3}{r^3}\omega^\xi_\xi\right)\right],\end{aligned} \tag{4.22c}$$

which is a viscous extension of the conservation law (4.13). ($\alpha =$ const. corresponds to NSV2 in KCO)

NSV3. Extension of the vorticity conservation law. This conservation law is given by

$$\begin{aligned}\Theta &= -\alpha^4\frac{B}{r^2}\left(\frac{r^2b^2}{B^2}\omega^\xi + \frac{r^4}{\alpha^3}\left(-\frac{b}{r}\omega^\eta + \frac{1}{\alpha}\omega^\xi\right)\right)\\ &= -\alpha^4\frac{B}{r^2}\left(\frac{r^2b^2}{B^2}\omega^\xi + \frac{r^4}{\alpha^3B}\omega^z\right),\end{aligned} \tag{4.23a}$$

$$\begin{aligned}\Phi^r = {}& \alpha^4\frac{rB}{\alpha^3}\Bigg(2u^r\left(\frac{1}{\alpha}u^\eta + \frac{b}{r}u^\xi\right) + b\left(u^r\omega^\eta - u^\eta\omega^r\right)\\ &- \frac{r^4 + r^2\alpha^2b^2 + b^4\alpha^4}{r^3\alpha}\left(u^r\omega^\xi - u^\xi\omega^r\right) + \dot\alpha\left(\frac{b}{\alpha}u^\xi + 2\alpha^2\frac{b^4}{r^3}u^\eta + \frac{b^2}{r}u^\eta\right)\Bigg)\\ &+ \alpha^4\nu\left[4\frac{B}{\alpha^3}\left(\frac{1}{\alpha}u^\eta + \frac{b}{r}u^\xi\right) - \frac{br}{\alpha^3}B\omega^\eta_r + \frac{B}{r^3}\left(b^4 - \frac{r^4}{\alpha^4} - \frac{r^6}{\alpha^4r^2 + \alpha^6b^2}\right)\omega^\xi\right.\\ &\left.+ \frac{B}{\alpha^4r^2}\left(r^4 + \alpha^2r^2b^2 + \alpha^4b^4\right)\omega^\xi_r + \frac{b}{\alpha B}\left(2 + \frac{r^4}{\left(r^2 + \alpha^2b^2\right)^2}\right)\omega^\eta\right],\end{aligned} \tag{4.23b}$$

$$\begin{aligned}\Phi^\xi = {}& \alpha^4\left(-\frac{1}{\alpha^3}bB\right)\Bigg(\left(u^r\right)^2 + \left(u^\eta\right)^2 - \left(u^\xi\right)^2 + r\left(u^\eta\omega^\xi - u^\xi\omega^\eta\right)\\ &- 2\frac{r}{\alpha b}u^\eta u^\xi + \dot\alpha\left(B\frac{r}{\alpha}\xi\omega^\eta + \frac{r}{\alpha}u^r - \frac{r^4 + r^2\alpha^2b^2 + b^4\alpha^4}{r^2\alpha^2b}B\xi\omega^\xi\right)\Bigg)\end{aligned}$$

$$+\alpha^4\nu\left[\frac{1}{\alpha^4 r^2}\left(r^4+\alpha^2r^2b^2+\alpha^4b^4\right)\omega^\xi_\xi-\frac{br}{\alpha^3}\omega^\eta_\xi-\frac{4bB}{\alpha^3 r}u^r+\frac{2B^4b}{r^3}\omega^r\right], \tag{4.23c}$$

which is a viscous extension of (4.15). (α = const. corresponds to NSV3 in KCO)

NSV4. Extension of an infinite family of vorticity conservation laws. The family of conservation laws (4.16), which holds for the helical invariant Euler equations, is carried over to the viscous case without change, as the viscosity does not appear explicitly. (α = const. corresponds to NSV4 in KCO)

NSV5. Extension of an infinite family of vorticity conservation laws. The infinite set of conservation laws (4.17) is extended by a viscous term. Its density and fluxes read

$$\Theta = M_r\omega^r+\frac{M_\xi}{B}\omega^\xi, \tag{4.24a}$$

$$\begin{aligned}\Phi^r=&\frac{M_\xi}{B}\left(u^r\omega^\xi-u^\xi\omega^r\right)-M_t\omega^r+\frac{\dot\alpha}{\alpha}\omega^r\left(M+\xi M_\xi\right)\\&+\nu\left[-\frac{M_{\xi\xi}}{B^2}\omega^r-\frac{M_r}{r}\left(r\omega^r\right)_r-\frac{2bBM_\xi}{\alpha r^2}\omega^\eta+\left(\frac{BM_\xi}{\alpha^2 r}+\frac{M_{r\xi}}{B}\right)\omega^\xi-\frac{M_\xi}{rB}\left(r\omega^\xi\right)_r\right],\end{aligned} \tag{4.24b}$$

$$\begin{aligned}\Phi^\xi=&M_r\left(u^\xi\omega^r-u^r\omega^\xi\right)-M_t\omega^\xi+\frac{\dot\alpha}{\alpha}\left(M\omega^\xi-B\xi M_r\omega^r\right)+\nu\left[\left(\frac{2B}{\alpha^2 r}-\frac{2}{rB}\right)M_\xi\omega^r\right.\\&\left.+\frac{M_{r\xi}}{B}\omega^r-\frac{M_r}{B}\omega^r_\xi+\frac{2bB^2M_r}{\alpha r^2}\omega^\eta-\left(\frac{2B^2M_r}{\alpha^2 r}+r\left(\frac{M_r}{r}\right)_r\right)\omega^\xi-\frac{M_\xi}{B^2}\omega^\xi_\xi\right],\end{aligned} \tag{4.24c}$$

while $M = M(\xi, r, t)$. As for (4.17) the previous conservation laws are a special case of the infinite family for viscous helical flows in Cheviakov and Oberlack (2014).

4.3 Proof of the absence of conservation of energy in time-dependent helical coordinates

It is well known that for the 3D time-dependent Euler system, the kinetic energy is conserved in coordinate systems which are not time-dependent. In the present section we will proof that in our spatially reduced time-dependent helically symmetric coordinate system the conservation of kinetic energy does not hold.

The proof can be done by contradiction: We rewrite the kinetic energy in conserved form in the helical time-dependent coordinates, i.e. (r, ξ, η^*) defined in (3.14a)-(3.14d). However, after imposing helical invariance, i.e. eliminating any η^*-dependence from the velocity and pressure, we would expect an energy equation, which is independent of η^*. However, we obtain an equation involving the helical coordinate η^* itself. As a result, it is not possible to write an energy conservation equation in a helically symmetric time-dependent coordinate system. The following steps may clarify the proceeding.

The energy equation can be written in a cylindrical coordinate system

$$\frac{\partial \Gamma^t}{\partial t} + \frac{\partial \Gamma^\varphi}{\partial \varphi} + \frac{\partial \Gamma^r}{\partial r} + \frac{\partial \Gamma^z}{\partial z} = 0, \tag{4.25}$$

where the fluxes read

$$\Gamma^t = r\tilde{K}, \tag{4.26a}$$
$$\Gamma^\varphi = u^\varphi \left(\tilde{K} + p\right), \tag{4.26b}$$
$$\Gamma^r = ru^r \left(\tilde{K} + p\right), \tag{4.26c}$$
$$\Gamma^z = ru^z \left(\tilde{K} + p\right). \tag{4.26d}$$

$\tilde{K}$ denotes the kinetic energy density, given by

$$\begin{aligned}\tilde{K} = \frac{1}{2}|\boldsymbol{u}|^2 &= \frac{1}{2}\left((u^r)^2 + (u^\varphi)^2 + (u^z)^2\right) \\ &= \frac{1}{2}\left[(u^r)^2 + B^2\left(\frac{b}{r}u^\xi + \frac{1}{\alpha}u^\eta\right)^2 + \left(B\left(\frac{1}{\alpha}u^\xi - \frac{b}{r}u^\eta\right) - \dot{\alpha}\eta^*\right)^2\right].\end{aligned} \tag{4.27a}$$

Replacing the cylindrical derivatives by the helical derivatives, the energy equation reads

$$\begin{aligned}&\frac{\partial}{\partial \tau}\left(r\tilde{K}\right) + \frac{\partial}{\partial r}\left(ru^r\left(\tilde{K} + p\right)\right) - \frac{\dot{\alpha}}{\alpha}\xi\frac{\partial}{\partial \xi}\left(r\tilde{K}\right) \\ &+ \frac{\partial}{\partial \xi}\left(\frac{\dot{\alpha}}{\alpha}\eta^*\left(r\tilde{K}\right) + \left(\frac{r}{\alpha}u^z + bu^\varphi\right)\left(\tilde{K} + p\right)\right) + \frac{\partial}{\partial \eta^*}\left(bu^\varphi\left(\tilde{K} + p\right)\right) = 0,\end{aligned} \tag{4.28}$$

Since the helical invariant coordinate η^* itself only occurs in the velocity component u^z and in the pressure p, these variables will be replaced by their corresponding helical expressions. Assuming helical invariance and simplifying the energy equation reads

$$\begin{aligned}R\left(\boldsymbol{\sigma}, \partial_j \boldsymbol{\sigma}\right) + &\left[\dot{\alpha}\left(r\frac{\dot{\alpha}}{\alpha}\xi\hat{u}_\xi - r\hat{u}_\tau - bu^\varphi_\xi\hat{u} + bu^\varphi\dot{\alpha} + bu^\varphi\hat{u}_\xi - \frac{r}{\alpha}\hat{u}_\xi\hat{u}\right.\right. \\ &+ \left(u^r + ru^r_r\right)\left(-\hat{u} - ru^r\hat{u}_r\right) - 2\hat{u}\hat{u}_\xi - \left(u^r u^r_\xi + u^\varphi u^\varphi_\xi\right) - \tilde{p}_\xi\Big) \\ &\left.+\ddot{\alpha}\left(-r\hat{u} + r\alpha bu^\varphi_\xi\xi + \left(u^r + ru^r_r\right)\alpha\xi + r\xi\hat{u}_\xi + \alpha\hat{u}\right)\right]\eta^* \\ &+ \left[\dot{\alpha}\left(r\ddot{\alpha} - \frac{\dot{\alpha}}{\alpha}r\hat{u}_\xi + \frac{1}{2}\left(u^r + ru^r_r\right)\dot{\alpha} + \frac{1}{2}u^\varphi_\xi\dot{\alpha} + \frac{1}{2}\frac{r}{\alpha}\dot{\alpha}\hat{u}_\xi + \dot{\alpha}\hat{u}_\xi - \ddot{\alpha}\alpha\right)\right. \\ &\left.+\ddot{\alpha}\left(-\frac{1}{2}r\alpha bu^\varphi_\xi - \frac{1}{2}\left(u^r + ru^r_r\right)\alpha - \frac{1}{2}r\right)\right](\eta^*)^2 = 0,\end{aligned} \tag{4.29}$$

where R is the collection of all η^*-independent terms and thus is a function of the helical dependent and independent variables $\boldsymbol{\sigma} \in \mathbb{R}^7$ defined in (A.4) and their first derivatives $\partial_j\boldsymbol{\sigma}$ $(j \in \{r, \xi, \tau\})$.

Here, the quantity $\hat{u}$ is the short form of the η^*-independent part of the u^z-velocity component, given by

$$\hat{u} := B\left(\frac{1}{\alpha}u^\xi - \frac{b}{r}u^\eta\right). \tag{4.30}$$

Apparently, (4.29) displays the above mentioned contradiction as velocity and pressure are assumed to be independent of η^*, while the equation still contains η^*. For $\alpha = \text{const.}$ all η^*-dependent terms vanish in equation (4.29) and, hence, the conservation of energy only holds true for the classical helically symmetric case.

4.4 Proof of the absence of conservation of helicity in time-dependent helical coordinates

In this section we prove that for the case of Euler's equations the conservation of helicity in helically symmetric flows in a spatially reduced time-dependent coordinate system does not hold. The proof is done in the same manner as for the conservation of kinetic energy. In cylindrical coordinates the density and fluxes of helicity conservation are given by

$$\Gamma^t = r\tilde{h}, \tag{4.31a}$$

$$\Gamma^\varphi = \omega^\varphi\left(E - (u^r)^2 - (u^z)^2\right) + u^\varphi\left(\tilde{h} - u^\varphi\omega^\varphi\right), \tag{4.31b}$$

$$\Gamma^r = r\omega^r\left(E - (u^\varphi)^2 - (u^z)^2\right) + ru^r\left(\tilde{h} - u^r\omega^r\right), \tag{4.31c}$$

$$\Gamma^z = r\omega^z\left(E - (u^r)^2 - (u^\varphi)^2\right) + ru^z\left(\tilde{h} - u^z\omega^z\right), \tag{4.31d}$$

where $\tilde{h} = \boldsymbol{u}\cdot\boldsymbol{\omega} = u^r\omega^r + u^\varphi\omega^\varphi + u^z\omega^z$ is helicity and

$$\begin{aligned} E &= \frac{1}{2}|\boldsymbol{u}|^2 + p = \frac{1}{2}\left((u^r)^2 + (u^\varphi)^2 + (u^z)^2\right) + p \\ &= \frac{1}{2}\left[(u^r)^2 + B^2\left(\frac{b}{r}u^\xi + \frac{1}{\alpha}u^\eta\right)^2 + \left(B\left(\frac{1}{\alpha}u^\xi - \frac{b}{r}u^\eta\right) - \dot{\alpha}\eta\right)^2\right] \\ &\quad + \tilde{p} - \frac{1}{2}\ddot{\alpha}\alpha\left(\xi - \eta^*\right)^2 \end{aligned} \tag{4.32}$$

is the total energy density (see e.g. KCO).

Rewriting the helicity conservation equation in the full 3D helical coordinate system (r, ξ, η^*) we obtain

$$\begin{aligned} &\frac{\partial}{\partial\tau}\left(r\tilde{h}\right) + \frac{\partial}{\partial r}\left(r\omega^r\left(\tilde{K} + p - \left(u^\xi\right)^2 - (u^\eta)^2 + 2B\left(\frac{1}{\alpha}u^\xi - \frac{b}{r}u^\eta\right)\dot{\alpha}\eta^* - \dot{\alpha}^2\left(\eta^*\right)^2\right)\right) \\ &\quad - \frac{\dot{\alpha}}{\alpha}\xi\frac{\partial}{\partial\xi}\left(r\tilde{h}\right) + \frac{\partial}{\partial\xi}\left(\frac{\dot{\alpha}}{\alpha}\eta^*\left(rh\right) + \left(\frac{r}{B}\omega^\xi\right)\left(\tilde{K} + p - (u^r)^2\right) + \left(\frac{r}{B}u^\xi - \frac{\dot{\alpha}}{\alpha}\eta^*\right)\tilde{h}\right. \end{aligned}$$

$$
\begin{aligned}
&- \frac{r}{B}\omega^{\xi}\left(\left(u^{\xi}\right)^{2} + (u^{\eta})^{2} - 2B\left(\frac{1}{\alpha}u^{\xi} - \frac{b}{r}u^{\eta}\right)\dot{\alpha}\eta^{*} + \dot{\alpha}^{2}\left(\eta^{*}\right)^{2}\right)\Bigg) \\
&+ \frac{\partial}{\partial\eta^{*}}\Bigg(b\omega^{\varphi}\left(\tilde{K} + p - (u^{r})^{2}\right) - b\omega^{\varphi}\left(\left(u^{\xi}\right)^{2} + (u^{\eta})^{2} - 2B\left(\frac{1}{\alpha}u^{\xi} - \frac{b}{r}u^{\eta}\right)\dot{\alpha}\eta^{*}\right. \\
&\left.+\dot{\alpha}^{2}\left(\eta^{*}\right)^{2}\right) + bu^{\varphi}\tilde{h}\Bigg) = 0. \qquad (4.33)
\end{aligned}
$$

In a second step imposing helical invariance onto equation (4.33), i.e. vorticity, velocity and pressure are $\eta^{*}-$independent, the helicity equation yields

$$
\begin{aligned}
\tilde{R}\left(\boldsymbol{\sigma}, \partial_{j}\boldsymbol{\sigma}\right) + &\left[\dot{\alpha}\left(\omega^{z}_{\xi}\frac{r}{\alpha}\hat{u} - r\omega^{z}_{\tau} + \frac{\dot{\alpha}}{\alpha}\xi r\omega^{z}_{\xi} + b\left(\omega^{\varphi}_{\xi}\hat{u} - \dot{\alpha}\omega^{\varphi}\hat{u}_{\xi} - u^{\varphi}_{\xi}\omega^{z} - u^{\varphi}\omega^{z}_{\xi}\right)\right.\right. \\
&\left.\left. + \left(r\omega^{r}\right)_{r}\hat{u} + r\hat{u}_{r}\omega^{r} - \left(ru^{r}\omega^{z}\right)_{r}\right) + \ddot{\alpha}\left(\omega^{z}_{\xi}r\xi + b\alpha\omega^{\varphi}_{\xi} + \left(r\omega^{r}\right)_{r}2\alpha\xi\right)\right]\eta^{*} \\
&+ \left[\dot{\alpha}\frac{1}{2}\left(-r\omega^{z}_{\xi}\frac{\dot{\alpha}}{\alpha} + b\omega^{\varphi}_{\xi}\dot{\alpha} - \left(r\omega^{r}\right)_{r}\dot{\alpha}\right) + \ddot{\alpha}\left(\frac{1}{2}r\omega^{z}_{\xi} - b\omega^{\varphi}_{\xi}\alpha - \left(r\omega^{r}\right)_{r}\alpha\right)\right]\left(\eta^{*}\right)^{2} \\
&= 0, \qquad (4.34)
\end{aligned}
$$

where $\tilde{R}$ is a collection of all η^{*}-independent terms and thus is a function of the reduced helical independent and dependent variables $\tilde{\boldsymbol{\sigma}} \in \mathbb{R}^{10}$, which consist of the two helical coordinates (r, ξ), the time (t), the three velocity components, pressure and the three vorticity components and their first derivatives $\partial_{j}\tilde{\boldsymbol{\sigma}}$, for $j \in \{r, \xi, \tau\}$. As for the energy equation the contradiction becomes apparent, as in (4.34) $\eta^{*}-$independence of all dependent variables was employed, still the equation contains η^{*} explicitly.

Likewise for the kinetic energy, for $\alpha = \text{const.}$ all η^{*}-dependent terms vanish in (4.34) and the conservation of helicity holds for the classical helically symmetric case.

5 Exact solutions of helically invariant Navier-Stokes equations

In this chapter we derive exact solutions to the classical system of helically invariant Navier-Stokes equations (3.19), which are the governing equations for helical flows at a constant pitch. The solutions can be assigned to two different classes. The solutions of the first class are based on an invariant solution ansatz emerging from the Galilean group in helical coordinates, which leads to linear functions in the helical coordinate $\xi = az + b\varphi$ for the two helical velocity components u^ξ and u^η. Starting from this approach, we derive a new equation for the radial velocity component u^r in the helical frame, for which we found two special solutions. The second class is based on an exact linearization of the Navier-Stokes equations by seeking exact solutions in form of Beltrami flows. Using separation of variables, we derive exponentially decaying time-dependent solutions, which consist of trigonometric functions in the helical coordinate ξ and of Confluent Heun-type functions in radial direction. First of all we present a short summary of well known exact solutions of the Navier-Stokes equations.

The present chapter is heavily based on the following publication of mine: Dierkes et al. (2020).

While no general solution is available for the full time-dependent nonlinear PDE system of Navier-Stokes equations, multiple families of exact and approximate solutions describing specific situations have been derived. Well-known examples of solutions of incompressible Navier-Stokes equations in primitive variables include the Couette flow and the Hagen-Poiseuille flow in a cylindrical pipe. Among the most famous solutions for the Navier-Stokes equations in vorticity formulation are axisymmetric vortex-type solutions, such as the Oseen-Lamb vortex and the Taylor vortex, which describe columnar vortices without axial stretching. An example of exact solutions of axisymmetric flows containing axial vortex stretching is the famous Burgers vortex, which is the first stretched vortex solution that models turbulent eddies (Wu et al., 2007).
A significant number of exact solutions of Navier-Stokes equations and related models, as well as of other nonlinear PDEs, have been derived in recent years with the help of techniques based on Lie groups, including local and nonlocal symmetries of PDEs, symmetry-invariant and partially invariant solutions, and their generalizations (see e.g. Ibragimov, 1995; Andreev et al., 1998; Meleshko and Pukhnachev, 1999; Bogoyavlenskij, 2003b; Pukhnachev, 2006; Bluman et al., 2010 and references therein). For example, in Ibragimov (1995), several classes of invariant solutions of the Navier-Stokes equations are presented. In many cases these solutions can be reduced to previously known solutions by choosing appropriate parameters. In Andreev et al. (1998), invariants of the Navier-Stokes equations in cylindrical coordinates were used to derive a system

of ordinary differential equations, for which exact solutions were obtained. In the following section we employ a similar approach to construct exact helically invariant solutions of Navier-Stokes equations.

5.1 A reduction with respect to Galilei group in helical coordinates

As it is shown in section 3.2.4 the helically invariant Navier-Stokes equations (3.19) admit four independent point symmetry groups: translations in space ξ and time t, translation of the pressure p and Galilean invariance in $\xi-$direction. If the transformed quantities for each group G^i, $i = 1,..4$ are denoted by $\left(r^*, \xi^*, t^*, (u^r)^*, (u^\xi)^*, (u^\eta)^*, p^*\right) = G^i\left(r, \xi, t, u^r, u^\xi, u^\eta, p\right)$ one has

$$G^1 = \left(r, \xi + \varepsilon, t, u^r, u^\xi, u^\eta, p\right), \tag{5.1a}$$

$$G^2 = \left(r, \xi, t + \varepsilon, u^r, u^\xi, u^\eta, p\right), \tag{5.1b}$$

$$G^3 = \left(r, \xi, t, u^r, u^\xi, u^\eta, p + \varepsilon f(t)\right), \tag{5.1c}$$

$$G^4 = \left(r, \xi + \varepsilon t, t, u^r, u^\xi + \varepsilon B(r), u^\eta - \varepsilon \frac{b}{ar} B(r), p\right). \tag{5.1d}$$

We note that no additional symmetries arise for two-component flows, where the velocity component in invariant direction vanishes, $u^\eta \equiv 0$.

The infinitesimal generators correspond to the symmetry groups (5.1) are given by

$$X_1 = \frac{\partial}{\partial t}, \tag{5.2a}$$

$$X_2 = \frac{\partial}{\partial \xi}, \tag{5.2b}$$

$$X_3 = f(t)\frac{\partial}{\partial p}, \tag{5.2c}$$

$$X_4 = t\frac{\partial}{\partial \xi} - \frac{b}{ar} B \frac{\partial}{\partial u^\eta} + B\frac{\partial}{\partial u^\xi}. \tag{5.2d}$$

For the Galilei symmetry G^4, X_4 we consider an invariant solution ansatz (see, e.g., Bluman et al., 2010). A solution $\boldsymbol{u} = \boldsymbol{\Theta}(r, t, \xi)$ with components $\boldsymbol{u} = \left(u^r, u^\xi, u^\eta, p\right)$ and $\boldsymbol{\Theta} = \left(\Theta^r, \Theta^\xi, \Theta^\eta, \Theta^p\right)$ is an invariant solution of the PDE system (3.19) with respect to the point symmetry (5.2d) if and only if $\boldsymbol{u} = \boldsymbol{\Theta}(r, t, \xi)$ satisfies

$$X_4\left(\boldsymbol{u} - \boldsymbol{\Theta}(r, \xi, t)\right)\big|_{\boldsymbol{u}=\boldsymbol{\Theta}(r,\xi,t)} = 0. \tag{5.3}$$

This leads to the characteristic ODE system given by

$$\frac{du^r}{0} = -\frac{ar}{bB} du^\eta = \frac{du^\xi}{B} = \frac{d\xi}{t} = \frac{dr}{0} = \frac{dt}{0} = \frac{dp}{0}. \tag{5.4}$$

The invariants for the independent variables are given by

$$I_1 = r, \quad I_2 = t, \tag{5.5}$$

and for the dependent variables, (5.4) leads to a form, which is slightly generalized to

$$u^r = u^r(r,t), \tag{5.6a}$$
$$u^\xi = F^\xi(r,t)\xi + G^\xi(r,t), \tag{5.6b}$$
$$u^\eta = F^\eta(r,t)\xi + G^\eta(r,t), \tag{5.6c}$$
$$p = p(r,t). \tag{5.6d}$$

where $u^r(r,t)$, $F^\xi(r,t)$, $G^\xi(r,t)$, $F^\eta(r,t)$, $G^\eta(r,t)$, and $p(r,t)$ are to be determined. The substitution of (5.6) into the Navier-Stokes equations (3.19) leads to quadratic expressions in ξ, where all unknown other functions do not depend on ξ. Hence all coefficients at independent expressions involving ξ must vanish. Consequently, as it is shown in Appendix B, which contains further details on the derivation of some subsequent equations, one obtains the restrictions

$$F^\eta = -\frac{b}{ar}F^\xi \tag{5.7}$$

and

$$F^\xi = -\frac{B}{r}\left(ru^r\right)_r, \tag{5.8}$$

relating the unknown functions F^η, F^ξ, and u^r. This leads to rewriting the helically invariant Navier-Stokes equations (3.19) as a system of four ξ-independent PDEs for the unknowns u^r, G^ξ, G^η, p, given by

$$u^r_t + u^r u^r_r - \frac{B^2}{r}\left(\frac{b}{r}G^\eta + aG^\xi\right)^2 + p_r - \nu\left[u^r_{rr} + \frac{1}{r}u^r_r - \frac{1}{r^2}u^r\right] = 0, \tag{5.9a}$$

$$ru^r_{rt} + u^r_t - u^r u^r_r - r\left(u^r_r\right)^2 + ru^r u^r_{rr} - \frac{2}{r}\left(u^r\right)^2 + \nu\left[-ru^r_{rrr} - 2u^r_{rr} - \frac{u^r}{r^2} + \frac{1}{r}u^r_r\right] = 0, \tag{5.9b}$$

$$G^\eta_t + u^r G^\eta_r + \frac{1}{B}G^\xi F^\eta + \frac{a^2B^2}{r}u^r G^\eta - \nu B\left[\frac{B''}{B^2}G^\eta + \frac{2B'}{B^2}G^\eta_r - \frac{2abB}{r^2}G^\xi_r\right.$$
$$\left. - \left(\frac{2ab}{r^2}G^\xi + \frac{b^2 - a^2r^2}{r^3}G^\eta\right)B' - \frac{B}{r^3}\left(b^2 - a^2r^2\right)G^\eta_r + \frac{1}{B}G^\eta_{rr} + \frac{\left(b^2 - a^2r^2\right)B}{r^4}G^\eta\right] = 0, \tag{5.9c}$$

$$G^\xi_t + u^r G^\xi_r + \frac{1}{B}G^\xi F^\xi + \frac{2abB^2}{r^2}u^r G^\eta + \frac{b^2B^2}{r^3}u^r G^\xi - \nu B\left[\frac{B''}{B^2}G^\xi + \frac{2B'}{B^2}G^\xi_r + \frac{2abB}{r^2}G^\eta_r\right.$$

$$+\left(\frac{2ab}{r^2}G^\eta-\frac{b^2-a^2r^2}{r^3}G^\xi\right)B'-\frac{B}{r^3}\left(b^2-a^2r^2\right)G^\xi_r+\frac{1}{B}G^\xi_{rr}-\frac{2abB}{r^3}G^\eta\Big]=0. \quad (5.9d)$$

Importantly, the PDE (5.9b) for u^r decouples from the rest of system of equations (5.9).

Substituting the ansatz expressions (5.6b) and (5.6c) into (3.17), one finds that for the Galilei-invariant helical flows, the cylindrical polar angle velocity component u^φ reduces to

$$u^\varphi=B\left(aG^\eta+\frac{b}{r}G^\xi\right), \quad (5.10)$$

and is independent of F^ξ and F^η. A linear combination of (5.9c) and (5.9d), where (5.9c) is multiplied by aB, and (5.9d) by bB/r, leads to a PDE for the u^φ-component, which is given by

$$u^\varphi_t+\frac{u^ru^\varphi}{r}+u^ru^\varphi_r-\nu\left(u^\varphi_{rr}+\frac{u^\varphi_r}{r}-\frac{u^\varphi}{r^2}\right)=0. \quad (5.11)$$

Every solution of (5.9) yields a solution of the helically invariant Navier-Stokes equations (3.19) through equations (5.6). Solutions of the reduced system (5.9), in fact, are related to the solutions of a single PDE (5.9b). Indeed, for every solution u^r of (5.9b), one may find F^ξ and F^η from (5.8) and (5.7), respectively. In the next step, the solutions for F^ξ and F^η may be used to solve (5.9c) and (5.9d) for G^ξ and G^η. Interestingly that PDEs (5.9c) and (5.9d) are linear PDEs for G^ξ and G^η with variable coefficients. Finally, one can obtain the pressure p from the PDE (5.9a).

The main equation (5.9b) can be brought into a particularly elegant form using the substitution

$$v(r,t)=r\,u^r(r,t), \quad (5.12)$$

leading to the PDE

$$v_{rt}+\left(\frac{vv_r}{r}\right)_r-2\frac{v_r^2}{r}-\nu\left[v_{rrr}+\frac{v_r}{r^2}-\frac{v_{rr}}{r}\right]=0. \quad (5.13)$$

satisfied by $v(r,t)$. In particular, the following statement holds: *every solution of the PDE* (5.13) *yields a solution of the helically invariant time-dependent Navier-Stokes equations* (3.19).

The *v-equation* (5.13) is a third-order nonlinear PDE which does not belong to any well-studied class of nonlinear PDEs, and for which consequently no exact solutions are known. The PDE (5.13) has a scaling symmetry and a translational symmetry in time, given by the infinitesimal generators

$$Y_1=r\frac{\partial}{\partial r}+2t\frac{\partial}{\partial t}, \quad (5.14a)$$

$$Y_2=\frac{\partial}{\partial t}. \quad (5.14b)$$

From (5.14) we generate the similarity variable

$$s = \frac{r}{\sqrt{4\nu\,(t+t_0)}}, \tag{5.15}$$

to seek invariant solutions of the PDE (5.13) in the form $v = v(s)$, which yields the ODE

$$s^3 v'' + 2s\left(v'\right)^2 + s^2 v' - 2svv'' + 2vv' + \nu\left[2s^2 v''' - 2sv'' + 2v'\right] = 0, \tag{5.16}$$

with prime denoting the derivative with respect to s. Two particular solution families of the ODE (5.16) can be readily constructed. The first solution family is obtained by demanding that both the linear and the nonlinear terms in (5.13) vanish separately, which leads to a consistent solution

$$v(r,t) = Ae^{-\frac{r^2}{4\nu(t+t_0)}}, \tag{5.17}$$

of the PDE (5.13), involving free constant parameters A and t_0. The second particular solution family is given by

$$v(r,t) = g(t) - \frac{r^2}{2\,(t+t_0)}, \tag{5.18}$$

where $g(t)$ is an arbitrary time-dependent function.

The next step in obtaining an explicit solution of the helically invariant flow is the solution of the (quite complex) linear PDEs (5.9c), (5.9d) for the unknown functions G^ξ, G^η. A simple but explicit solution of the helically invariant Navier-Stokes system (3.19) can be immediately obtained if one assumes $G^\xi = G^\eta = 0$, which corresponds to a helically symmetric flow where the polar velocity component u^φ vanishes (cf. (5.10)), but all three helical velocity components u^r, u^η, u^ξ remain nonzero. In this case, the solution (5.17) can be used to obtain the radial velocity component u^r using (5.12), the pressure using (5.9a), and the remaining velocity components (5.6b), (5.6c) using (5.7) and (5.8). The full solution is given by

$$u^r = \frac{A}{r}\,e^{-\frac{r^2}{4\nu(t+t_0)}}, \qquad u^\eta = -\frac{AbB\xi}{2\nu ar\,(t+t_0)}\,e^{-\frac{r^2}{4\nu(t+t_0)}}, \tag{5.19a}$$

$$u^\xi = \frac{AB\xi}{2\nu\,(t+t_0)}\,e^{-\frac{r^2}{4\nu(t+t_0)}}, \qquad p = -\frac{A^2}{2r^2}\,e^{-\frac{r^2}{2\nu(t+t_0)}} + f(t), \tag{5.19b}$$

where $f(t)$ is an arbitrary function of time. In a similar manner, for the solution (5.18) of (5.13), one obtains the explicit exact solution

$$u^r = \frac{g(t)}{r} - \frac{r}{2\,(t+t_0)}, \qquad u^\eta = -\frac{bB\xi}{ar\,(t+t_0)}, \tag{5.20a}$$

$$u^\xi = \frac{B\xi}{t+t_0}, \qquad p = -\frac{3}{8}\frac{r^2}{(t+t_0)^2} - \frac{g(t)^2}{2r^2} - g'(t)\,\ln r + h(t), \tag{5.20b}$$

involving an additional pressure gauge given by an arbitrary function $h(t)$. Unlike the first solution family (5.19), the second solution family (5.20) does not involve an arbitrary scaling parameter A.

We note again that both solutions (5.19), (5.20) of the helically invariant Navier-Stokes equations (3.19) are neither periodic in ξ, nor regular on the z-axis. These solutions should be understood as essentially local, i.e. defined in some helical annular sector, or in other words, a rectangle

$$0 < r_1 \le r \le r_2, \quad 0 \le \xi_1 \le \xi \le \xi_2 < 2\pi b$$

in the helical coordinates (r, ξ). Using the non-dimensionalization

$$\begin{array}{llll} \hat{r} = r/b, & \hat{z} = z/b, & \hat{\xi} = \xi/b = a\hat{z} + \phi, & \hat{t} = \nu t/b^2, \\ \hat{u}^r = u^r/u_0, & \hat{u}^\eta = u^\eta/u_0, & \hat{u}^\xi = u^\xi/u_0, & \hat{p} = p/u_0^2, \\ \hat{A} = A/(bu_0), & u_0 = \nu/b, & \hat{B} = \hat{r}/\sqrt{a^2\hat{r}^2+1} & \end{array}$$

and the corresponding modifications of the arbitrary functions, the solutions (5.19) and (5.20) can be written respectively as

$$\hat{u}^r = \frac{\hat{A}}{\hat{r}}\, e^{-\frac{\hat{r}^2}{4(\hat{t}+\hat{t}_0)}}, \qquad \hat{u}^\eta = -\frac{\hat{A}\hat{B}\hat{\xi}}{2a\hat{r}\,(\hat{t}+\hat{t}_0)}\, e^{-\frac{\hat{r}^2}{4(\hat{t}+\hat{t}_0)}}, \tag{5.21a}$$

$$\hat{u}^\xi = \frac{\hat{A}\hat{B}\hat{\xi}}{2\,(\hat{t}+\hat{t}_0)}\, e^{-\frac{\hat{r}^2}{4(\hat{t}+\hat{t}_0)}}, \qquad \hat{p} = -\frac{\hat{A}^2}{2\hat{r}^2}\, e^{-\frac{\hat{r}^2}{2(\hat{t}+\hat{t}_0)}} + \hat{f}(\hat{t}), \tag{5.21b}$$

and

$$\hat{u}^r = \frac{\hat{g}(\hat{t})}{r} - \frac{\hat{r}}{2\,(\hat{t}+\hat{t}_0)}, \qquad \hat{u}^\eta = -\frac{\hat{B}}{a\hat{r}\hat{\xi}\,(\hat{t}+\hat{t}_0)}, \tag{5.22a}$$

$$\hat{u}^\xi = \frac{\hat{B}\hat{\xi}}{\hat{t}+\hat{t}_0}, \qquad \hat{p} = -\frac{3}{8}\frac{\hat{r}^2}{(\hat{t}+\hat{t}_0)^2} - \frac{\hat{g}(\hat{t})^2}{2\hat{r}^2} - \hat{g}'(\hat{t})\,\ln\hat{r} + \hat{h}(\hat{t}). \tag{5.22b}$$

For a flow with the velocity field $\boldsymbol{u}(t, \boldsymbol{x})$, the *instantaneous streamlines* are defined as parametric curves

$$\frac{d}{d\gamma}\boldsymbol{x}(\gamma) = \boldsymbol{u}(t, \boldsymbol{x}(\gamma)), \quad \boldsymbol{x}(0) = \boldsymbol{x}_0, \tag{5.23}$$

where γ is a nonnegative scalar parameter. For a generic time-dependent flow, instantaneous streamlines (5.23) change with time, and no fluid parcel has to follow any instantaneous streamline. On the other hand for equilibrium flows that are independent of time, as well as for special time-dependent flows, streamline curves can be fixed, and thus followed by physical fluid parcels.

For both of the above solutions, streamlines are curves in the plane $\phi = \text{const.}$. For the first solution family (5.21), the streamlines are not fixed but change in time, since the time-dependence of the velocity components is different. In particular, as $t \to \infty$, the

streamlines tend to radial curves. For the second solution family (5.22), the streamlines are fixed if and only if $g(t) = 0$.

The dimensionless vorticity is defined as $\hat{\boldsymbol{\omega}} = b\boldsymbol{\omega}/u_0$, with components of $\boldsymbol{\omega}$ given by (3.27), and the dimensionless helicity density of the flow is computed as $\hat{h}_H = \hat{\boldsymbol{u}} \cdot \hat{\boldsymbol{\omega}}$.

For the first solution family (5.21), the velocity and vorticity magnitudes and the helicity density are given by

$$|\hat{\boldsymbol{u}}|^2 = \frac{\hat{A}^2 e^{-\frac{\hat{r}^2}{2(\hat{t}+\hat{t}_0)}}}{4a^2\hat{r}^2(\hat{t}+\hat{t}_0)^2}\left(4a^2(\hat{t}+\hat{t}_0)^2 + \hat{r}^2\hat{\xi}^2\right), \tag{5.24a}$$

$$|\hat{\boldsymbol{\omega}}|^2 = \frac{\hat{A}^2 e^{-\frac{\hat{r}^2}{2(\hat{t}+\hat{t}_0)}}}{16a^2\hat{r}^2(\hat{t}+\hat{t}_0)^4}\left(4(\hat{t}+\hat{t}_0)^2 + \hat{r}^4\hat{\xi}^2\right), \tag{5.24b}$$

$$\hat{h}_H = \frac{\hat{A}^2 e^{-\frac{\hat{r}^2}{2(\hat{t}+\hat{t}_0)}}}{2a\hat{r}^2(\hat{t}+\hat{t}_0)}. \tag{5.24c}$$

Figure 5.1 shows streamlines, pressure profiles, the helical surface patch $\eta = \text{const.}$, and examples of velocity and vorticity magnitude level surfaces $|\hat{\boldsymbol{u}}| = \text{const.}$, $|\hat{\boldsymbol{\omega}}| = \text{const.}$ for the first solution family (5.21), for a sample set of dimensionless parameters.

For the second solution family (5.22), the velocity and vorticity magnitudes and the flow helicity density are given by

$$|\hat{\boldsymbol{u}}|^2 = \frac{a^2(2\hat{g}(\hat{t})(\hat{t}+\hat{t}_0) - \hat{r}^2)^2 + 4\hat{r}^2\hat{\xi}^2}{4a^2\hat{r}^2(\hat{t}+\hat{t}_0)^2}, \tag{5.25a}$$

$$|\hat{\boldsymbol{\omega}}| = \frac{1}{a\hat{r}(\hat{t}+\hat{t}_0)}, \tag{5.25b}$$

$$\hat{h} = \frac{\hat{g}}{a\hat{r}^2(\hat{t}+\hat{t}_0)} - \frac{1}{2a(\hat{t}+\hat{t}_0)^2}. \tag{5.25c}$$

In particular, in (5.25), for a fixed time t, the vorticity magnitude $|\hat{\boldsymbol{\omega}}|$ and the helicity density $\hat{h}$ are constant on circular cylinders $r = \text{const.}$. We do not provide plots for this rather simple solution family because they are somewhat less physically appealing, and can be obtained in a straightforward way.

5.2 The exact linearization of the Navier-Stokes equations; Beltrami-type solutions

The vector momentum equation in the Navier-Stokes model (3.1) is often written in the form

$$\boldsymbol{u}_t + (\nabla \times \boldsymbol{u}) \times \boldsymbol{u} + \nabla P - \nu \nabla^2 \boldsymbol{u} = 0, \tag{5.26}$$

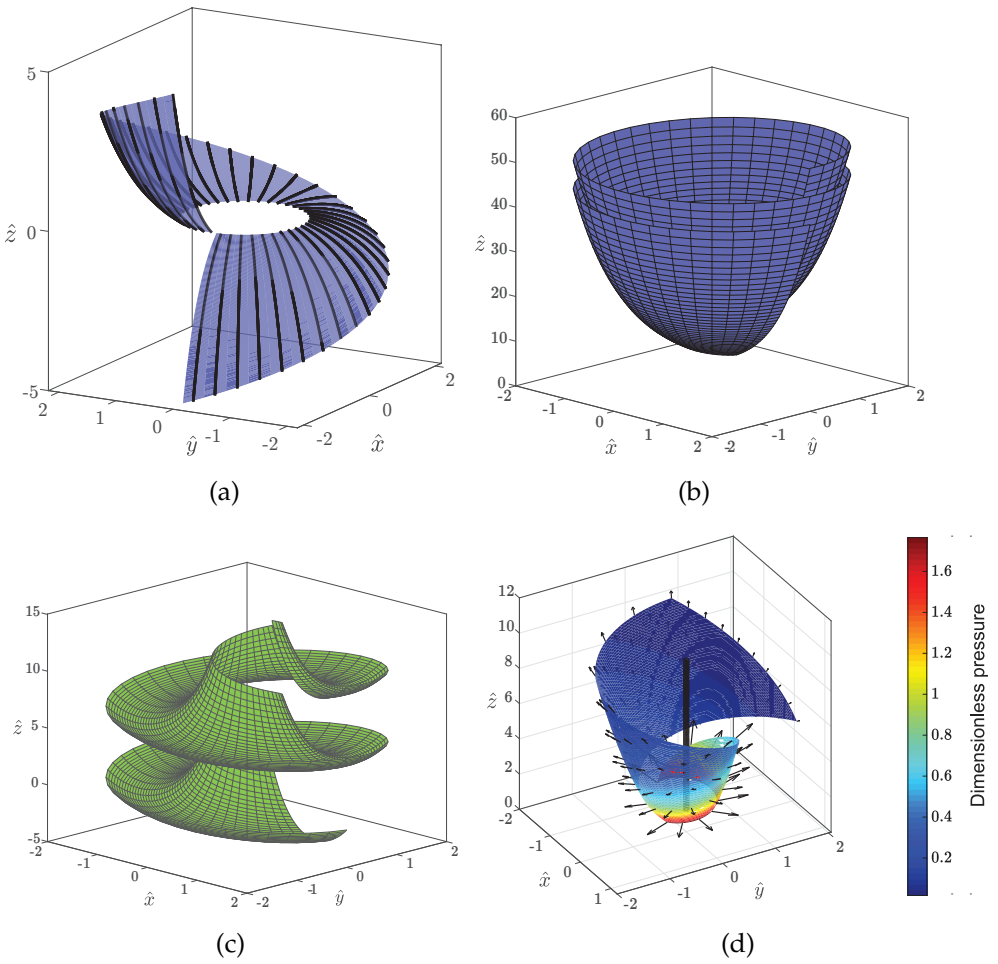

Figure 5.1: Dimensionless flow parameters and the helical surface for the exact helically invariant solution (5.21) with $\hat{t} = 1$, $\hat{t}_0 = 0$, $\hat{A} = \hat{f} = 1$. (a) The streamlines emanating from the circle $\hat{z} = 0, \hat{r} = 1$. (b) The velocity magnitude isosurface $|\hat{\boldsymbol{u}}| = 10$, plotted for $0 \leq \phi \leq 4\pi$, $\xi \geq 0$. (c) The vorticity magnitude isosurface $|\hat{\boldsymbol{\omega}}| = 2$, plotted for $0 \leq \phi \leq 4\pi$, $\xi \geq 0$. (d) the helical coordinate rectangle $\hat{\eta} = -6$, $0.5 \leq \hat{r} \leq 2$, $0 \leq \hat{\xi} \leq 2\pi$ in the physical space, with velocity vectors and pressure $\hat{p}$ color map.

where the modified pressure is given by

$$P = p + \frac{1}{2}|\boldsymbol{u}|^2. \tag{5.27}$$

The essential nonlinearity is contained in the advection term $(\nabla \times \boldsymbol{u}) \times \boldsymbol{u}$. The linearization idea of Beltrami consisted in setting it to zero, i.e. seeking exact solutions of the Navier-Stokes system that satisfy the *Beltrami flow* ansatz of vorticity and velocity collinearity,

$$\boldsymbol{\omega} \equiv \nabla \times \boldsymbol{u} = \vartheta \boldsymbol{u}, \tag{5.28}$$

where $\vartheta = \vartheta(\boldsymbol{x}, t)$ is an arbitrary scalar function. The seven scalar equations made up of the constant-density Navier-Stokes model (3.1) and the PDEs (5.28) make up an overdetermined linear system in terms of five unknown scalar functions given by $\boldsymbol{u}$, P, and ϑ. Even though overdetermined, these equations are known to have physically meaningful solutions (e.g., Bogoyavlenskij, 2003a,b). It should be noted that due to the constraint (5.28), vortex stretching is inhibited, which is always the case for two-dimensional flows. Nevertheless, our newly found Beltrami-type exact solutions contain three non-zero velocity components and hence essentially differ from two-dimensional flows.

In the helically invariant setting, the subsequently presented linear equations (5.30) describing Beltrami flows follow from (3.19). They are given by seven PDEs for the unknowns $u^r(t,r,\xi)$, $u^\xi(t,r,\xi)$, $u^\eta(t,r,\xi)$, $P(t,r,\xi)$, $\vartheta(t,r,\xi)$. The continuity equation reads

$$\frac{1}{r}u^r + (u^r)_r + \frac{1}{B}(u^\xi)_\xi = 0, \tag{5.29}$$

while the momentum equations reduce to the linear PDEs

$$\begin{aligned}
(u^r)_t = &-P_r + \nu\left[\frac{1}{r}(r(u^r)_r)_r + \frac{1}{B^2}(u^r)_{\xi\xi} - \frac{1}{r^2}u^r\right.\\
&\left.-\frac{2bB}{r^2}\left(a(u^\eta)_\xi + \frac{b}{r}(u^\xi)_\xi\right)\right], &(5.30a)\\
(u^\eta)_t = &\nu\left[\frac{1}{r}(r(u^\eta)_r)_r + \frac{1}{B^2}(u^\eta)_{\xi\xi} + \frac{a^2B^2(a^2B^2-2)}{r^2}u^\eta\right.\\
&\left.+\frac{2abB}{r^2}\left((u^r)_\xi - \left(Bu^\xi\right)_r\right)\right], &(5.30b)\\
(u^\xi)_t = &-\frac{1}{B}P_\xi + \nu\left[\frac{1}{r}(r(u^\xi)_r)_r + \frac{1}{B^2}(u^\xi)_{\xi\xi} + \frac{a^4B^4-1}{r^2}u^\xi\right.\\
&\left.+\frac{2bB}{r}\left(\frac{b}{r^2}(u^r)_\xi + \left(\frac{aB}{r}u^\eta\right)_r\right)\right], &(5.30c)
\end{aligned}$$

and the three Beltrami conditions (5.28) together with the definition of the vorticity vector in helical coordinates in (3.27) are given by

$$\omega^r = -\frac{1}{B}(u^\eta)_\xi = \vartheta u^r, \tag{5.31a}$$

$$\omega^\eta = \frac{1}{B}(u^r)_\xi - \frac{1}{r}\left(ru^\xi\right)_r - \frac{2abB^2}{r^2}u^\eta + \frac{a^2B^2}{r}u^\xi = \vartheta u^\eta, \tag{5.31b}$$

$$\omega^\xi = (u^\eta)_r + \frac{a^2B^2}{r}u^\eta = \vartheta u^\xi. \tag{5.31c}$$

The linear homogeneous model (5.30), (5.31) is autonomous in t and ξ, and thus admits a separation of variables ansatz for all dependent variables:

$$f(t, r, \xi) = T(t)\, R(r)\, \Xi(\xi), \tag{5.32}$$

where f stands for each dependent variable: u^r, u^ξ, u^η, P. Moreover, any linear combination of separated solutions (5.32) yields an exact solution of the linear homogeneous PDE system (5.30), (5.31), and thus of the helically symmetric Navier-Stokes equations (3.19) subject to the Beltrami condition (5.28).

From the form of the momentum equations (5.30), it follows that an admissible form of the time dependence for the velocity components (and hence for the other unknowns, as it follows from the remaining PDEs) is given by exponential functions. In particular, for all velocity components, the time dependence is the same. Moreover, from the point of view of ξ-periodicity and the nature of differential relations, where spatial derivatives of the unknowns and the unknowns themselves are present in the equations, it is natural to assume the harmonic dependence of the unknowns on ξ: $h(\xi) \sim \exp(i\lambda\xi)$, $\lambda = \text{const.} \in \mathbb{R}$. For the linear homogeneous model, both the real and the imaginary part of each solution component yield solutions of the Beltrami model. (For simplicity, we will explicitly consider real functions.) From the form of Beltrami equations (5.28), it follows that the only admissible dependence of the Beltrami parameter ϑ is on the radial variable r. With the above assumptions, the general real form of the separated solutions is given by

$$u^r = e^{-\nu Q^2 t}(K_1 \cos\lambda\xi + K_2 \sin\lambda\xi) R_1(r), \tag{5.33a}$$

$$u^\xi = e^{-\nu Q^2 t}(K_3 \cos\lambda\xi + K_4 \sin\lambda\xi) R_2(r), \tag{5.33b}$$

$$u^\eta = e^{-\nu Q^2 t}(K_5 \cos\lambda\xi + K_6 \sin\lambda\xi) R_3(r), \tag{5.33c}$$

$$\vartheta = R_a(r), \tag{5.33d}$$

$$P = e^{-\nu Q^2 t}(K_7 \cos\lambda\xi + K_8 \sin\lambda\xi) R_p(r) \tag{5.33e}$$

The chosen form of the negative time exponent $-\nu Q^2 < 0$, $Q = \text{const.} \in \mathbb{R}$, is natural for the given parabolic problem (5.29),(5.30). The exponentially decaying time-dependent term $e^{-\nu Q^2 t}$ makes the solutions (5.33) similar to the two-dimensional 2D Taylor's decaying vortices (e.g., Taylor (1923)).

Due to the periodicity of the helical variable ξ with its period given in equation (3.20), it follows that one must have

$$\lambda = \lambda_n = n/b, \quad n = 0, 1, 2, \ldots, \tag{5.34}$$

i.e., only discrete *modes* in ξ-direction satisfy the periodicity conditions.

The relationships between the parameters K_i, $i = 1, \ldots, 8$ and the radial functions R_i, $i = 1, 2, 3$ and R_p in (5.33) are derived in Appendix B.2. In particular, it is shown that

$$\vartheta(r) = \text{const.} = Q, \quad R_p(r) = 0.$$

It follows that the modified pressure P is zero, which in turn leads to the final expression for the pressure

$$p = p_0 - \frac{1}{2}|\boldsymbol{u}|^2, \quad p_0 = \text{const.}, \tag{5.35}$$

and thus the level surfaces of pressure and the velocity magnitude coincide. It is further shown that the nonzero constants K_i in (5.33) are related by

$$\frac{K_2}{K_5} = -\frac{K_1}{K_6}, \quad \frac{K_3}{K_5} = \frac{K_4}{K_6}, \quad \frac{K_7}{K_8} = -\frac{K_4}{K_3}, \tag{5.36}$$

and $R_1(r)$ is a solution of a second-order ODE

$$\frac{\mathrm{d}^2 R_1}{\mathrm{d}r^2} + \frac{B^2}{r}\left(\frac{3b^2}{r^2} + a^2\right)\frac{\mathrm{d}R_1}{\mathrm{d}r} - \left(\frac{\lambda^2}{B^2} + \frac{2a^2B^2 - 1}{r^2} - \vartheta^2 - \frac{2ab\vartheta B^2}{r^2}\right)R_1 = 0. \tag{5.37}$$

The remaining parameters $R_2(r)$ and $R_3(r)$ are related to $R_1(r)$ by

$$R_3 = -\frac{K_1}{K_6}\frac{\vartheta B}{\lambda}R_1, \quad R_2 = \frac{K_2}{K_3}\frac{B}{\lambda r}\left(R_1 + rR_1'\right). \tag{5.38}$$

The general solution of the ODE (5.37) cannot be written in terms of elementary functions, but is related to the solution of the *confluent Heun ODE* (Ronveaux, 1995)

$$\begin{aligned} &Y''(z) + \frac{\alpha z^2 + (\beta - \alpha + \gamma + 2)z + \beta + 1}{z(z-1)}Y'(z) \\ &\quad + \frac{((\beta + \gamma + 2)\alpha + 2\delta)z - (\beta + 1)\alpha + (\gamma + 1)\beta + 2\eta + \gamma}{2z(z-1)}Y(z) = 0, \end{aligned} \tag{5.39}$$

involving five constant parameters $\alpha, \beta, \gamma, \delta, \eta$. While the original Heun ODE with an independent variable z has four singularities $z = 0$, $z = 1$, $z = a$, and $z = \infty$, the confluent Heun equation (5.39) is obtained from it by displacing the singularity $z = a$ to infinity, under an appropriate redefinition of the constant parameters (see, e.g., Kristensson (2010)). Both the original Heun ODE and its confluent version are relatively well studied (e.g., Arscott 1995; Kristensson 2010; Ishkhanyan and Grigoryan 2014; El-Jaick and Figueiredo 2008 and references therein). Existing literature includes asymptotic forms, recursion relations, series representations of Heun functions in

terms of powers of z or hypergeometric functions, and so on. Heun functions are known to arise in various physical applications (Hortaçsu, 2013). We also note that Heun functions can be efficiently numerically approximated (Motygin, 2015).

The solution of the ODE (5.37) is given by

$$R_1(r) = R_{1\,n}(r) = C_1 r^{n-1} H_{C^+} + C_2 r^{-n-1} H_{C^-}, \tag{5.40}$$

where C_1, C_2 are arbitrary constants, and

$$H_{C^+} = H_C\left(\alpha, \beta, \gamma, \delta, \eta, -a^2 r^2/b^2\right), \tag{5.41a}$$

$$H_{C^-} = H_C\left(\alpha, -\beta, \gamma, \delta, \eta, -a^2 r^2/b^2\right), \tag{5.41b}$$

are confluent Heun functions with parameters

$$\alpha = 0, \quad \beta = b\lambda_n = n, \quad \gamma = -2, \quad \delta = \frac{a^2 n^2 - \vartheta^2 b^2}{4a^2}, \quad \eta = \frac{a^2(4-n^2) + \vartheta b(2a+\vartheta b)}{4a^2}. \tag{5.42}$$

The remaining radial dependencies are found from (5.38) and are given by

$$\begin{aligned} R_2(r) = R_{2\,n}(r) = &-\frac{K_1 B b}{K_4}\left(C_1 r^{n-2} H_{C^+} - C_2 r^{-n-2} H_{C^-}\right) \\ &+ \frac{2K_1 B a^2}{K_4 n b}\left(C_1 r^n H'_{C^+} + C_2 r^{-n} H'_{C^-}\right), \end{aligned} \tag{5.43a}$$

$$R_3(r) = R_{3\,n}(r) = -\frac{K_1 b\vartheta B}{K_6 n}\left(C_1 r^{n-1} H_{C^+} + C_2 r^{-n-1} H_{C^-}\right). \tag{5.43b}$$

It is convenient to write the complete solution for the separated helical velocity components in terms of dimensionless variables

$$\begin{aligned} &\tilde{r} = \frac{ar}{b}, \quad \tilde{z} = \frac{az}{b}, \quad \tilde{\xi} = \tilde{z} + \varphi, \quad \tilde{t} = \nu\vartheta^2 t, \quad \gamma = \frac{b\vartheta}{a}, \\ &\tilde{B}(\tilde{r}) = aB(\tilde{r}) = \frac{\tilde{r}}{\sqrt{\tilde{r}^2+1}}, \quad \tilde{\boldsymbol{u}} = \frac{b}{\nu}\boldsymbol{u}, \quad \tilde{p} = \frac{b^2}{\nu^2}p. \end{aligned} \tag{5.44}$$

It is given by

$$\tilde{u}_n^r = e^{-\tilde{t}}\left(\tilde{C}_{1\,n}\tilde{r}^{n-1} H_{C^+} + \tilde{C}_{2\,n}\tilde{r}^{-n-1} H_{C^-}\right)\left(K_1\cos(n\tilde{\xi}) + K_2\sin(n\tilde{\xi})\right), \tag{5.45a}$$

$$\begin{aligned} \tilde{u}_n^\xi = e^{-\tilde{t}}\,\tilde{B}\Bigg[&\tilde{C}_{1\,n}\left(\tilde{r}^{n-2} H_{C^+} - \frac{2}{n}\tilde{r}^n H'_{C^+}\right) \\ &-\tilde{C}_{2\,n}\left(\tilde{r}^{-n-2} H_{C^-} + \frac{2}{n}\tilde{r}^{-n} H'_{C^-}\right)\Bigg]\left(K_2\cos(n\tilde{\xi}) - K_1\sin(n\tilde{\xi})\right), \end{aligned} \tag{5.45b}$$

$$\tilde{u}_n^\eta = e^{-\tilde{t}}\,\frac{\gamma\tilde{B}}{n}\left(\tilde{C}_{1\,n}\tilde{r}^{n-1} H_{C^+} + \tilde{C}_{2\,n}\tilde{r}^{-n-1} H_{C^-}\right)\left(K_2\cos(n\tilde{\xi}) - K_1\sin(n\tilde{\xi})\right), \tag{5.45c}$$

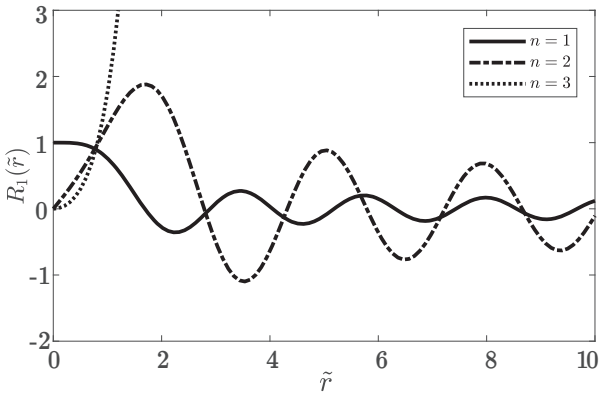

Figure 5.2: An illustration of the radial part $R_{1\,n}(\tilde{r})$ (5.40) of the velocity component $\tilde{u}^r_n$ (5.47a) of the Beltrami solution (5.47) for $n = 1, 2, 3$, $\tilde{C}_{1\,n} = 1$, $\tilde{C}_{2\,n} = 0$, $\gamma = -3$.

and the pressure $\tilde{p}$ is found from (5.35). In terms of the dimensionless variables (5.44), the confluent Heun functions are given by

$$H_{C^\pm} = H_C\left(0, \pm n, -2, \frac{n^2-\gamma^2}{4}, 1 + \frac{\gamma(\gamma+2)-n^2}{4}, -\tilde{r}^2\right). \tag{5.46}$$

One may denote $K_1 = K\sin\psi$, $K_2 = K\cos\psi$, where K, ψ is a different pair of arbitrary parameters ($K^2 = K_1 + K_2$, $\psi = \arctan(K_1/K_2)$). Without loss of generality, we set $K = 1$. Then (5.45) takes a simpler form

$$\tilde{u}^r_n = e^{-\tilde{t}}\,\left(\tilde{C}_{1\,n}\,\tilde{r}^{n-1}H_{C^+} + \tilde{C}_{2\,n}\,\tilde{r}^{-n-1}H_{C^-}\right)\sin(n\tilde{\xi} + \psi_n), \tag{5.47a}$$

$$\tilde{u}^\xi_n = e^{-\tilde{t}}\,\tilde{B}\left[\tilde{C}_{1\,n}\left(\tilde{r}^{n-2}H_{C^+} - \frac{2}{n}\tilde{r}^n H'_{C^+}\right)\right.$$
$$\left. -\tilde{C}_{2\,n}\left(\tilde{r}^{-n-2}H_{C^-} + \frac{2}{n}\tilde{r}^{-n}H'_{C^-}\right)\right]\cos(n\tilde{\xi} + \psi_n), \tag{5.47b}$$

$$\tilde{u}^\eta_n = e^{-\tilde{t}}\,\frac{\gamma\tilde{B}}{n}\left(\tilde{C}_{1\,n}\tilde{r}^{n-1}H_{C^+} + \tilde{C}_{2\,n}\tilde{r}^{-n-1}H_{C^-}\right)\cos(n\tilde{\xi} + \psi_n), \tag{5.47c}$$

$$\tilde{p}_n = p_{0\,n} - \frac{1}{2}\left(|\tilde{u}^r_n|^2 + |\tilde{u}^\xi_n|^2 + |\tilde{u}^\eta_n|^2\right). \tag{5.47d}$$

Depending on the choice of the constant parameters $n \in \mathbb{N}$ and $C_1, C_2, \gamma \in \mathbb{R}$, the separated space-time modes (5.47) may be bounded or unbounded functions, regular or singular at the origin. For example, for the choice $\tilde{C}_{2\,n} = 0$, $\gamma < 0$, $n = 1, 2$ the radial parts of solution (5.47) components are bounded functions for all $\tilde{r}$, and are regular on the $\tilde{z}$-axis; for the same constants when $n \geq 3$, the Heun functions (5.46) diverge as $\tilde{r} \to \infty$. As an example, radial parts of the velocity component $\tilde{u}^r_n$ (5.47a) are shown in Figure 5.2 for $n = 1, 2, 3$, $C_1 = 1$, $C_2 = 0$, $\gamma = -3$. While single-mode solutions

present physical interest, since the Beltrami model (5.30), (5.31) is linear homogeneous, it follows that any linear combination of physical solutions (5.33)

$$\tilde{u}^r = \sum_n \tilde{u}^r_n, \quad \tilde{u}^\xi = \sum_n \tilde{u}^\xi_n, \quad \tilde{u}^\eta = \sum_n \tilde{u}^\eta_n, \quad \tilde{p} = \sum_n p_n \tag{5.48}$$

(involving arbitrary parameter families $\tilde{C}_{1\,n}$, $\tilde{C}_{2\,n}$, ψ_n) yields a $\tilde{\xi}$-periodic physical exact solution of the helically invariant Navier-Stokes equations (3.19). We note that such solutions still have the same spatial period $\tau_{\tilde{\xi}}$ (3.20) in the $\tilde{\xi}$-direction.
It is important to remark that the time dependence both for modes (5.47) and for the general solution (5.48) is the same, i.e., all modes decay at the same rate. The following properties consequently hold for every solution:

1. The set of constant-pressure surfaces $\tilde{p}(\tilde{t}, \tilde{r}, \tilde{\xi}) = \text{const.}$ (coinciding with level surfaces $|\boldsymbol{u}(\tilde{t}, \tilde{r}, \tilde{\xi})|^2 = \text{const.}$, $|\boldsymbol{\omega}(\tilde{t}, \tilde{r}, \tilde{\xi})|^2 = \text{const.}$) are time-invariant, in the sense that the common time dependence factors out, and for the given value of $\tilde{p}$ (or $|\tilde{\boldsymbol{u}}|$, $|\tilde{\boldsymbol{\omega}}|$), the surfaces at different times $\tilde{t}$ are just different surfaces within the same set; no shape change occurs.

2. The streamlines (5.23) for the flow defined by an exact solution (5.48) are fixed, and are followed by the particles. In particular, the velocity vector field never changes direction, only changing its magnitude exponentially in time.

In Figures 5.3a, 5.4a, the cross-section is periodic in $\tilde{\xi}$ with the period π, which is a half of the period $\tau_{\tilde{\xi}}$ (3.20) because the figures correspond to the isosurfaces of squared velocities. Note that these isosurfaces coincide with the isosurfaces of helicity density, since for all Beltrami flows, (5.28) holds, and the helicity density of such flows is given by $\tilde{h} = \vartheta|\tilde{\boldsymbol{u}}|^2$, with $\vartheta = \text{const.} = Q$ for the solutions (5.47).
A sample set of upward-directed streamlines for the separated solution (5.47) with $n = 2$ is shown in Figure 5.5. Both the solutions with $n = 1$ and $n = 2$ for the same set of other parameters include lines that are (on average) directed upward or downward. For some lines, the $\tilde{z}$-projection of the fluid velocity changes sign once or more per helical period.

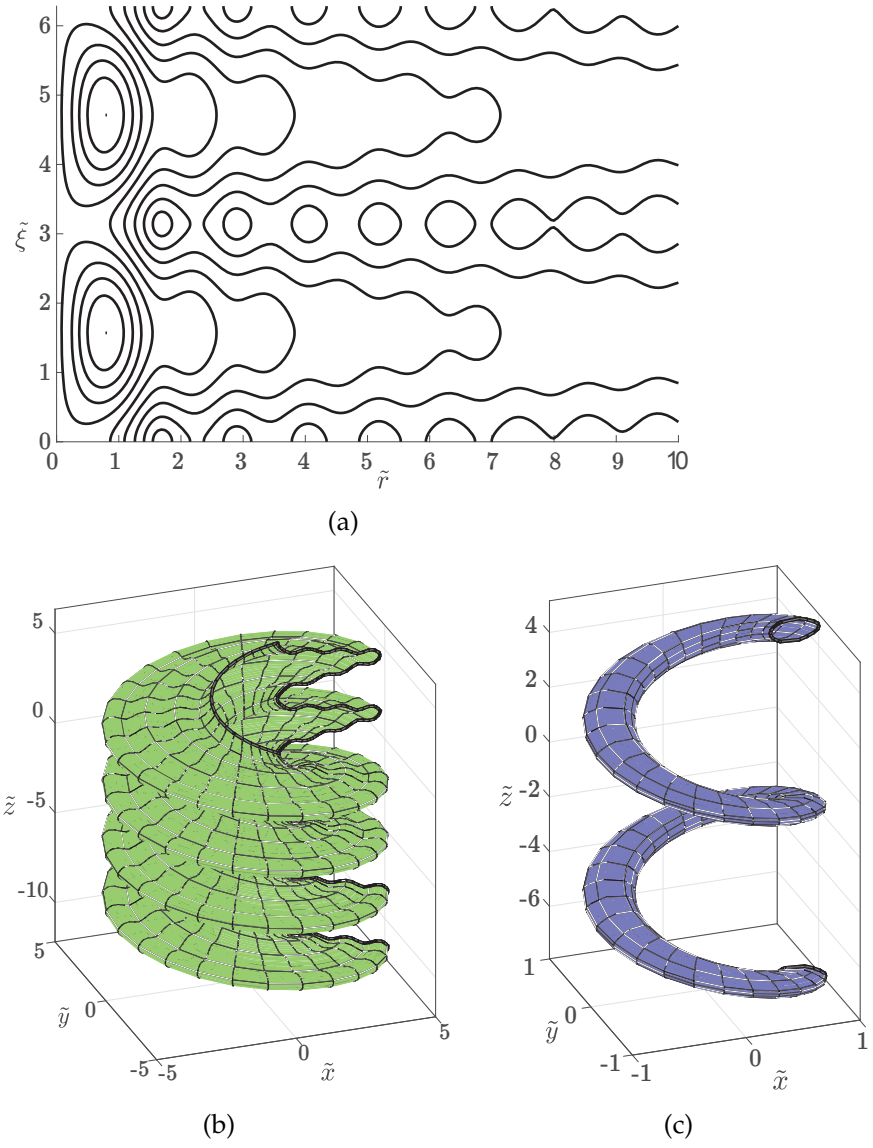

Figure 5.3: Level surfaces $|\tilde{\boldsymbol{u}}|^2 = \text{const.}$ (equivalently, $\tilde{p} = \text{const.}$, $|\tilde{\boldsymbol{\omega}}|^2 = \text{const.}$, or $\tilde{h} = \text{const.}$) for the exact dimensionless Beltrami solution (5.47) for $n = 1$, $C_1 = 1$, $C_2 = 0$, $\psi = -\pi/2$. (a) A cross-section of level surfaces plot $|\tilde{\boldsymbol{u}}|^2 = \text{const.}$, for one period $0 \leq \tilde{\xi} \leq 2\pi$. (b) A connected component of the level surface $|\tilde{\boldsymbol{u}}|^2 = 0.4$. (c) A connected component of the level surface $|\tilde{\boldsymbol{u}}|^2 = 2.6$.

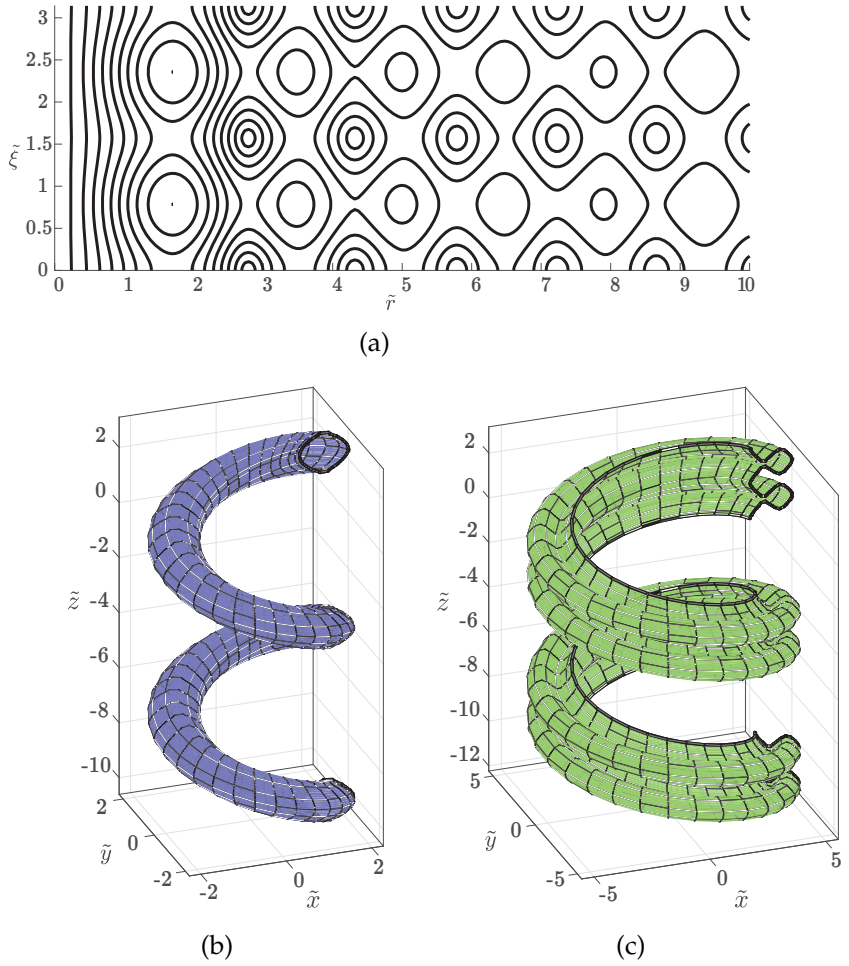

Figure 5.4: Level surfaces $|\tilde{\boldsymbol{u}}|^2 = \text{const.}$ (equivalently, $\tilde{p} = \text{const.}$, $|\tilde{\boldsymbol{\omega}}|^2 = \text{const.}$, or $\tilde{h} = \text{const.}$) for the exact dimensionless Beltrami solution (5.47) for $n = 2$, $C_1 = 1$, $C_2 = 0$, $\psi = -\pi/2$. (a) A cross-section of level surfaces plot $|\tilde{\boldsymbol{u}}|^2 = \text{const.}$, for one period $0 \leq \tilde{\xi} \leq 2\pi$. (b) A connected component of the level surface $|\tilde{\boldsymbol{u}}|^2 = 3.54$. (c) A connected component of the level surface $|\tilde{\boldsymbol{u}}|^2 = 0.97$.

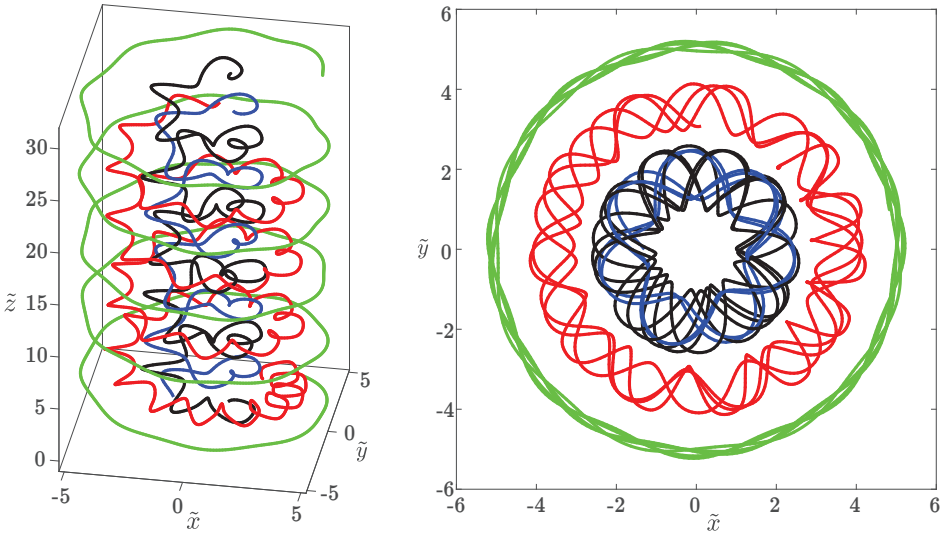

(a) (b)

Figure 5.5: Four sample streamlines for the exact dimensionless Beltrami solution (5.47) for $n = 2$, $C_1 = 1$, $C_2 = 0$, emanating from various points in the plane $z = 1$. (a) Side view. (b) Top view.

Part II

Numerics

6 The DG discretization of the helically invariant Navier-Stokes equations

In this chapter we present the numerical discretization of the helically invariant Navier-Stokes equations (3.19). We derive periodicity conditions for the helical coordinate ξ in section 6.1 and a condition for uniqueness at the centerline axis $r = 0$ in analogy to Khorrami et al. (1989) who considered *"boundedness"* and *"smoothness"* conditions at the central axis in cylindrical coordinates within a stability analysis of swirling flows. Combining both of these conditions, in section 6.3 a reduced DG space is introduced and the numerical fluxes of the spatial discretization of (3.19) are presented. Finally, a semi-explicit scheme for the temporal discretization is discussed in 6.4.

The helical coordinate system (r, ξ, η) has been introduced by Kelbin et al. (2013). It is given by

$$r, \quad \xi = az + b\varphi, \quad \tilde{\eta} = a\varphi - bz/r^2, \tag{6.1}$$

where $a, b = \text{const.}$, $a^2 + b^2 > 0$ and (r, φ, z) are the usual cylindrical coordinates. In the present work we use a new invariant coordinate η, given by

$$\eta = -bz + ar^2\varphi\,, \tag{6.2}$$

which has two important advantages. First, the coordinate lines of η (lines where $\eta = \text{const.}$) are orthogonal to lines where $\xi = \text{const.}$ and second, the coordinate η is not singular at the centerline $r = 0$, i.e. lines where $\eta = \text{const.}$ do not collapse to one single point at the origin $(r, z) = (0, 0)$. However, the choice of the invariant coordinate η is important for the formulation of appropriate conditions at the centerline of the helix $r = 0$, which we consider in the following. The derivation of the coordinate (6.2) is provided in Appendix C.

6.1 Periodicity conditions at the centerline

The transformation from helical to cylindrical coordinates is given by the mapping

$$\begin{pmatrix} r\varphi \\ z \end{pmatrix} = \begin{bmatrix} \boldsymbol{v}^c & \boldsymbol{w}^c \end{bmatrix} \begin{pmatrix} \xi \\ \eta \end{pmatrix} = \begin{bmatrix} v_1^c & w_1^c \\ v_2^c & w_2^c \end{bmatrix} \begin{pmatrix} \xi \\ \eta \end{pmatrix}. \tag{6.3}$$

The inverse relation reads

$$\begin{pmatrix} \xi \\ \eta \end{pmatrix} = \underbrace{\begin{bmatrix} \frac{b}{r} & a \\ ar & -b \end{bmatrix}}_{\boldsymbol{M}} \begin{pmatrix} r\varphi \\ z \end{pmatrix}, \tag{6.4}$$

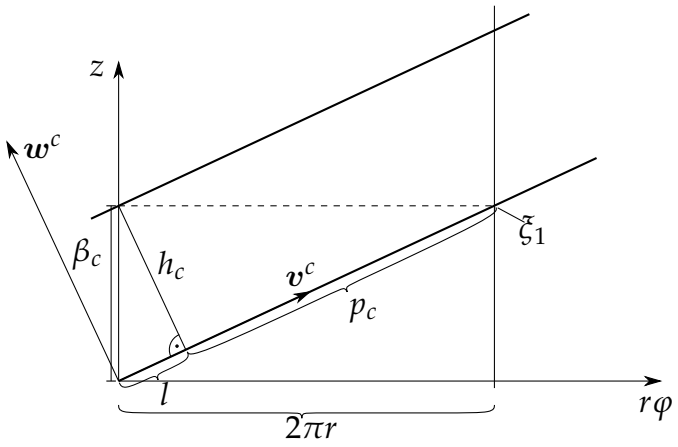

Figure 6.1: An illustration of the geometric correlations for one helical turn. The coordinate lines of constant ξ are presented in the $r\varphi - z-$plane. β_c is the pitch of the helix and h_c the distance of two points on two helical turns.

where

$$\boldsymbol{M}^{-1} = \frac{1}{-\frac{b^2}{r} - a^2 r} \begin{bmatrix} -b & -a \\ -ar & \frac{b}{r} \end{bmatrix}.$$

Using the geometric function $B(r)$ defined in (3.15f) leads to

$$\begin{pmatrix} r\varphi \\ z \end{pmatrix} = \begin{bmatrix} \frac{b}{r}B^2 & \frac{a}{r}B^2 \\ aB^2 & -\frac{b}{r^2}B^2 \end{bmatrix} \begin{pmatrix} \xi \\ \eta \end{pmatrix}. \tag{6.5}$$

Since we know that after one helical turn $\varphi = 2\pi$

$$v_1^c \cdot \xi_1 = 2\pi r, \tag{6.6}$$

we can compute the point ξ_1 which is given by

$$\xi_1 = \frac{2\pi r^2}{bB^2}. \tag{6.7}$$

Using that, the pitch of the helix reads

$$\beta_c = v_2^c \cdot \xi_1 = aB^2 \cdot \frac{2\pi r^2}{bB^2} = 2\frac{a}{b}\pi r^2. \tag{6.8}$$

From Figure 6.1, one may observe that

$$h_c^2 + p_c^2 = 4\pi^2 r^2 \tag{6.9}$$

and further, using $h_c^2 = l \cdot p_c$, defining $x_c := l + p_c$ and employing both into (6.9) leads to

$$p_c = \frac{4\pi^2 r^2}{x} = 2\pi b B, \tag{6.10}$$

where we employed the trigonometric relation $x_c^2 = \beta_c^2 + 4\pi^2 r^2$ and (6.8). From (6.10) it follows that for the case when $r \to 0$ the length p_c vanishes, which means that we have $\xi-$independence at the centerline. Similarly, knowing that $p_c = x_c - l$ we obtain

$$l = \frac{\beta_c^2}{\sqrt{\beta_c^2 + 4\pi^2 r^2}}. \tag{6.11}$$

Finally, we compute the periodic conditions ξ_p, ξ_l, η_p considering the following relations of distances for one helical pitch

$$p_c : (l + p_c) = \xi_{p_c} : \xi_1, \tag{6.12a}$$
$$l : (l + p_c) = \xi_l : \xi_1, \tag{6.12b}$$
$$\xi_l \cdot \boldsymbol{v}^c + \eta_{p_c} \cdot \boldsymbol{w}^c = \begin{pmatrix} 0 \\ \xi_1 v_2^c \end{pmatrix}, \tag{6.12c}$$

which are given by

$$\xi_{p_c} = \frac{8\pi^3 r^4}{(\beta_c^2 + 4\pi^2 r^2)\, bB^2} = 2\pi b, \tag{6.13a}$$
$$\xi_l = \frac{2\pi\beta^2 r^2}{(\beta_c^2 + 4\pi^2 r^2)\, bB^2} = \frac{2\pi r^2 a^2}{b}, \tag{6.13b}$$
$$\eta_{p_c} = -\frac{8\pi^3 r^4}{(\beta_c^2 + 4\pi^2 r^2)\, bB^2} \frac{ar^2}{b} = -2\pi r^2 a. \tag{6.13c}$$

In the following section we derive a condition for uniqueness and boundedness of all physical variables at the centerline axis $r = 0$.

6.2 Condition for uniqueness at the centerline

For the derivation of uniqueness conditions at the centerline axis, we follow Khorrami et al. (1989) who considered the following conditions in cylindrical coordinates, given by

$$\lim_{r\to 0} \frac{\partial \boldsymbol{u}}{\partial \varphi} = 0, \qquad \lim_{r\to 0} \frac{\partial p}{\partial \varphi} = 0. \tag{6.14}$$

For $r > 0$, one may consider a ring around the z-axis where different values for the velocities in circumferential direction may be given at each point. For $r \to 0$ this circle reduces to a single point at the z-axis, where a unique velocity and pressure must be given. This leads to the condition that the velocity must not change in circumferential direction for $r \to 0$. Expanding (6.14) for a cylindrical velocity vector $\boldsymbol{u} = \left(u^r, u^\phi, u^z\right)$, we obtain

$$\lim_{r\to 0} \frac{\partial \boldsymbol{u}}{\partial \varphi} = \lim_{r\to 0} \left(\frac{\partial u^r}{\partial \varphi} \boldsymbol{e}_r + u^r \frac{\partial \boldsymbol{e}_r}{\partial \varphi} + \frac{\partial u^\varphi}{\partial \varphi} \boldsymbol{e}_\varphi + u^\varphi \frac{\partial \boldsymbol{e}_\varphi}{\partial \varphi} + \frac{\partial u^z}{\partial \varphi} \boldsymbol{e}_z + u^z \frac{\partial \boldsymbol{e}_z}{\partial \varphi} \right). \tag{6.15}$$

The derivatives w.r.t. circumferential direction of the three cylindrical unit vectors are given by

$$\frac{\partial \boldsymbol{e}_z}{\partial \varphi} = 0, \qquad \frac{\partial \boldsymbol{e}_r}{\partial \varphi} = \boldsymbol{e}_\varphi, \qquad \frac{\partial \boldsymbol{e}_\varphi}{\partial \varphi} = -\boldsymbol{e}_r. \tag{6.16}$$

Hence, we obtain

$$\lim_{r\to 0} \frac{\partial \boldsymbol{u}}{\partial \varphi} = \lim_{r\to 0} \left(\left(\frac{\partial u^r}{\partial \varphi} - u^\varphi \right) \boldsymbol{e}_r + \left(\frac{\partial u^\varphi}{\partial \varphi} + u^r \right) \boldsymbol{e}_\varphi + \left(\frac{\partial u^z}{\partial \varphi} \right) \boldsymbol{e}_z \right). \tag{6.17}$$

The components must vanish for $r \to 0$ separately, which leads to

$$\lim_{r\to 0} \left(\frac{\partial u^r}{\partial \varphi} - u^\varphi \right) = 0, \qquad \lim_{r\to 0} \left(\frac{\partial u^\varphi}{\partial \varphi} + u^r \right) = 0, \qquad \lim_{r\to 0} \left(\frac{\partial u^z}{\partial \varphi} \right) = 0. \tag{6.18}$$

Next, we express the derived conditions (6.18) in helical coordinates derived in KCO. Employing the velocity components (3.17) and the derivative

$$\frac{\partial}{\partial \varphi} = ar^2 \frac{\partial}{\partial \eta} + b \frac{\partial}{\partial \xi}, \tag{6.19a}$$

and imposing helical invariance, i.e. $\left(\frac{\partial}{\partial \eta} \equiv 0 \right)$, leads to

$$\lim_{r\to 0} \left(b u^r_\xi - B \left(\frac{b}{r} u^\xi + a u^\eta \right) \right) = 0, \tag{6.20a}$$

$$\lim_{r\to 0} \left(B \frac{b^2}{r} u^\xi_\xi - B b a u^\eta_\xi + u^r \right) = 0, \tag{6.20b}$$

$$\lim_{r\to 0} \left(B b a u^\xi_\xi - \frac{b^2}{r} B u^\eta_\xi \right) = 0. \tag{6.20c}$$

B(r) is the geometric function, for which $\lim_{r\to 0} B(r) = 0$ holds. If we now assume

$$\lim_{r\to 0} u^r < \pm\infty, \qquad \lim_{r\to 0} \frac{\partial u^\xi}{\partial \xi} < \pm\infty, \qquad \lim_{r\to 0} \frac{\partial u^\eta}{\partial \xi} < \pm\infty, \tag{6.21}$$

i.e. u^r is limited and u^η and u^ξ are smooth with respect to ξ for $r \to 0$, we obtain

$$\lim_{r\to 0} \left(b u^r_\xi - \frac{b}{\sqrt{a^2 r^2 + b^2}} u^\xi \right) = 0, \tag{6.22a}$$

$$\lim_{r\to 0} \left(\frac{b^2}{\sqrt{a^2 r^2 + b^2}} u^\xi_\xi - u^r \right) = 0, \tag{6.22b}$$

$$\lim_{r\to 0} \left(\frac{b^2}{\sqrt{a^2 r^2 + b^2}} u^\eta_\xi \right) = 0. \tag{6.22c}$$

Finally, the centerline conditions are given by

$$b u^r_\xi = u^\xi, \qquad b u^\xi_\xi = -u^r, \qquad u^\eta_\xi = 0 \tag{6.23}$$

for $r = 0$. For the pressure, the condition is given by

$$\lim_{r\to 0} \frac{\partial p}{\partial \varphi} = \frac{\partial p}{\partial \xi} = 0. \tag{6.24}$$

6.3 The spatial discretization

In section 6.1 we have seen that the periodic length p_c vanishes at $r = 0$. A zero length of the helix would mean that there are infinitely many helical turns at the centerline axis. Hence, we conclude that all velocity components and the pressure must be ξ-independent, i.e. $\frac{\partial}{\partial \xi} = 0$ at $r = 0$. Combining the periodicity conditions and the uniqueness conditions for the helical velocity components and the pressure (6.23) derived in section 6.2 finally leads to centerline conditions, choosen as

$$u^r = 0, \quad u^\xi = 0, \quad u^\eta_\xi = 0, \quad p_\xi = 0, \tag{6.25a-d}$$

which means that the radial and helical velocity components vanish whereas the velocity component in invariant direction and the pressure are constant with respect to spatial coordinates. Taking into account the conditions (6.25) we can formulate a reduced DG space which is presented subsequently.

6.3.1 Reduced DG spaces ensuring the centerline conditions

In standard DG formulation, the velocity and pressure are discretized in DG spaces of order k and $k' = k - 1$, respectively, in order to comply the Ladyženskaja-Babuška-Brezzi (LBB) condition (see Babuška, 1973; Brezzi and Fortin, 2012). In this case, the DG space is usually given by

$$(\boldsymbol{u}, p) \in \mathbb{P}_k(\mathcal{K})^3 \times \mathbb{P}_{k-1}(\mathcal{K}) := \mathbb{V}_k\,. \tag{6.26}$$

In contrast to that, for the discretization helically invariant Navier-Stokes equations (3.19) we need to introduce a reduced DG space $\mathbb{V}_k^0$ due to the centerline conditions at the central axis $r = 0$. We distinguish between two different spatial domains in the following. The first domain is a cylindrical shell where the centerline axis $r = 0$ is omitted (domain #1). Afterwards, we consider the full domain including the centerline axis which we denote as the second case (domain #2). For both, we distinguish between a mixed-order and an equal-order formulation of the DG discretization. For the DG discretization on the cylindrical shell we seek solutions in the DG space $\mathbb{V}_k$ where we additionally demand that the integral of the pressure over one cell vanishes, i.e. $\int_{K_0} p = 0$. For the DG discretization in the full domain, the underlying DG space is denoted as $\mathbb{V}_k^0$. The different DG spaces for the four distinct cases are presented in Table 6.1. The validation of the implementation in the cylidrical shell is presented in chapter 7 followed by the validation in the full domain in chapter 8.

Geometry	mixed-order	equal-order
Domain #1 $r_0 \vee\mid r \vee\mid 1$	$\mathbb{V}_k^0 = \left\{(\boldsymbol{u}, p) \in \mathbb{P}_k(\mathcal{K})^3 \times \mathbb{P}_{k-1}(\mathcal{K}), \text{ s.t. } \int_{K_0} p = 0\right\}$	$\mathbb{V}_k^0 = \left\{(\boldsymbol{u}, p) \in \mathbb{P}_k(\mathcal{K})^3 \times \mathbb{P}_k(\mathcal{K}), \text{ s.t. } \int_{K_0} p = 0\right\}$
Domain #2 $0 \vee\mid r \vee\mid 1$	$\mathbb{V}_k^0 = \left\{(\boldsymbol{u}, p) \in \mathbb{P}_k(\mathcal{K})^3 \times \mathbb{P}_{k-1}(\mathcal{K}), \text{ s.t. } u^r = u^\xi = 0,\ u^\eta_\xi = 0,\ p_\xi = 0\right\}$	$\mathbb{V}_k^0 = \left\{(\boldsymbol{u}, p) \in \mathbb{P}_k(\mathcal{K})^3 \times \mathbb{P}_k(\mathcal{K}), \text{ s.t. } u^r = u^\xi = 0,\ u^\eta_\xi = 0,\ p_\xi = 0\right\}$

Table 6.1: DG spaces for different geometries and DG formulations. $\mathbb{P}_k(\mathcal{K})$ and $\mathbb{P}_{k-1}(\mathcal{K})$ are the spaces of smooth polynomial functions up to order k and $k-1$, respectively.

6.3.2 Boundary conditions

For the DG discretization of the helically invariant Navier-Stokes equations (3.19), we use the following Dirichlet and periodic boundary conditions

$$\begin{aligned} \boldsymbol{u} &= \boldsymbol{u}_D \quad \text{on } \Gamma_D\,, \\ \boldsymbol{u} &= \boldsymbol{u}_P \quad \text{on } \Gamma_P\,, \end{aligned} \tag{6.27}$$

where Γ_D is the Dirichlet boundary and Γ_P is the boundary where periodic BCs are assumed. For the Dirichlet BC we distinguish between the two spatial domains (i) the cylindrical shell and (ii) the full domain including $r = 0$. In the case (i) we assume Dirichlet boundary conditions at the inner and the outer cylindrical walls, given by

$$\Gamma_D = \left\{(r, \xi) \in \mathbb{R}^2 \mid r = r_0 > 0 \vee r = 1\right\}, \tag{6.28}$$

whereas in case (ii) Dirichlet BCs are assumed only at the outer cylindrical wall, i.e.

$$\Gamma_D = \left\{(r, \xi) \in \mathbb{R}^2 \mid r = 1\right\}. \tag{6.29}$$

At the inner axis $r = 0$ the centerline conditions (6.25) are used. In both cases periodic boundary conditions are implemented on the following boundaries

$$\Gamma_P = \left\{(r, \xi) \in \mathbb{R}^2 \mid \xi = 0 \vee \xi = 2\pi\right\}. \tag{6.30}$$

6.3.3 The spatial discretization of the helically invariant Navier-Stokes equations

We propose the following discretization of the helically invariant Navier-Stokes equations (3.19), using the boundary conditions (6.27) in the DG space: find $(\boldsymbol{u}, p) \in \mathbb{V}_k^0$ such that for all $(\tilde{\boldsymbol{v}}, \tau) \in \mathbb{V}_k^0$

$$\mathrm{Ns}\left(\boldsymbol{u}, (\boldsymbol{u}, p), (\tilde{\boldsymbol{v}}, \tau)\right) = \mathrm{rhsNs}\left((\tilde{\boldsymbol{v}}, \tau)\right), \tag{6.31}$$

where the Navier-Stokes form $\mathrm{Ns}(-,-,-)$ is given by

$$\mathrm{Ns}\left(\boldsymbol{u}, (\boldsymbol{u}, p), (\tilde{\boldsymbol{v}}, \tau)\right) = n\left(\boldsymbol{u}, \boldsymbol{u}, \tilde{\boldsymbol{v}}\right) - a\left(p, \boldsymbol{u}, \tilde{\boldsymbol{v}}\right), \tag{6.32}$$

which consists of a trilinear form $\mathcal{N}(-,-,-)$ representing the convective terms, and a bilinear form $\mathcal{A}(p, \boldsymbol{u}, \tilde{\boldsymbol{v}})$, representing the pressure gradient and the viscous terms of the Navier-Stokes equations (3.19). Note that (6.31) is the discrete spatial formulation of (3.19), neglecting the transient term, which will be taken into account in section 6.4. The right-hand side of the discretized Navier-Stokes equations (3.19),

$$\mathrm{rhsNs}\left((\tilde{\boldsymbol{v}}, \tau)\right) = s\left(\tilde{\boldsymbol{v}}\right) + q\left(\tilde{\boldsymbol{v}}\right) + r\left(\tau\right), \tag{6.33}$$

is the sum of three linear forms, representing body forces by $s\left(\tilde{\boldsymbol{v}}\right)$, boundary conditions for the momentum equations by $q\left(\tilde{\boldsymbol{v}}\right)$ and boundary conditions for the continuity equation by $r(\tau)$.

The momentum equations of the helically invariant Navier-Stokes equations (3.19) are presented component-wise in radial direction as well as in the helical "ξ" and "η"-direction. For brevity, we introduce the following naming for the DG space

$$\mathbb{V}_{k,i}^0 := \left\{ u_i \mid (u_1, u_2, u_3, u_4) = (\boldsymbol{u}, \tau) \in \mathbb{V}_k^0 \right\} \tag{6.34}$$

and using that, we write the system (6.31) component-wise as follows

$$\mathcal{C}\left(\boldsymbol{u}, \tau\right) = 0 \qquad \forall \tau \in \mathbb{V}_{k,4}^0, \tag{6.35a}$$

$$\mathcal{N}_1\left(\boldsymbol{u}, \boldsymbol{u}, \tilde{v}_1\right) - \mathcal{A}_1\left(p, \boldsymbol{u}, \tilde{v}_1\right) = b_1\left(\tilde{v}_1\right) \qquad \forall \tilde{v}_1 \in \mathbb{V}_{k,1}^0, \tag{6.35b}$$

$$\mathcal{N}_2\left(\boldsymbol{u}, \boldsymbol{u}, \tilde{v}_2\right) - \mathcal{A}_2\left(\boldsymbol{u}, \tilde{v}_2\right) = b_2\left(\tilde{v}_2\right) \qquad \forall \tilde{v}_2 \in \mathbb{V}_{k,2}^0, \tag{6.35c}$$

$$\mathcal{N}_3\left(\boldsymbol{u}, \boldsymbol{u}, \tilde{v}_3\right) - \mathcal{A}_3\left(p, \boldsymbol{u}, \tilde{v}_3\right) = b_3\left(\tilde{v}_3\right) \qquad \forall \tilde{v}_3 \in \mathbb{V}_{k,3}^0, \tag{6.35d}$$

where the index "1" denotes the terms of the momentum equation in radial direction, the index "2" and "3" represent terms of the η- and ξ-Momentum equation. Note that the η-momentum equation equation has no pressure. Furthermore, (6.35a) is the discrete form of the continuity equation.

In the following, we present the DG discretization of each term in (6.35). The velocity divergence (6.35a) is discretized as follows

$$\mathcal{C}(\boldsymbol{u},\tau) = -\int_\Omega \left[u^r \cdot \left(\frac{\mathrm{d}f}{\mathrm{d}_h r}\tau + f\partial_{r,h}\tau \right) + \frac{f}{B}u^\xi \partial_{\xi,h}\tau - \frac{f}{r}u^r\tau \right] \mathrm{d}V + \oint_\Gamma \left[\{u^r\}\, \boldsymbol{e}_r\cdot\boldsymbol{n} + \frac{1}{B}\left\{u^\xi\right\} \boldsymbol{e}_\xi\cdot\boldsymbol{n} \right] f\,[\![\tau]\!]\,\mathrm{d}S\,, \quad (6.36)$$

where $f = f(r)$ is a metric function, which we introduce to remove singularities in the coefficients of the PDEs at the centerline axis $r = 0$. In the present thesis we choose $f = B^2(r)$. The convective terms are discretized in a "super weak form", by partially integrating twice

$$\mathcal{N}(\boldsymbol{w},u,\tilde{v}) = \int_\Omega \nabla u\cdot\boldsymbol{w} f\tilde{v}\,\mathrm{d}V + \oint_\Gamma \left(\widehat{u\boldsymbol{w}\boldsymbol{n}} - u\boldsymbol{w}\boldsymbol{n}\right) f\tilde{v}\,\mathrm{d}S\,. \quad (6.37)$$

The parameter $\boldsymbol{w} = \left(w_0^r, w_0^\eta, w_0^\xi\right)$ is taken from the initial condition and linearizes the convective part. The operator n is the sum of the convective terms of the component-wise discretization (6.35), i.e. $\mathcal{N} = \mathcal{N}_1 + \mathcal{N}_2 + \mathcal{N}_3$. The scalar quantity u is the velocity component for each momentum equation, e.g. $u = u^r$ for the r-momentum equation. For the flux $\widehat{u\boldsymbol{w}\boldsymbol{n}}$, we use the upwind formulation,

$$f_{upw}(u,\boldsymbol{w},\boldsymbol{n}) := \widehat{u\boldsymbol{w}\boldsymbol{n}} = \begin{cases} u^-\boldsymbol{w}\cdot\boldsymbol{n} & \text{if } \boldsymbol{w}\cdot\boldsymbol{n}\geq 0 \\ u^+\boldsymbol{w}\cdot\boldsymbol{n} & \text{if } \boldsymbol{w}\cdot\boldsymbol{n} < 0\,. \end{cases} \quad (6.38)$$

For brevity, we introduce the flux

$$f_{sw}(u,\boldsymbol{w},\boldsymbol{n}) := f_{upw} - u\boldsymbol{w}\boldsymbol{n}, \quad (6.39)$$

such that the convective terms in (6.35) read

$$\mathcal{N}_1(\boldsymbol{u},\boldsymbol{w},\tilde{v}_1) = \int_\Omega \left[u_0^r\partial_{r,h}u^r + \frac{1}{B}u_0^\xi\partial_{\xi,h}u^r - \frac{B^2}{r}\left(\frac{b}{r}u_0^\xi + au_0^\eta\right)\left(\frac{b}{r}u^\xi + au^\eta\right)\right] f\tilde{v}_1\mathrm{d}V + \oint_\Gamma \left(f_{sw}(u^r, w_0^r\boldsymbol{e}_r,\boldsymbol{n}) + \frac{1}{B}f_{sw}\left(u^r, w_0^\xi\boldsymbol{e}_\xi,\boldsymbol{n}\right)\right)[\![\tilde{v}_1]\!]\, f\mathrm{d}S\,, \quad (6.40a)$$

$$\mathcal{N}_2(\boldsymbol{u},\boldsymbol{w},\tilde{v}_2) = \int_\Omega \left[u_0^r\partial_{r,h}u^\eta + \frac{1}{B}u_0^\xi\partial_{\xi,h}u^\eta + \frac{a^2B^2}{r}u_0^ru^\eta\right] f\tilde{v}_2\mathrm{d}V + \oint_\Gamma \left(f_{sw}(u^\eta, w_0^r\boldsymbol{e}_r,\boldsymbol{n}) + \frac{1}{B}f_{sw}\left(u^\eta, w_0^\xi\boldsymbol{e}_\xi,\boldsymbol{n}\right)\right)[\![\tilde{v}_2]\!]\, f\mathrm{d}S\,, \quad (6.40b)$$

$$\mathcal{N}_3(\boldsymbol{u},\boldsymbol{w},\tilde{v}_3) = \int_\Omega \left[u_0^r\partial_{r,h}u^\xi + \frac{1}{B}u_0^\xi\partial_{\xi,h}u^\xi + 2\frac{abB^2}{r^2}u_0^ru^\eta + \frac{b^2B^2}{r^3}u_0^ru^\xi\right] f\tilde{v}_3\mathrm{d}V + \oint_\Gamma \left(f_{sw}\left(u^\xi, w_0^r\boldsymbol{e}_r,\boldsymbol{n}\right) + \frac{1}{B}f_{sw}\left(u^\xi, w_0^\xi\boldsymbol{e}_\xi,\boldsymbol{n}\right)\right)[\![\tilde{v}_3]\!]\, f\mathrm{d}S\,. \quad (6.40c)$$

To discretize the viscous terms, we employ a non-standard symmetric interior penalty (SIP) method to receive

$$
\begin{aligned}
\mathcal{A}_1\left(p,\boldsymbol{u},\tilde{v}_1\right) = &-\nu\int_\Omega\left[\left(-p+\partial_{r,h}u^r\right)\left(\frac{\mathrm{d}f}{\mathrm{d}r}\tilde{v}_1+f\partial_{r,h}\tilde{v}_1\right)+u^r\left(\frac{\frac{\mathrm{d}f}{\mathrm{d}r}\cdot r-f}{r^2}\tilde{v}_1+\frac{f}{r}\partial_{r,h}\tilde{v}_1\right)\right.\\
&\left.+\left(\frac{1}{B^2}\partial_\xi u^r+C^{r,\eta}u^\eta+C^{r,\xi}u^\xi\right)f\partial_{\xi,h}\tilde{v}_1-\frac{f}{r}u^r\tilde{v}_1\right]\mathrm{d}V\\
&+\nu\oint_\Gamma\left[\left(-p+\frac{1}{r}\left\{u^r\right\}+\left\{\partial_{r,h}u^r\right\}\right)\boldsymbol{e}_r\cdot\boldsymbol{n}\right.\\
&\left.+\left(\frac{1}{B^2}\left\{\partial_{\xi,h}u^r\right\}+C^{r,\eta}\left\{u^\eta\right\}+C^{r,\xi}\left\{u^\xi\right\}\right)\boldsymbol{e}_\xi\cdot\boldsymbol{n}\right]\cdot f\left[\!\left[\tilde{v}_1\right]\!\right]\mathrm{d}S\\
&+\nu\oint_\Gamma\left(\left\{\partial_{r,h}\tilde{v}_1\right\}\boldsymbol{e}_r+\frac{1}{B^2}\left\{\partial_{\xi,h}\tilde{v}_1\right\}\boldsymbol{e}_\xi\right)\cdot\boldsymbol{n}\,f\left[\!\left[u^r\right]\!\right]\,\mathrm{d}S\\
&+\nu\oint_\Gamma\eta_{\mathrm{SIP}}\left[\!\left[u^r\right]\!\right]\left[\!\left[\tilde{v}_1\right]\!\right]\,\mathrm{d}S\,, \qquad (6.41a)\\
\mathcal{A}_2\left(\boldsymbol{u},\tilde{v}_2\right) = &\int_\Omega\left[\partial_{r,h}u^\eta\left(\frac{\mathrm{d}f}{\mathrm{d}r}\tilde{v}_2+f\partial_{r,h}\tilde{v}_2\right)+u^\eta\left(\frac{\frac{\mathrm{d}f}{\mathrm{d}r}r-f}{r^2}\tilde{v}_2+\frac{f}{r}\partial_{r,h}\tilde{v}_2\right)\right.\\
&+\partial_{\xi,h}u^\eta\partial_{\xi,h}\tilde{v}_2\frac{f}{B^2}+u^rC^\eta f\partial_{\xi,h}\tilde{v}_2-Bu^\xi\left(\partial_{r,h}C^\eta f\tilde{v}_2+C^\eta\frac{\mathrm{d}f}{\mathrm{d}r}\tilde{v}_2+C^\eta f\partial_{r,h}\tilde{v}_2\right)\\
&\left.-\frac{a^2B^2\left(a^2B^2-2\right)}{r^2}u^\eta f\tilde{v}_2\right]\mathrm{d}V\\
&+\oint_\Gamma\left[\left(\left\{\partial_{r,h}u^\eta\right\}+\frac{1}{r}\left\{u^\eta\right\}-B\left\{u^\xi\right\}\right)\boldsymbol{e}_r\cdot\boldsymbol{n}\right.\\
&\left.+\left(\frac{1}{B^2}\left\{\partial_{\xi,h}u^\eta\right\}+C^\eta\left\{u^r\right\}\right)\boldsymbol{e}_\xi\cdot\boldsymbol{n}\right]\cdot f\left[\!\left[\tilde{v}_2\right]\!\right]\mathrm{d}S\\
&+\nu\oint_\Gamma\left(\left\{\partial_{r,h}\tilde{v}_2\right\}\boldsymbol{e}_r+\frac{1}{B^2}\left\{\partial_{\xi,h}\tilde{v}_2\right\}\boldsymbol{e}_\xi\right)\cdot\boldsymbol{n}\,f\left[\!\left[u^\eta\right]\!\right]\,\mathrm{d}S\\
&+\nu\oint_\Gamma\eta_{\mathrm{SIP}}\left[\!\left[u^\eta\right]\!\right]\left[\!\left[\tilde{v}_2\right]\!\right]\,\mathrm{d}S\,, \qquad (6.41b)\\
\mathcal{A}_3\left(p,\boldsymbol{u},\tilde{v}_3\right) = &-\int_\Omega\left[\left(-\frac{1}{B}p+\frac{1}{B^2}\partial_{\xi,h}u^\xi+C^{\xi,r}u^r\right)f\partial_{\xi,h}\tilde{v}_3\right.\\
&+\partial_{r,h}u^\xi\left(\frac{\mathrm{d}f}{\mathrm{d}r}\tilde{v}_3+f\partial_{r,h}\tilde{v}_3\right)+u^\xi\left(\frac{\frac{\mathrm{d}f}{\mathrm{d}r}r-f}{r^2}\tilde{v}_3+\frac{f}{r}\partial_{r,h}\tilde{v}_3\right)\\
&\left.+\frac{aB}{r}u^\eta C^{\xi,\eta}\left(\partial_{r,h}f\tilde{v}_3+\frac{\mathrm{d}f}{\mathrm{d}r}\tilde{v}_3+f\partial_{r,h}\tilde{v}_3\right)-\frac{a^4B^4-1}{r^2}u^\xi f\tilde{v}_3\right]\mathrm{d}V\\
&+\oint_\Gamma\left[\left(\left\{\partial_{r,h}u^\xi\right\}+\frac{1}{r}\left\{u^\xi\right\}+C^{\xi,\eta}\frac{aB}{r}\left\{u^\eta\right\}\right)\boldsymbol{e}_r\cdot\boldsymbol{n}\right.\\
&\left.+\left(\frac{1}{B^2}\left\{\partial_{\xi,h}u^\xi\right\}+C^{\xi,r}\left\{u^r\right\}-\frac{1}{B}p\right)\boldsymbol{e}_\xi\cdot\boldsymbol{n}\cdot f\left[\!\left[\tilde{v}_3\right]\!\right]\right]\mathrm{d}S\\
&+\nu\oint_\Gamma\left(\left\{\partial_{r,h}\tilde{v}_3\right\}\boldsymbol{e}_r+\frac{1}{B^2}\left\{\partial_{\xi,h}\tilde{v}_3\right\}\boldsymbol{e}_\xi\right)\cdot\boldsymbol{n}\,f\left[\!\left[\left[\!\left[u^\xi\right]\!\right]\right]\!\right]\,\mathrm{d}S
\end{aligned}
$$

$$+\nu \oint_{\Gamma} \eta_{\mathrm{SIP}} \left[\!\left[u^{\xi} \right]\!\right] [\![\tilde{v}_3]\!] \, \mathrm{d}S \,, \tag{6.41c}$$

where, for brevity, we use the following abbreviations for the coefficients

$$\begin{aligned} C^{r,\eta} &:= -\frac{2abB}{r^2}\,, \qquad C^{\xi,r} := \frac{2b^2B}{r^3} = -C^{r,\xi}\,, \qquad C^{\eta} := \frac{2abB}{r^2} = -C^{r,\eta}\,, \\ C^{r,\xi} &:= -\frac{2b^2B}{r^3}\,, \qquad C^{\xi,\eta} := \frac{2bB}{r}\,. \end{aligned} \tag{6.42}$$

The first upper index corresponds to the momentum equation, whereas the second index indicates the corresponding velocity component. E.g.: $C^{r,\eta}$ is the coefficient of the u^{η} term in the r-momentum equation.

6.4 The temporal discretization

For the temporal discretization we use a semi-explicit scheme, given in Shahbazi et al. (2007). The main idea is to split the full spatial operator into a Stokes operator, which is discretized implicitly and a nonlinear term, which we implement explicitly. The reason for such a treatment of the temporal discretization is a resulting time-independent uniform grid. Using that, we have a great advantage in performance: we need to solve the Stokes system only once and can compute many time steps with low computational cost by evaluating the convective terms explicitly. We use first and third order BDF scheme for the transient term and a third-order extrapolation (**EX3**) for the nonlinear term in case of the third order BDF scheme. For a uniform timestep size Δt the Navier-Stokes equations (3.1) are discretized as follows

$$\mathcal{C}\left(\boldsymbol{u}^{n+1}, \tau\right) = 0 \qquad \forall \tau \in \mathbb{V}^0_{k,4} \tag{6.43a}$$

$$\begin{aligned} &\frac{\beta_0}{\Delta t} \int_{\Omega} \boldsymbol{u}^{n+1} \tilde{\boldsymbol{v}} \, \mathrm{d}V + \mathcal{A}\left(p^{n+1}, \boldsymbol{u}^{n+1}, \tilde{\boldsymbol{v}}\right) = \int_{\Omega} \left(\frac{\beta_1}{\Delta t} \boldsymbol{u}^{n} + \frac{\beta_2}{\Delta t} \boldsymbol{u}^{n-1} + \frac{\beta_3}{\Delta t} \boldsymbol{u}^{n-2} \right) \tilde{\boldsymbol{v}} \, \mathrm{d}V \\ &- \left(\gamma_1 \, n\left(\boldsymbol{u}^{n}, \boldsymbol{w}^{n}, \tilde{\boldsymbol{v}}\right) + \gamma_2 \, n\left(\boldsymbol{u}^{n-1}, \boldsymbol{w}^{n-1}, \tilde{\boldsymbol{v}}\right) + \gamma_3 \, n\left(\boldsymbol{u}^{n-2}, \boldsymbol{w}^{n-2}, \tilde{\boldsymbol{v}}\right) \right) \\ &\qquad \forall \tilde{\boldsymbol{v}} \in \mathbb{V}^0_{k,i},\ i = 1, \ldots 3 \end{aligned} \tag{6.43b}$$

where $\mathcal{A}$ is the bilinearform (6.41), $\mathbb{V}^0_{k,i}$ is the DG space defined in (6.34) and $\mathcal{C}$ is the discretized velocity divergence, given by (6.36). For a BDF scheme of first order the coefficients are given by $\beta_0 = 1, \beta_1 = \beta_2 = \beta_3 = 0$ and $\gamma_1 = 1, \gamma_2 = \gamma_3 = 0$, whereas for a BDF scheme of third order the coefficients are given by $\beta_0 = \frac{11}{6}, \beta_1 = 3, \beta_2 = -\frac{3}{2}, \beta_3 = \frac{1}{3}$ and $\gamma_1 = 3, \gamma_2 = -3, \gamma_3 = 1$ for the third-order extrapolation (**EX3**). The key advantage of this method is that the left-hand-side of (6.43b) is constant in time. Thus, we can use a direct solver and save the factorization which means that a computationally expensive factorization must be done only once.

6.5 Test cases

As a test case for the numerical implementation of the helically invariant system of Navier-Stokes equations we consider the following time-dependent manufactured solution, which is given by

$$u^r = \left(1 - e^{-r^2}\right) \sin(\xi) \cos(t), \tag{6.44a}$$

$$u^\xi = \left(2rBe^{-r^2} \cos\xi + \frac{B}{r}\left(1 - e^{-r^2}\right) \cos(\xi)\right) \cos(t), \tag{6.44b}$$

$$u^\eta = \left(1 - e^{-r^2}\right) \cos(\xi) \cos(t), \tag{6.44c}$$

$$p = \left(1 - e^{-r^2}\right) \sin(\xi) \cos(t). \tag{6.44d}$$

The present solution is periodic in $\xi-$direction and thus fulfills the periodicity conditions

$$u^j(r,\xi) = u^j(r,\xi + 2\pi) \qquad \text{for } j = r,\xi,\eta \tag{6.45}$$

and

$$p(r,\xi) = p(r,\xi + 2\pi). \tag{6.46}$$

Additionally, the manufactured solution (6.44) is divergence-free, i.e. the continuity equation is fulfilled. For this ansatz residual terms arise, which are implemented as source terms in the momentum equations of the helically invariant Navier-Stokes system. To test the steady Navier-Stokes system, we reduce the maufactured solution (6.44) by assuming $\cos(t) = 1$, which leads to the following expressions for the velocity and pressure

$$u^r = \left(1 - e^{-r^2}\right) \sin(\xi), \tag{6.47a}$$

$$u^\xi = 2rBe^{-r^2} \cos\xi + \frac{B}{r}\left(1 - e^{-r^2}\right) \cos(\xi), \tag{6.47b}$$

$$u^\eta = \left(1 - e^{-r^2}\right) \cos(\xi), \tag{6.47c}$$

$$p = \left(1 - e^{-r^2}\right) \sin(\xi). \tag{6.47d}$$

The second transient test case that we use in this thesis is the exact solution that we derived in section 5.1, given by equations (5.19).

7 Convergence studies on a cylindrical shell and results

In the present chapter, the computational domain will be restricted to a cylindrical shell, i.e. the centerline axis is excluded and the radial coordinate will be $R_0 \leq r \leq R_1$, where $R_0 > 0$. The focus of this chapter lies on the verification of the DG discretization that was shown previously. Therefore in Section 6.5 a benchmark test, given by a manufactured solution is constructed which is used for the spatial and temporal convergence studies in sections 7.2 and 7.3.

7.1 The condition number of the operator matrix

To the best of the author's knowledge, there are no investigations of the existence and uniqueness of solutions of the helically invariant system of Navier-Stokes equations (3.19). However, recent research has shown that exact solutions exist, which is one crucial hint for the well-posedness of the system. In this section we show that the condition number is finite and hence is acceptable even for fine meshes.

The condition number κ of a matrix $\boldsymbol{T}$, with respect to a matrix norm $\|\cdot\|_*$ is given by

$$\kappa(\boldsymbol{T}) = \|\boldsymbol{T}\|_* \|\boldsymbol{T}^{-1}\|_*, \tag{7.1}$$

which we compute by using MATLAB's command *"condest"* for sparse matrices. The algorithm that MATLAB uses is based on the 1-norm estimator of Hager, given in Hager (1984).

We compute the condition numbers of the full spatial operator which results from the DG discretization of the steady helically invariant Navier-Stokes equations (3.19) presented in Section (6) for various grids consisting of 4×4 cells to 32×32 cells and different DG degrees varying between $k = 1$ and $k = 3$.

It turns out that the slope of the lines in Figure 7.1 is less than $|m| = 2$ and approximately independent of the DG degree. The largest condition number for DG degree $k = 3$ and 1024 cells is $\kappa \approx 10^5$, which is feasible for the given grid.

7.2 Spatial convergence studies

For the spatial convergence study we consider a uniform Cartesian grid with 4×4 cells for the coarsest and 64×64 cells for the finest grid. Since the computational domain is rectangular, each cell also has a rectangular shape and we may choose the shortest edge as the cell size, i.e. $h = \min(\mathrm{d}r, \mathrm{d}\xi)$. The convergence study was performed for each component of the helical velocity vector $\mathbf{u}$, as well as for the pressure p. We

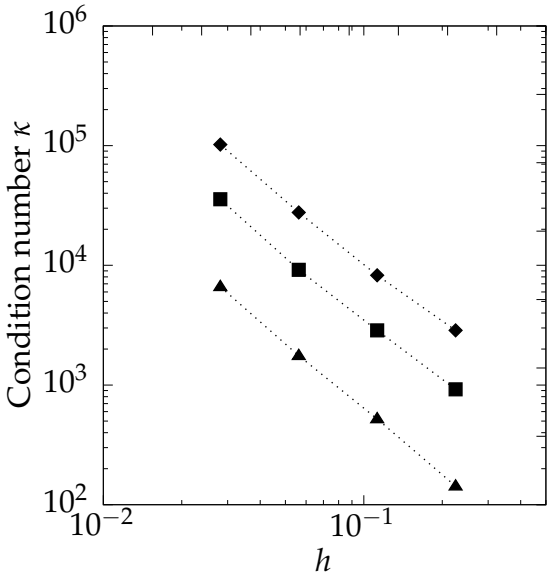

k	$\lvert m \rvert$
1	1.83
2	1.75
3	1.73

Figure 7.1: Condition numbers of the spatial operator matrix versus grid spacing h for polynomial degrees degrees $k = 1, \ldots, 3$ and $k' = 0, \ldots, 2$, respectively. The mesh is varied from 4×4 up to 32×32 cells. Mixed order formulation. The absolute value of the slope $|m|$ of each line is less than $|m| = 2$ for all polynomial degrees.

investigate different polynomial orders, varying from $k = 1$ to $k = 3$ for the velocity and $k' = 0, \ldots, 2$ for the pressure. For each DG degree and each velocity component we obtain the convergence rate of $k + 1$, which we expect from theory. For the pressure p we observe super-convergence due to (i) a highly regular mesh in the whole fluid domain and (ii) the fact, that we use the exact solution (6.47) of the problem on all boundaries (cf. Fig. 7.2).

In addition to that, we present an equal order formulation of the spatial discretization of the system (3.19). In order to control pressure jumps across interfaces, we add an addtional stability term in the continuity equation (6.35a), as proposed in Di Pietro and Ern (2011). Hence, the continuity equation reads

$$c\left(\boldsymbol{u}, \tau\right) + \lambda_{\text{Stab}}\left(p, \tau\right) = 0 \qquad \forall \tau \in \mathbb{V}_k^0, \tag{7.2}$$

where the stabilization term is given by

$$\lambda_{\text{Stab}}\left(p, \tau\right) := \oint_\Gamma h_\Gamma \left[\!\left[p\right]\!\right] \left[\!\left[\tau\right]\!\right] f(r) \, \mathrm{d}S. \tag{7.3}$$

Herein, h_F is a local length scale for which we choose the longest edge of each cell, i.e. $\max\left(\Delta r, \Delta\xi\right)$. As before, $f(r)$ is the metric function, which is set to $f(r) = 1$ for computations on the cylindrical shell. Figure 7.3 shows the results of a $h-$convergence study, using analogous settings as in the studies for the mixed-order DG formulation shown in Figure 7.2. Comparing both convergence studies, the results for the velocity components are rather similar. Concerning the pressure, the mixed-order formulation

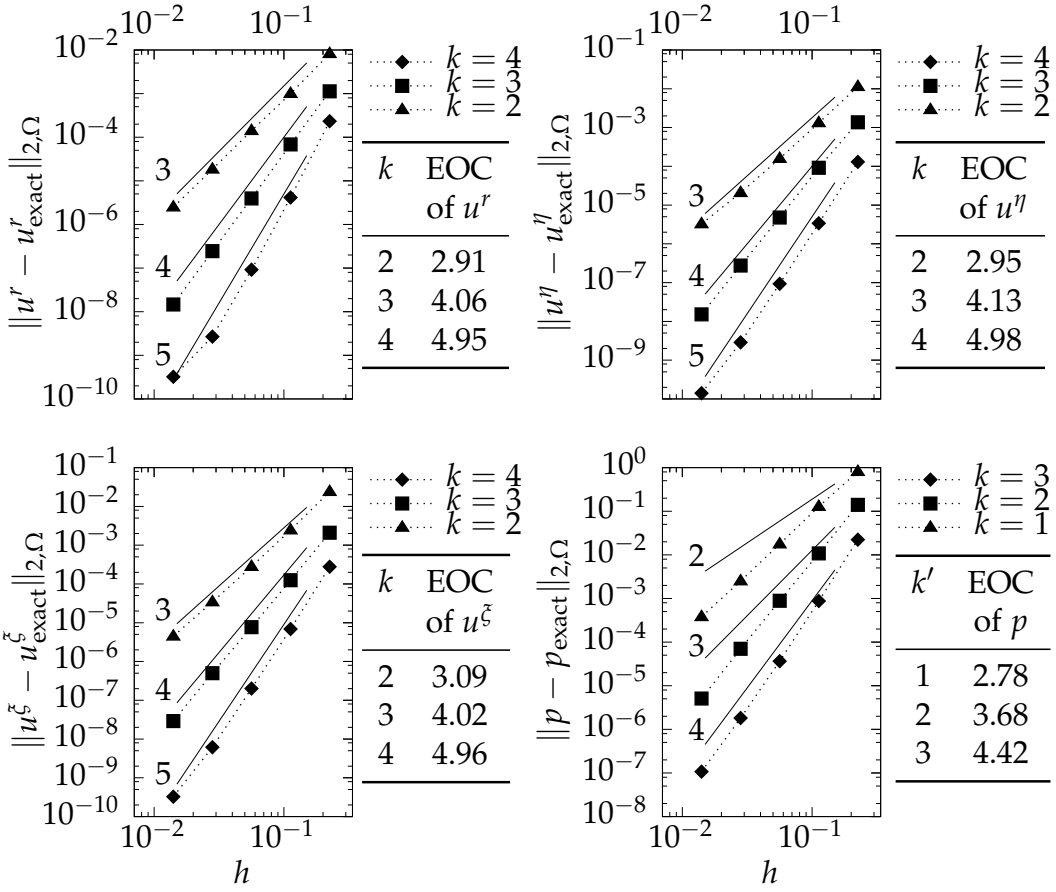

Figure 7.2: L^2 norm errors, measured with respect to the manufactured solution (6.47) for the velocity $\boldsymbol{u}$ and pressure p v.s. the grid size h. For comparison the solid lines are plotted to show the slopes $m = (3,4,5)$ for the velocity and $m = (2,3,4)$ for the pressure, respectively. Computations for $4 \times 4, \ldots, 64 \times 64$ cells and DG degrees $k = 1, \ldots, 3$ and $k' = 0, \ldots, 2$ on a domain $\Omega = [r \times \xi] = [0.1, \ldots, 1 \times 0, \ldots, 2\pi]$. Mixed order formulation.

shows better results for low DG degrees, whereas for DG degree $k = 4$ also the equal order formulation reaches approximately the expected convergence rate. Due to these results, we subsequently will keep the focus on the mixed-order formulation.

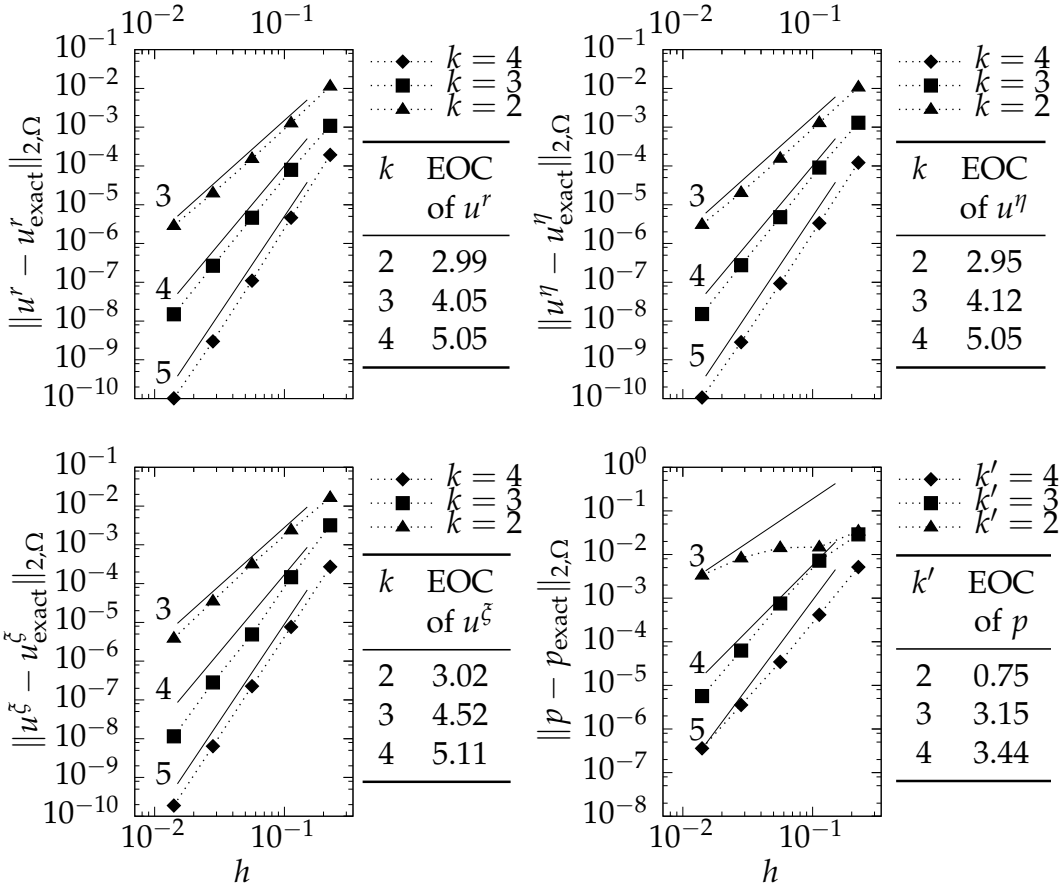

Figure 7.3: L^2 norm errors, measured with respect to the manufactured solution (6.47) for the velocity $\boldsymbol{u}$ and pressure p v.s. the grid size h. Computations for $4 \times 4, \ldots, 64 \times 64$ cells and DG degrees $k = k' = 2, \ldots, 4$ on a domain $\Omega = [r \times \xi] = [0.1, \ldots, 1 \times 0, \ldots, 2\pi]$. Equal order formulation with pressure stabilization in the continuity equation (7.2).

7.3 Temporal convergence study

For the temporal discretization we consider a BDF scheme of third order with time step sizes from $\Delta t = 3.125 \times 10^{-2}$ to $\Delta t = 0.25$. The polynomial order is chosen to be $k = 4$ for the velocity and $k' = 3$ for the pressure. All computations are conducted on a grid of 32×32 cells, such that the temporal error dominates the error of the spatial operator. For all physical quantities, i.e. all velocity components and the pressure the expected convergence rate of three is approximately obtained (cf. Figure 7.4).

Furthermore, we consider a temporal convergence study using the exact solution (5.21) of the helically invariant Navier-Stokes equations (3.19) to verify the accuracy of the semi-explicit timestepping method presented in section 6.4. The computational domain

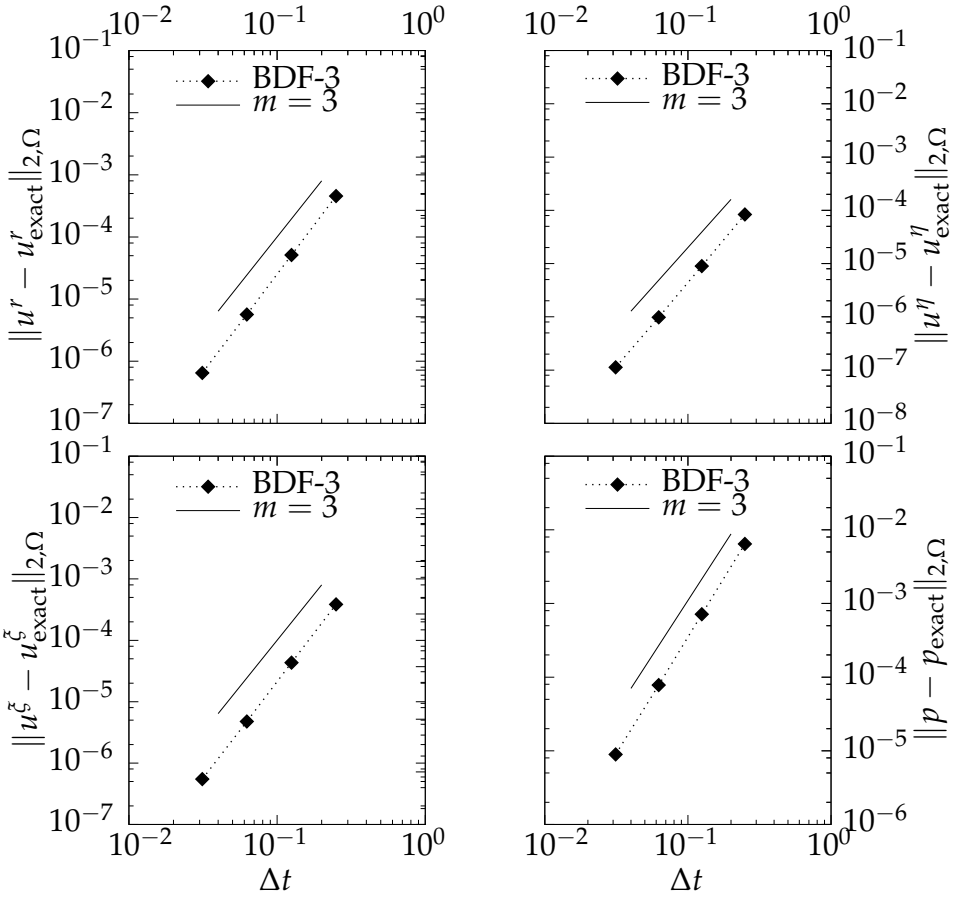

Figure 7.4: Temporal convergence studies, using the test case (6.44). The L^2 norm errors are plotted for the velocity $\boldsymbol{u}$ and pressure p v.s. the time step size Δt. Computations for 32×32 cells and DG degrees $k = 4$ and $k' = 3$ on a domain $\Omega = [r \times \xi] = [0.1, \ldots, 1 \times 0, \ldots, 2\pi]$. Mixed order formulation.

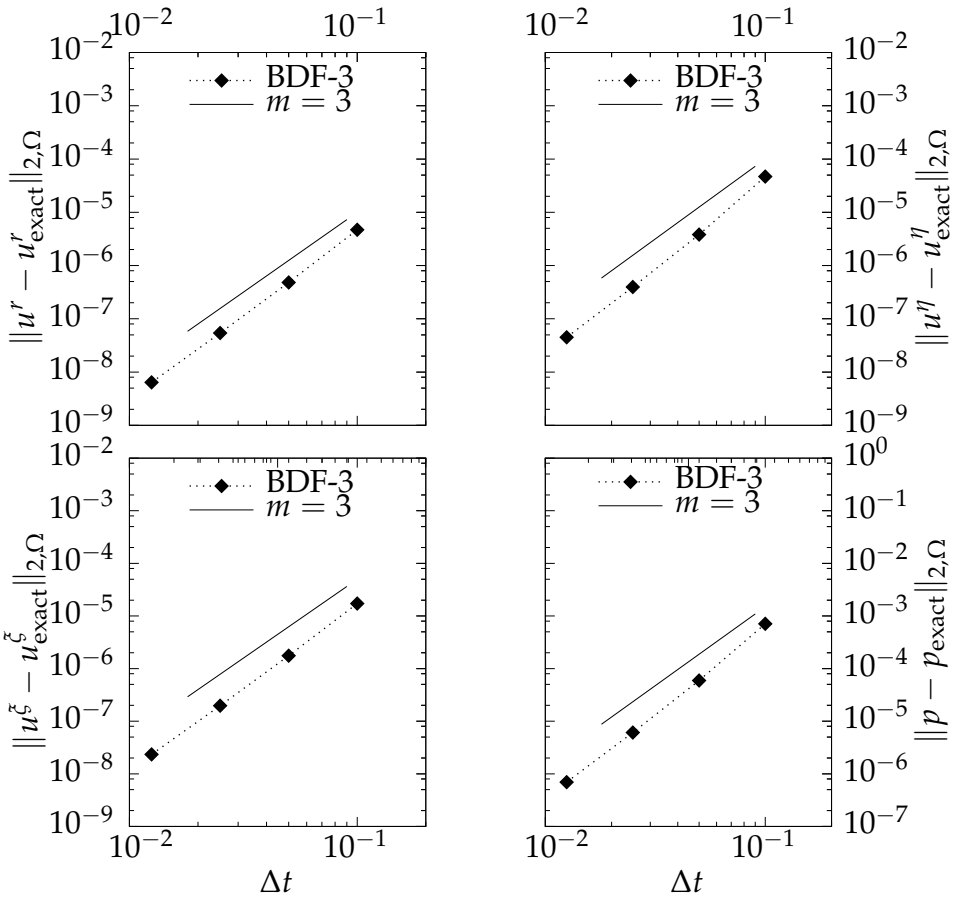

Figure 7.5: Temporal convergence studies for the velocity $\boldsymbol{u}$ and pressure p v.s. the time step size Δt. The calculation of the L^2 norm errors is based on the exact solution (5.21). Computations for 16×16 cells and DG degrees $k = 4$ and $k' = 3$ on a cylindrical shell $\Omega = [r \times \xi] = [1, \ldots, 2 \times 0, \ldots, 2\pi]$. Mixed order formulation.

for the present benchmark test is set to $\Omega = [r \times \xi] = [1 \ldots 2 \times 0 \ldots 2\pi]$, avoiding a range around the centerline axis $r = 0$ where the exact solution is not defined. The Navier-Stokes equations are solved for a viscosity $\nu = 1$ and helical parameters $a = 1$ and $b = 1$. Further parameters involved in the exact solution are set to $A = 1$ and $t_0 = 1$. The mixed order formulation of polynomial degrees $k = 4$ for the velocity and $k' = 3$ for the pressure is used. The mesh consists of 16×16 cells and time step sizes varying from $\Delta t = 0.1$ to $\Delta t = 0.0125$ are considered, such that the temporal error dominates the spatial error. The number of time steps are $n_s = 5, 10, 20, 40$, which results in a total integration time $T = 0.5$. The temporal convergence rate that is expected from theory has been obtained for all variables (cf. Figure 7.5). The L^2 norm errors for the velocity e_u and the pressure e_u are calculated as follows

$$e_u = \|\boldsymbol{u}^{n_s} - \boldsymbol{u}_h\,(n_s \Delta t)\|^2_{L^2(\Omega)}\,, \qquad e_p = \|p^{n_s} - p_h\,(n_s \Delta t)\|^2_{L^2(\Omega)}\,, \tag{7.4}$$

where $\boldsymbol{u}^{n_s}$, p^{n_s} is the exact solution at $t = n_s \Delta t$.

8 Convergence studies on the full domain and results

In this section we consider the DG discretization of the helically invariant Navier-Stokes equations (3.19) in the full cylindrical domain, including the centerline axis at $r = 0$. In this case the DG approximation is based on the DG space $\mathbb{V}_k^0$ defined in table 6.1 ensuring the centerline conditions that have been introduced in section 6.3.1. At the beginning of this chapter we present a method to reduce the DOFs of the DG discretization at $r = 0$, which is equivalent to a change of the DG basis and is the result of the conditions (6.25).

8.1 Implementation of the reduced DG space $\mathbb{V}_k^0$

In each timestep the evaluation of the spatial operator and the matrix assembly rely on in the DG space $\mathbb{V}_k$. Since the reduced DG space $\mathbb{V}_k^0$ is a linear subspace of the DG space $\mathbb{V}_k$, i.e. $\mathbb{V}_k^0 \leq_{\mathbb{R}} \mathbb{V}_k$, a basis $\boldsymbol{\Psi}^{\boldsymbol{B}}$ of $\mathbb{V}_k^0$ can readily be written as $\boldsymbol{\Psi}^{\boldsymbol{B}} = \boldsymbol{\Phi}^{\boldsymbol{B}} \cdot \boldsymbol{A}$, where $\boldsymbol{\Phi}^{\boldsymbol{B}}$ is a basis of $\mathbb{V}_k$ and $\boldsymbol{A} \in \mathbb{R}^{\dim(\mathbb{V}_k)\times\dim\left(\mathbb{V}_k^0\right)}$ is a non-quadratic matrix. The reduction of the DG space can be done component-wise for each component of the velocity vector $\boldsymbol{u}$ as well as for the pressure p. In the following we distinguish two different cases of DG space reductions. In the first case we discuss the DG space reduction using the conditions (6.25a,b), which are cell-local conditions. The second case is a global DG space reduction where the conditions, given by (6.25c,d) are used. Hence the first case is more restrictive and is implemented locally on each cell at the centerline, whereas the second case represents a global relation connecting the neighboring cells in ξ-direction at $r = 0$.

8.1.1 Case 1: Cell-local reduction of the DG space $\mathbb{V}_k$

In this first case the two centerline conditions $u^r = 0$ and $u^\xi = 0$ are implemented. Let $\left(\Phi_{j,1}^B, \ldots, \Phi_{j,N_k}\right)$ be a basis of a DG space of degree k in cell K_j which is located at the centerline $r = 0$, i.e. $\overline{K_j} \cap (\{0\} \times \mathbb{R}) \neq 0$. For both velocity components u^i, with $i = \{r, \xi\}$, we consider the ansatz $u^i(r,\xi) = \sum_{n=1}^{N_k} \Phi_{j,n}^B(r,\xi)\, \tilde{u}_{j,n}^i \stackrel{!}{=} 0$ for $r = 0$ and the nodes at the centerline in K_j $\xi = \xi_1, \xi_2, \ldots, \xi_{N_k+1}$, where $\xi_1 < \xi_2 < \ldots < \xi_{N_k+1}$ and $(0, \xi_k) \in \overline{K_j}$. The ansatz leads to a system of equations, given by

$$\underbrace{\begin{bmatrix} \Phi_{j,1}^B(0,\xi_1) & \cdots & \Phi_{j,N_k}^B(0,\xi_1) \\ \vdots & & \vdots \\ \Phi_{j,1}^B(0,\xi_{N_k+1}) & \cdots & \Phi_{j,N_k}^B(0,\xi_{N_k+1}) \end{bmatrix}}_{\boldsymbol{B}} \begin{bmatrix} \tilde{u}_{j,1}^i \\ \vdots \\ \tilde{u}_{j,N_k}^i \end{bmatrix} = \boldsymbol{0}, \tag{8.1}$$

for the velocity components u^r and u^ξ. Equation (8.1) is a linear system of the form $\boldsymbol{B}\,\tilde{\boldsymbol{u}} = \boldsymbol{0}$, where $\boldsymbol{B}$ denotes the matrix of the basis functions, evaluated at the centerline $r = 0$. In a next step we need to find a matrix $\boldsymbol{A} \in \mathbb{R}^{\dim(\mathbb{V}_k)\times\dim\left(\mathbb{V}_k^0\right)}$ such that the columns of $\boldsymbol{A}$ represent a solution of (8.1), i.e. $\boldsymbol{B}\cdot\boldsymbol{A} = \boldsymbol{0}$. Using that, it follows that

$$\left(\Psi_{j,1},\ldots,\Psi_{j,l}\right) = \left(\Phi_{j,1},\ldots,\Phi_{j,N_k}\right)\boldsymbol{A} \tag{8.2}$$

is a basis which fulfills the centerline conditions (6.25a,b). The matrix $\boldsymbol{A}$ can be obtained e.g. from the row echelon form of $\boldsymbol{B}$, which is a generalized Gaussian elimination.

8.1.2 Case 2: Global reduction of the DG space $\mathbb{V}_k$

In the second case the centerline conditions, given by (6.25c,d) are implemented. The implementation is divided into two steps. In the first step we proceed in anlogy to the first case. The DG space is locally reduced in each cell at the centerline but this time using the $\xi-$derivative of the basis functions $\partial_\xi\Phi^B_{j,k}$. Hence, in this case the system of equations $\boldsymbol{B}\,\tilde{\boldsymbol{u}} = \boldsymbol{0}$ is given by

$$\begin{bmatrix} \partial_\xi\Phi^B_{j,1}\left(0,\xi_1\right) & \cdots & \partial_\xi\Phi^B_{j,N_k}\left(0,\xi_1\right) \\ \vdots & & \vdots \\ \partial_\xi\Phi^B_{j,1}\left(0,\xi_{N_k+1}\right) & \cdots & \partial_\xi\Phi^B_{j,N_k}\left(0,\xi_{N_k+1}\right) \end{bmatrix} \begin{bmatrix} \tilde{u}^i_{j,1} \\ \vdots \\ \tilde{u}^i_{j,N_k} \end{bmatrix} = \boldsymbol{0}. \tag{8.3}$$

From that, a matrix $\boldsymbol{A}^*$ can be obtained in analogy to the proceeding in section 8.1.1. In the second step we connect the neighboring cells at $r = 0$. For that, we consider two cells K_j and K_l and demand that

$$u^\eta\left(0,\xi_1\right) = u^\eta\left(0,\xi_2\right), \tag{8.4}$$

for nodes $(0,\xi_1) \in \overline{K_j}$ and $(0,\xi_2) \in \overline{K_l}$. The same condition is used for the pressure p. Using the polynomial DG ansatz, (8.4) can be written as

$$\Bigg[\underbrace{\Phi^B_{j,1}\left(0,\xi_1\right),\ldots,\Phi^B_{j,N_k}\left(0,\xi_1\right),-\Phi^B_{l,1}\left(0,\xi_2\right),\ldots,-\Phi^B_{l,N_k}\left(0,\xi_2\right)}_{\left[\boldsymbol{B}_1^*,\,-\boldsymbol{B}_2^*\right]}\Bigg] \cdot \begin{bmatrix} \tilde{u}^\eta_{j,1} \\ \vdots \\ \tilde{u}^\eta_{j,N_k} \\ \tilde{u}^\eta_{l,1} \\ \vdots \\ \tilde{u}^\eta_{l,N_k} \end{bmatrix} = \boldsymbol{0}. \tag{8.5}$$

Just as before, a matrix $\boldsymbol{R}$ needs to be determined such that the following transformation holds

$$\underbrace{\begin{bmatrix} \boldsymbol{I} & \boldsymbol{0} \\ \boldsymbol{R}_{21} & \boldsymbol{R}_{22} \end{bmatrix}}_{\boldsymbol{R}} \begin{bmatrix} \tilde{u}^{\eta}_{j,1} \\ \vdots \\ \tilde{u}^{\eta}_{j,N_k} \\ \tilde{u}^{\eta}_{l,1} \\ \vdots \\ \tilde{u}^{\eta}_{l,N_k} \end{bmatrix} = \begin{bmatrix} \tilde{u}^{*\eta}_{j,1} \\ \vdots \\ \tilde{u}^{*\eta}_{j,N_k} \\ \tilde{u}^{*\eta}_{l,1} \\ \vdots \\ \tilde{u}^{*\eta}_{l,N_k} \end{bmatrix}, \tag{8.6}$$

where $\tilde{u}^{*\eta}_{j,1}, \ldots, \tilde{u}^{*\eta}_{l,N_k}$ are the DG coordinates in the reduced DG space. The transformation is constructed as such that the coordinates in cell K_j are maintained. Similar to section 8.1.1 we find the solution space of $[\boldsymbol{B}^*_1,\ -\boldsymbol{B}^*_2]$ through a solution of

$$[\boldsymbol{B}^*_1,\ -\boldsymbol{B}^*_2] \begin{bmatrix} \boldsymbol{I} & \boldsymbol{0} \\ \boldsymbol{R}_{21} & \boldsymbol{R}_{22} \end{bmatrix} = \boldsymbol{0}. \tag{8.7}$$

It follows that the block $\boldsymbol{R}_{22}$ is determined by the solution space of $\boldsymbol{B}^*_2$ and $\boldsymbol{R}_{21}$ can be obtained by the solution of

$$\boldsymbol{B}^*_2 \cdot \boldsymbol{R}_{21} = \boldsymbol{B}^*_1, \tag{8.8}$$

using the least squares method for underdetermined systems. The final transformation matrix $\boldsymbol{Q}$ that combines both steps (i) the cell-local reduction by evaluation of the $\xi-$derivatives of the basis functions and (ii) the reduction connecting neighbor cells is given by

$$\boldsymbol{Q} = \boldsymbol{A}^* \cdot \boldsymbol{R}. \tag{8.9}$$

8.2 The condition number

In this section we consider the condition number of the operator matrix obtained from the DG discretization and investigate the behaviour for different grid sizes and DG degrees. In Figure (8.1) it is shown that the values of the condition numbers as well as the growth, measured by the slope decrease significantly by the introduction of a penalty scaling which we denote as $s_P(r)$. In the present case we choose $s_P(r) = B(r)^2$ with B being the geometric function defined in (3.15f). Hence, the penalty terms in the discretization of the viscous part (6.41) are given by

$$\oint_{\Gamma} \eta_{\mathrm{SIP}}\, s_P(r) \left[\!\left[u^i\right]\!\right] \left[\!\left[v_j\right]\!\right] \,\mathrm{d}S \tag{8.10}$$

where u^i with $i = \{r, \xi, \eta\}$ denotes the three helical velocity components and $j = \{1, 2, 3\}$ the three test functions used in the corresponding momentum equations. For the present studies on the condition number, the centerline conditions (6.25) and the implementation for the reduced DG space $\mathbb{V}^0_K$ are used. At the outer boundary, i.e. at $r = 1$ we use the manufactured solution (6.47) as a Dirichlet boundary condition which has already been applied for testing the discretization of the steady Navier-Stokes equations in the helically symmetric frame. The grid is varied from 4×4 up to 32×32

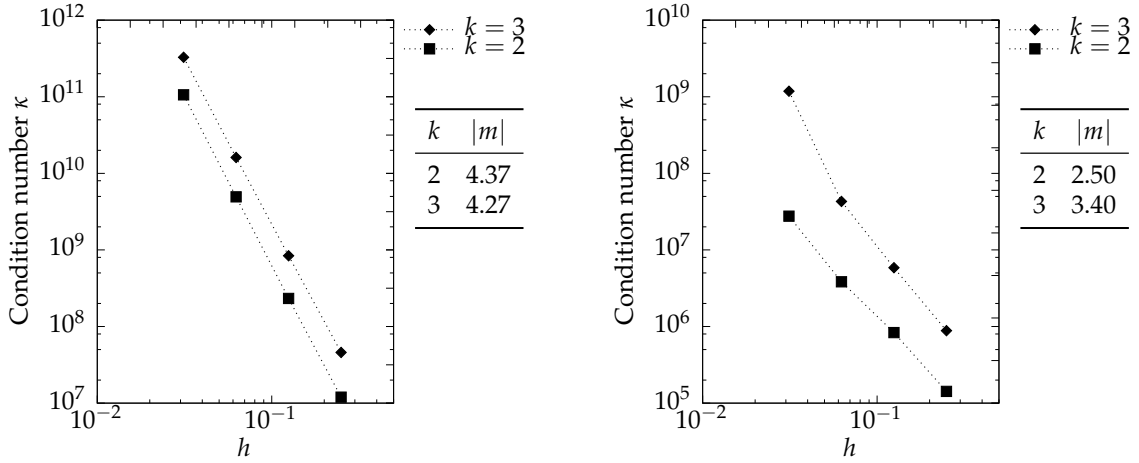

Figure 8.1: Condition numbers κ of the operator matrix over the grid size h (a) without a penalty scaling and (b) using a penalty scaling of $B(r)^2$. Mixed order formulation with polynomial degrees $k = (2, 3)$ for the velocities and $k' = (1, 2)$ for the pressure.

cells and the polynomial degrees are chosen to be $k = 2$ and $k = 3$ for the velocities and $k' = 1$ and $k' = 2$ for the pressure, respectively. Figure 8.1a shows the results without a scaling, i.e. $s_P = 1$ whereas in Figure 8.1b the results for a penalty scaling $s_P = B(r)^2$ are presented.
The choice of the penalty scaling may not yet be optimal, so that the task of future research remains to find better scalings that further reduce the values and the growth of the condition numbers.

8.3 Convergence studies

As before for the cylindrical shell domain, we present a spatial and temporal convergence study for our test case (6.47). Since in the full cylindrical domain, in order to remove singularities in the coefficients of the helically invariant Navier-Stokes equations (3.19), the PDEs are multiplied by a metric function $f = B^2(r)$ (with $B(r)$ defined in (3.15f)). Hence, we introduce the following norm, given by

$$\left\| u^i - u^i_{\text{exact}} \right\|_B := \left\| B(r) \left(u^i - u^i_{\text{exact}} \right) \right\|_2, \tag{8.11}$$

where the numerical errors are scaled by the metric function $B(r)$ and the u^i denote the components of the velocity vector, i.e. u^r, u^ξ and u^η.

Since the solution of the pressure is only unique up to a constant c, we need to find c such that

$$\int_\Omega \left(p_{\text{err}} - c \right)^2 B(r)^2 \, \mathrm{d}\Omega \quad \rightarrow \quad \min, \tag{8.12}$$

where $p_{\text{err}} = p - p_{\text{exact}}$. A quick calculation shows that

$$c = \frac{\int_\Omega p_{\text{err}} B(r)^2 \, \mathrm{d}\Omega}{\int_\Omega B(r)^2 \, \mathrm{d}\Omega}. \tag{8.13}$$

8.3.1 Spatial convergence study

In Fig. 8.2 convergence plots for the mixed order formulation are presented. In particular for DG degrees $k = 2$ and $k = 3$, the convergence rates are very close to what we expect from theory. Fig. 8.3 shows convergence plots for the equal order formulation. Here, for the velocity components of polynomial degrees $k = 2$ and $k = 3$ the expected convergence rate is reached. The pressure converges with a rate of $EOC \propto h^p$.

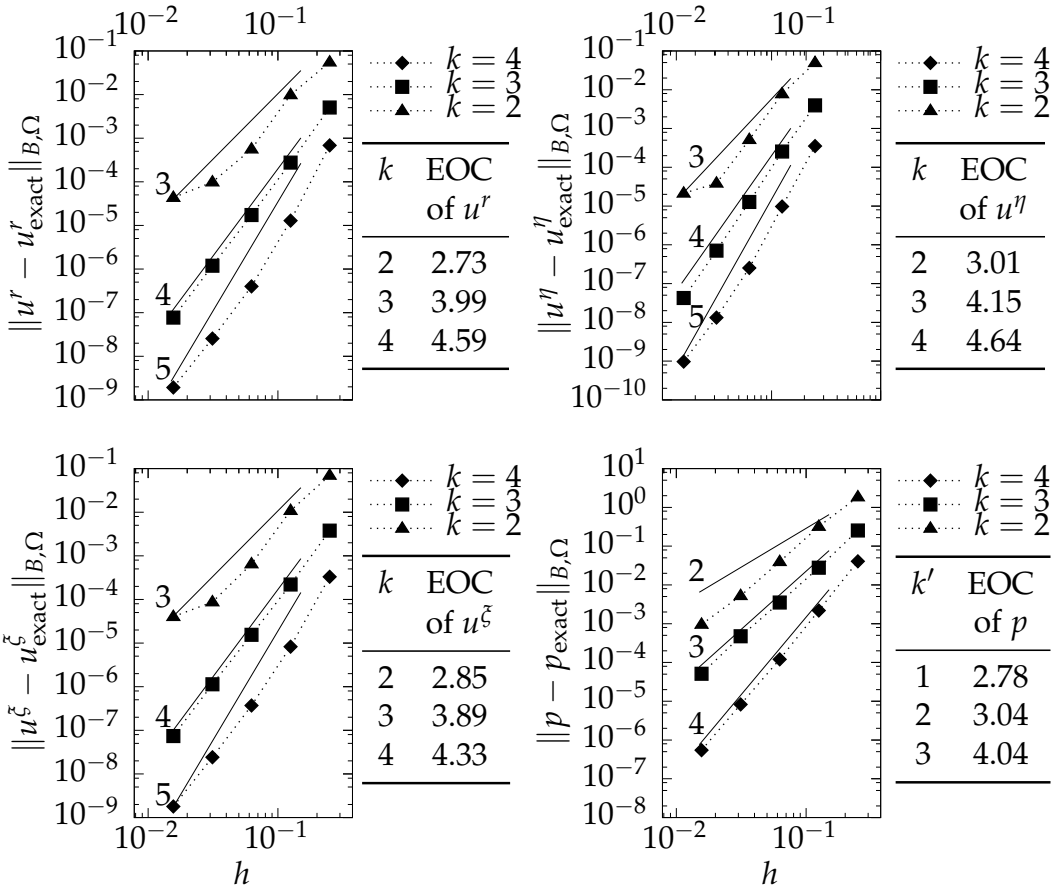

Figure 8.2: Numerical errors, measured in the $B-$norm defined by (8.11) with respect to the manufactured solution (6.47). The errors for the velocity $\boldsymbol{u}$ and pressure p are plotted v.s. the grid size h. Computations for $4 \times 4, \ldots, 64 \times 64$ cells and DG degrees $k = 2 \ldots 4$ and $k' = 1, \ldots, 3$ on the full domain $\Omega = [r \times \xi] = [0, \ldots, 1 \times 0, \ldots, 2\pi]$. Mixed order formulation.

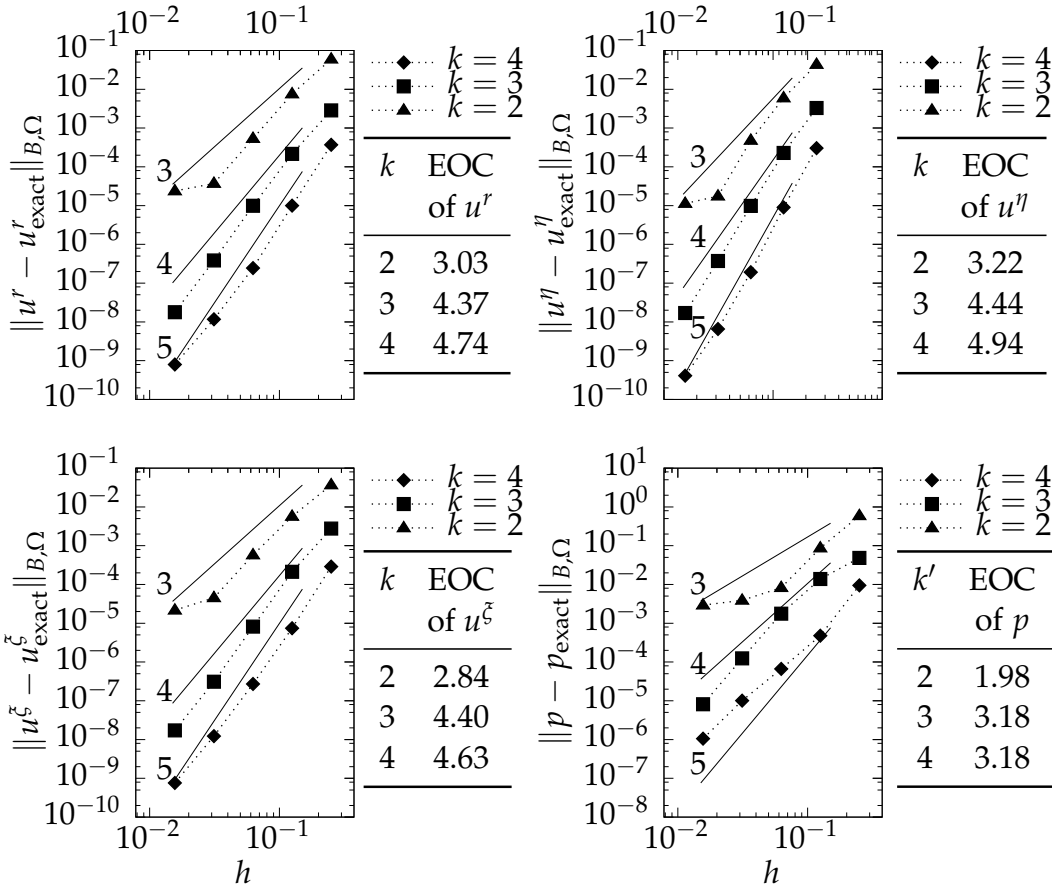

Figure 8.3: Numerical errors, measured in the $B-$norm defined by (8.11) with respect to the manufactured solution (6.47). The errors for the velocity $\boldsymbol{u}$ and pressure p are plotted v.s. the grid size h. Computations for $4 \times 4, \ldots, 64 \times 64$ cells and DG degrees $k = k' = 2, \ldots, 4$ on the full domain $\Omega = [r \times \xi] = [0, \ldots, 1 \times 0, \ldots, 2\pi]$. Equal order formulation.

8.3.2 Temporal convergence study

As before in section 7.3, we consider the temporal convergence rates of the numerical discretization of the transient PDEs using the semi-explicit BDF3 scheme introduced in 6.4. For time step sizes from $\Delta t = 3 \times 10^-2$ to $\Delta t = 0.25$, the polynomial order $k = 4$ and $k' = 3$ for the velocity and pressure and a spatial grid consisting of 32×32 cells, we obtain the expected convergence rate for a third-order time integration scheme on the full cylindrical computational domain, which is shown in Fig. 8.4

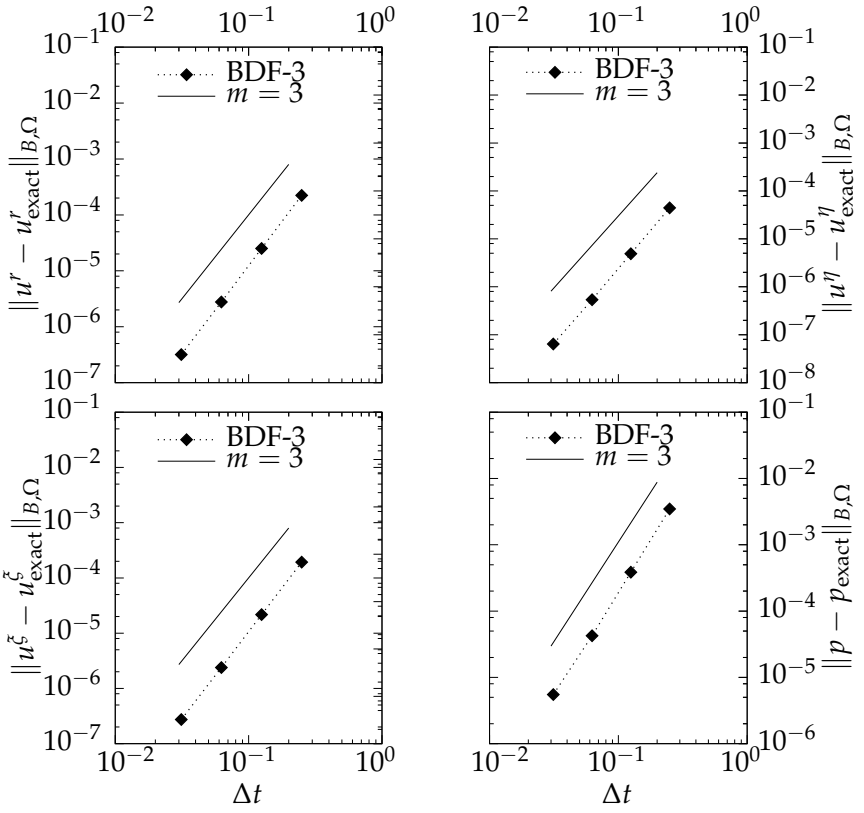

Figure 8.4: Temporal convergence studies, using the test setup (6.44). The numerical errors are measured in the $B-$norm, defined by (8.11). The velocity $\boldsymbol{u}$ and pressure p is plotted v.s. the time step size Δt. Computations for 32×32 cells and DG degrees $k = 4$ and $k' = 3$ on a full cylindrical domain $\Omega = [r \times \xi] = [0, \ldots, 1 \times 0, \ldots, 2\pi]$. Mixed order formulation.

9 Direct numerical simulations and results

In this chapter, we apply the newly developed DG code to perform direct numerical simulations of helically invariant flows at Reynolds numbers around $Re = 2400$. We perform two different simulations. In the first simulation (I) a forcing is applied by boundary conditions which are periodic in ξ-direction. For the second simulation (II) a shearing is employed through initial conditions. In that case Kelvin-Helmholtz instabilities are observed. Finally for simulation (I) the temporal evolution of the energy spectra is discussed. In addition to the convergence studies in chapters 7 and 8, these physically meaningful results also verify a correct DG discretization of the helically invariant Navier-Stokes equations.

9.1 Two simulations of helically invariant flows

In simulation (I) we consider a parameter domain $(r \times \xi) = [0, \ldots, 4 \times 0, \ldots, 2\pi]$ with the following BCs

$$u^r = -\frac{r}{2}\cos(\xi), \tag{9.1a}$$
$$u^\eta = K_P \cos(\xi), \tag{9.1b}$$
$$u^\xi = B(r)\sin(\xi), \tag{9.1c}$$
$$p = 0, \tag{9.1d}$$

where $K_P = 2$ and $B(r)$ the geometric function (3.15f). At the left boundary (where $r = 0$) a zero gradient condition in radial direction is assumed. The initial conditions are given by

$$u^r = 0, \tag{9.2a}$$
$$u^\eta = K_P \left(2 - \left(\frac{r}{4}\right)^2\right)\cos(\xi), \tag{9.2b}$$
$$u^\xi = K_P \left(2 - \left(\frac{r}{4}\right)^2\right)\sin(\xi), \tag{9.2c}$$
$$p = 0, \tag{9.2d}$$

such that the maximal velocity is given by $u_0^{\max} = 4$. The viscosity is chosen to be $\nu = 6.5 \cdot 10^{-3}$ which leads to a Reynolds number $Re = \frac{u_0^{\max} L_r}{\nu} = 2461$. We choose a polynomial degree of $k = 5$ for the velocity and $k' = 4$ for the pressure, respectively. The grid consists of 100 cells in each direction resulting in $7.8 \cdot 10^5$ DoF. The simulation is conducted with a time step size of $\Delta t = 10^{-5}$ for $n_s = 10^5$ time steps such that we

have a total simulation time of $T = 1\ s$. The result is presented in Figure 9.1, where the velocity component u^η is shown at different times t. One may observe the evolution of a vortex that is formed in the top left corner of the computational domain.

In simulation (II) we consider a shear flow, where the initial conditions for velocity and pressure are given by

$$u^\eta = u^\xi = \begin{cases} K_S \cdot r & \text{for } r \leq \frac{L_r}{2} \\ 0.1 \cdot (2 - r) & \text{for } r > \frac{L_r}{2} \end{cases}, \tag{9.3a}$$

$$u^r = p = 0. \tag{9.3b}$$

We choose $K_S = 8$ and for the radial length of the domain $L_r = 2$. Further parameters for the simulation are assumed as follows: time step size $\Delta t = 10^{-4}$, spatial domain $(r \times \xi) = [0, \ldots, 2 \times 0, \ldots, 2\pi]$, boundary conditions $\boldsymbol{u} = 0$ at $r = 2$ and $\nabla \boldsymbol{u} \cdot \boldsymbol{e}_r = \mathbf{0}$ at $r = 0$, viscosity $\nu = 6.7 \cdot 10^{-3}$, the Reynolds number $Re = 2388$, and a polynomial degree $k = 5$ and $k' = 4$ for the DG approximation. In Figure 9.2 snapshots at different times of the development of Kelvin-Helmholtz instabilities are shown for the velocity component u^η.

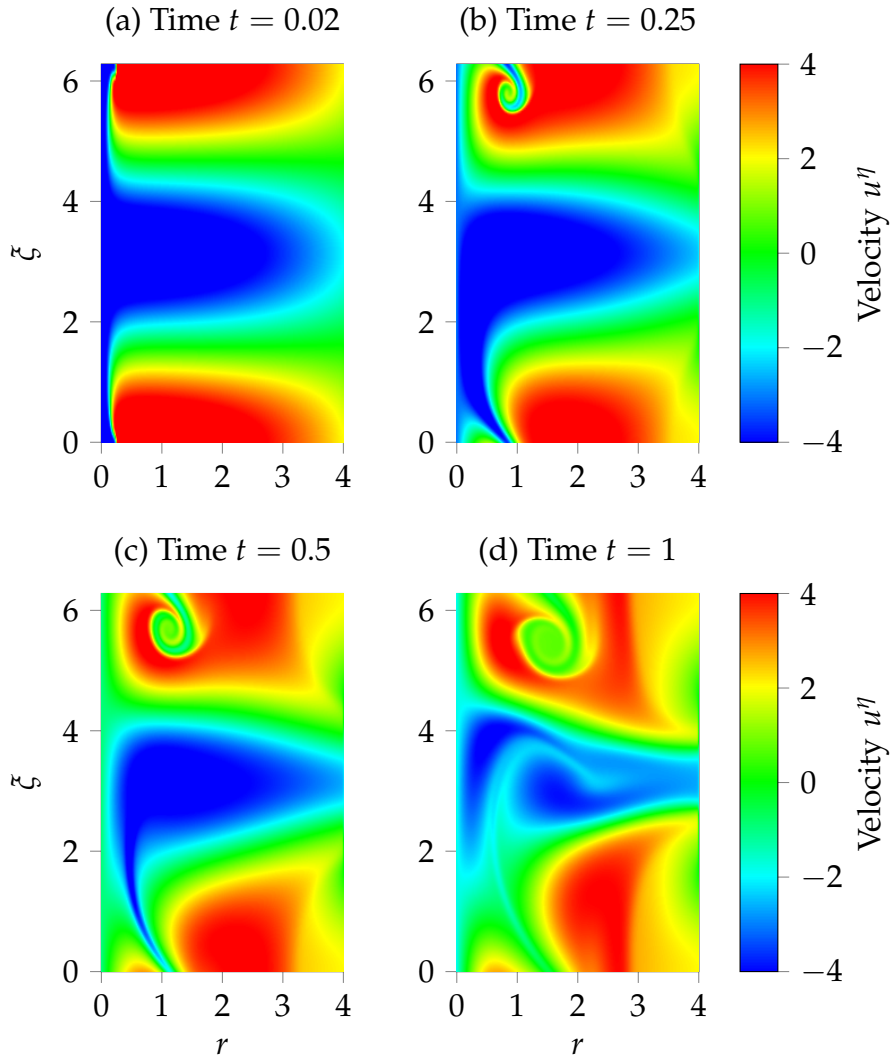

Figure 9.1: Time evolution of a vortex in the helically symmetric parameter domain r, ξ. The results are obtained for a simulation using a polynomial degree $k = 5$ for velocities and $k' = 4$ for the pressure. The Reynolds number for the flow is $Re = 2461$. Snapshots for the velocity component u^η are shown for times $t = 0.02, \ldots, 1$.

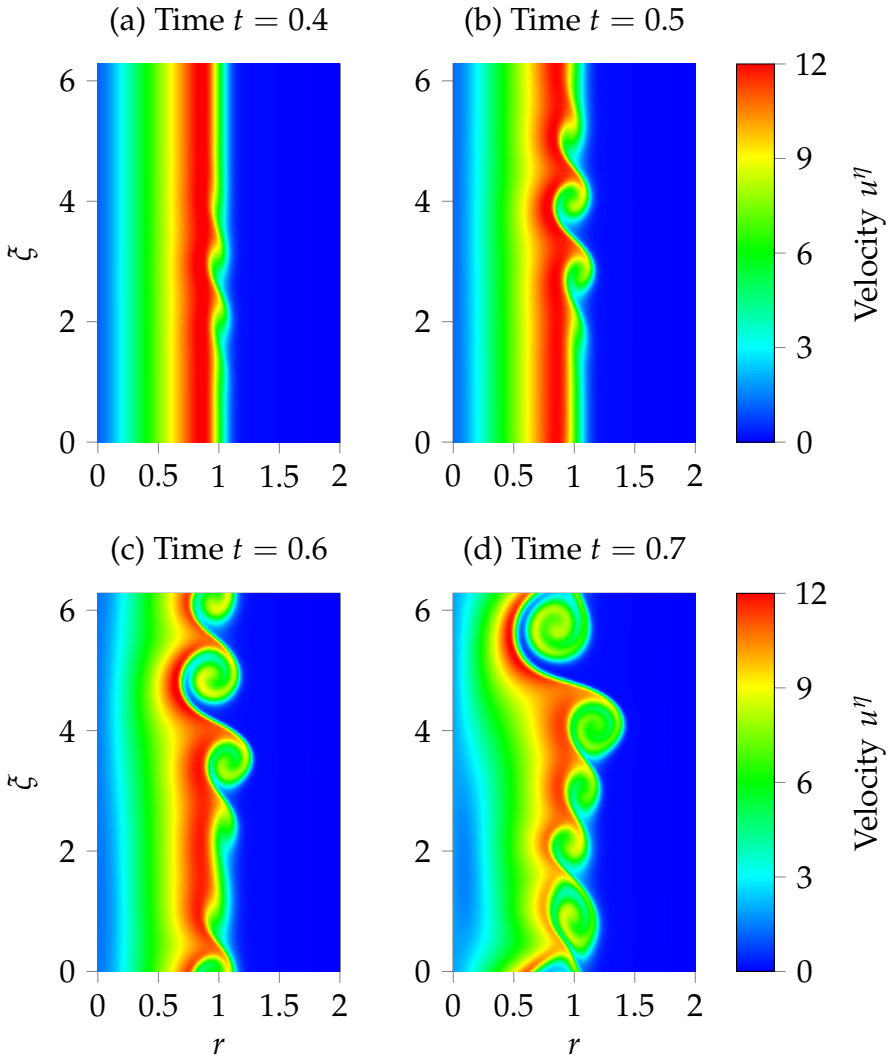

Figure 9.2: Development of the Kelvin-Helholtz instabilities in the helically symmetric parameter domain r, ξ. The results are obtained for a simulation using a polynomial degree $k = 5$ for velocities and $k' = 4$ for the pressure. The Reynolds number for the flow is $Re = 2388$. Snapshots for the velocity component u^η are shown for times $t = 0.4, \ldots, 0.7$.

9.2 Energy spectra of helically invariant flows

For simulation (I) (see Figure 9.1), energy spectra are considered at different times $t = [0.5, 0.6, 0.7, 1.0]$. Since the spatial domain is only periodic in ξ-direction, we employ a fast Fourier transform (FFT) on a line $r = \text{const.}$ for the kinetic energy, determined from the helical velocity as follows

$$\tilde{K} = \frac{1}{2}\left((u^r)^2 + (u^\eta)^2 + \left(u^\xi\right)^2\right). \tag{9.4}$$

In the present case we choose $r = 1$ (and $n_F = 500$ points) such that the line hits the vortex which is formed in the top-left corner of the domain. Figures 9.3 and 9.4 show the temporal development of the energy spectra. In Figure 9.3 one may observe that with increasing time, the energy decreases for all scales with the exception of a small range of wave numbers $6 \leq k_h \leq 10$. The scaling law of $k_h^{-5/3}$ predicted by Kolmogorov (see e.g. Pope and Pope, 2000) is plotted in 9.4 for comparison. One may observe that the scaling of the energy spectra for the present flow is different compared to Kolmogorov's law. Furthermore, the spectra becomes steeper as time increases. To determine the exact scaling of the energy spectra could be one possible and quite important task for future research of turbulent helically invariant flows.

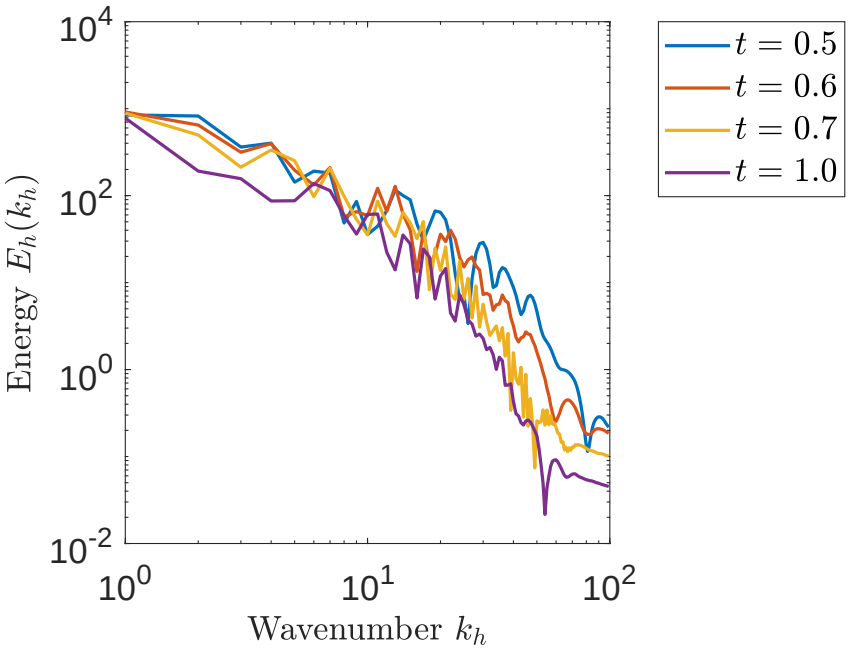

Figure 9.3: Comparison of energy spectra at different times $t = [0.5, 0.6, 0.7, 1.0]$ for the simulation of a turbulent helical flow with initial conditions (9.2) at $Re = 2461$. The kinetic energy $E_h(k)$ is plotted as a function of the wavenumber k_h.

In addition, Figures 9.3 and 9.4 show the characteristic ranges of turbulent energy spectra known from the literature (e.g. Pope and Pope, 2000). For small wave numbers, i.e. on the large scales, the energy-containing range can be observed. In that range,

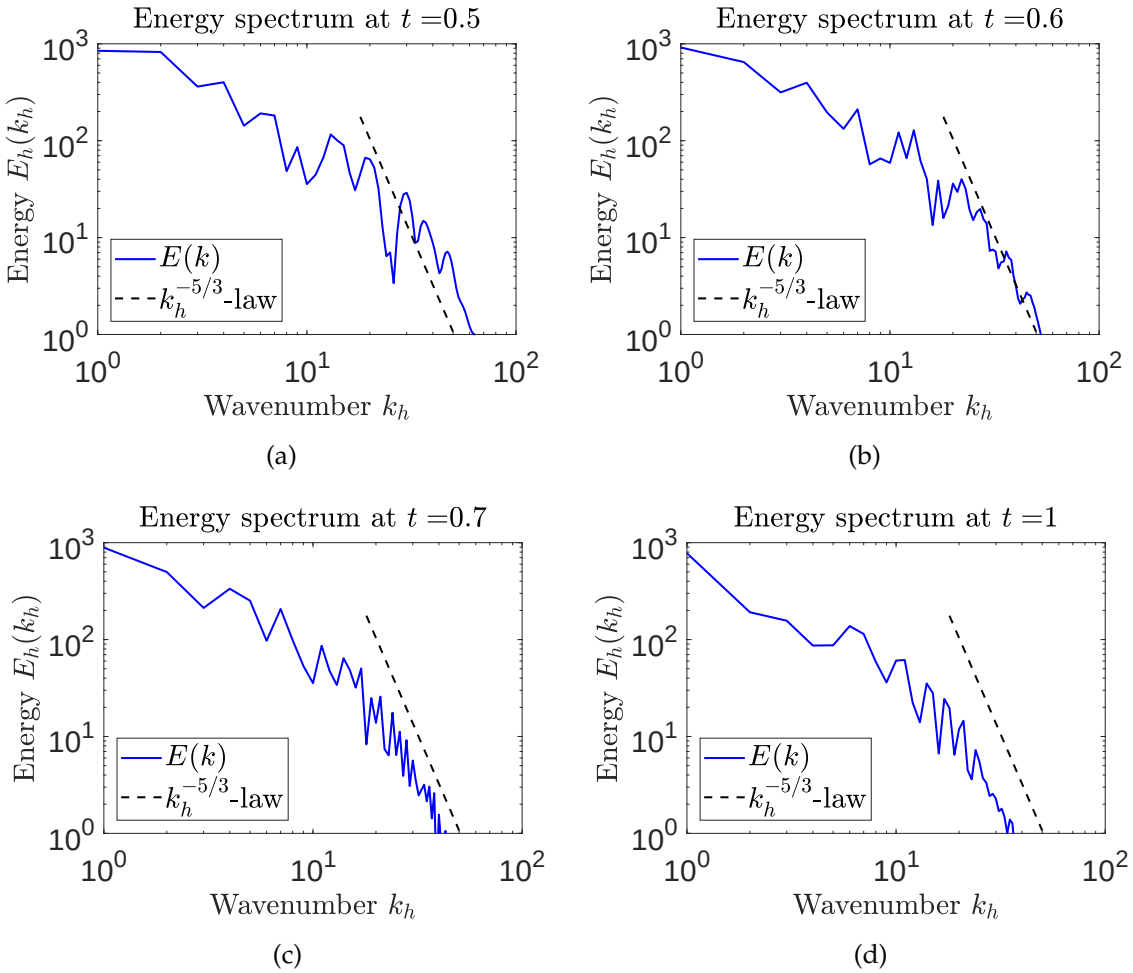

Figure 9.4: Energy spectra at different times $t = [0.5, 0.6, 0.7, 1.0]$ for the simulation of a turbulent helical flow with initial conditions (9.2) at $Re = 2461$. The kinetic energy $E_h(k)$ is plotted over the wavenumber k_h. The dashed line represents Kolmogorov's $k_h^{-5/3}$-law.

energy is injected into the system. For larger wave numbers, i.e. for $k_h = 10^1, \ldots, 6 \cdot 10^1$ the inertial subrange can be identified, where energy is transferred between the vortices. The third and last region of a turbulent energy spectrum, the dissipation range, is indicated in Figure 9.3 at wave numbers around $k_h = 10^2$, but is not shown completely. The reason for this is that the smallest scales (the Kolmogorov scales) have not yet been completely resolved in the simulation. Larger calculations with finer grids also reveal the dissipation range, so that finally a statement regarding the energy transfer for helically symmetric flows (towards the small scales or vice versa) can be made. The performance of simulations with sufficiently fine grid resolutions is the subject of future research on the turbulence of helically invariant flows.

The investigations of the energy spectra discussed in this chapter present a first view of the behavior of energy and the time evolution. For further investigations of the energy spectra and in particular for a statement concerning the questions in how far helical flows are more like 2D or 3D flows, it is necessary to perform a series of FFT in the whole computational domain (e.g for a series of different lines $r = \text{const.}$). Additionally, simulations using more DoF in order to resolve the smallest eddies are needed, as well as a different external forcing to trigger turbulence in helically symmetric flows. Nevertheless, the simulations show that one can generate vortices and hence turbulence using the newly developed numerical code.

10 Conclusion and outlook

The present thesis is separated into two parts. In the first part analytic methods such as the Lie symmetry groups and the direct method for seeking conservation laws of PDEs are applied. The analysis of the helically symmetric Navier-Stokes equations leads to new conservation laws as well as new exact solutions of the system of equations.
In the second part of this thesis, we develop a numerical code based on the DG method that solves the transient incompressible helically invariant Navier-Stokes equations. In addition, we provide two numerical simulations for high Reynolds number flows. The results show the formation of vortices, Kelvin-Helmholtz instabilities, and a scaling of energy spectra which we compare with the well-known scaling law predicted by Kolmogorov in the turbulence theory. A summary of the results from both parts of this thesis is provided in the following. Some paragraphs of the present chapter are heavily based on the articles Dierkes and Oberlack (2017) and Dierkes et al. (2020) which are publications of mine.

10.1 Results of the analytic part

First we extended the classical case of a helical coordinate system provided in KCO by applying the method of group invariant reduction. Based on these new coordinates we derived a reduced system of time-independent helically invariant Euler and Navier-Stokes equations, where the spatial dependence of all dependent variables has been reduced by one. For the development of the new helical coordinate system, the helical symmetry of the Euler and Navier-Stokes equations has been considered, which relies on the combination of two Lie symmetry groups: (i) Generalized Galilean invariance, which comprises classical Galilean group and axial translation and (ii) the rotation about the same axis. In contrast to the coordinate system that is used for classical helical flows given in KCO, where all coordinates are time-dependent, the present helical coordinate ξ is time-dependent. Nevertheless, particularly for the helical coordinate, there is a high analogy between the classical and the extended case. The only difference is that the parameter a in the classical helical setting is replaced by the time-dependent parameter $\frac{1}{\alpha(t)}$. Moreover, the helically invariant Euler and Navier-Stokes equations are extended by terms involving the time-derivative of the parameter function $\alpha(t)$. Using the newly derived time-dependent helical coordinate system new conservation laws were sought, which were obtained from the new helical invariant system of equations. However, for every CL in KCO a corresponding CL has been found from the Euler and Navier-Stokes equations in primitive variables and in vorticity formulation for the time-dependent coordinates. Only the conservation of energy and helicity does not hold in the time-dependent coordinate system, which is proven in the sections 4.3 and 4.4. However, the assumption of helical invariance gives rise to new conservation laws

which exist in addition to the known CLs in three dimensions, e.g. the conservation of mass, momentum and energy. The derivation of the time-dependent coordinate system together with the construction of new CL represent the first milestone of this thesis.

The second milestone of this thesis is the derivation of exact solutions of the helically invariant Navier-Stokes equations which can be divided into two different types. The first type arises from the invariant solution ansatz with respect to the Galilei group (5.1d) admitted by the helically invariant Navier-Stokes equations (3.19). We derive a new nonlinear PDE of third order (5.13), for which we present two particular solutions, given by (5.17) and (5.18). From that, complete solutions to the Navier-Stokes system are derived and given by (5.19) and (5.20). It remains an open problem to derive further physically relevant particular solutions, as well as the general solution of the v-equation (5.13). We verified that the v-equation does not admit nonclassical symmetries, hence, the nonclassical method (e.g., Bluman et al., 2010) and the equivalent "direct method" of Clarkson and Kruskal (1989) cannot be used to construct additional exact solutions.

The second type of solutions of the helically invariant system of Navier-Stokes equations (3.19) is based on an exact linearization of the Navier-Stokes equations, where we seek solutions that satisfy the Beltrami condition (5.28). We note that for such flows, the most important mechanism in turbulence, the vortex stretching, is not active, since the velocity and the vorticity vectors are parallel. Nevertheless, in order to seek exact solutions, the Beltrami assumption is extremely helpful, as the PDE system (3.19) becomes linear. A family of separated solutions of this system is described by an exponentially decaying in time, $\xi-$periodic ansatz (5.33), leading to a linear system of ODEs ((B.14) in Appendix B.2). Exact solutions (5.47) were found in the case of a constant Beltrami parameter ϑ. These solutions involve confluent Heun functions. While all such separated solutions are $\xi-$periodic, the radial dependence may be regular or singular on the z-axis, and the solutions may grow or decay as $r \to \infty$. However, all solutions (5.47) are regular in annular domains $0 < r_1 \leq r \leq r_2$. We also note that though the solutions (5.47) are time-dependent, all streamlines, as well as level surfaces of helicity density, velocity and vorticity magnitude are time-invariant (see Figures 5.3, 5.4 and 5.5).

10.2 Results of the numerical part

The third milestone of this thesis is the development of a DG code to solve the helically invariant Navier-Stokes equations numerically. In order to do that we first derive periodicity conditions which hold in the helical frame. The derivation is based on the fact that all physical variables are periodic along a helical line which means that the values at the beginning and at the end of one helical turn coincide. We further derive a uniqueness condition for the physical variables at the centerline axis. The proceeding is analogous to Khorrami et al. (1989) where similar conditions for axisymmetric flows are discussed. Combining both of these steps, we found a set of conditions at the centerline. Using that result, we introduce a reduced DG space $\mathbb{V}_k^0$ (see Table 6.1) that includes the newly derived conditions.

After these preliminaries we proceed with a spatial discretization using the DG method with polynomial approximations of the solutions by polynomial functions of order k for the velocity components and k' for the pressure. The computational domain is chosen to be the parameter domain (r, ξ) and is divided into non-overlapping rectangular elements and approximated by the grid consisting of cells $K_1, \dots K_N$. For the boundary conditions we choose Dirichlet BCs at the outer wall, i.e. at $r = 1$ and periodic BCs in $\xi-$direction at the top and bottom boundaries of the domain. The viscous terms are discretized using the SIP method whereas for the nonlinear terms of the Navier-Stokes equations a "super weak" form is obtained by double partial integration. For the fluxes of the nonlinear terms, we use a standard upwind formulation.

Following Shahbazi et al. (2007), we employ a semi-explicit scheme for the temporal discretization, where the full operator is split into a Stokes operator and the nonlinear terms. The Stokes operator consists of the viscous terms and the pressure gradient and is discretized implicitly whereas the nonlinear terms are treated explicitly. The great advantage is that once having solved the Stokes system, solutions of each time step may be obtained by an explicit treatment of the nonlinear terms. In this powerful method of time integration we use a BDF scheme of third-order for the transient term and a third-order extrapolation of the nonlinear terms.

The correct implementation of the DG discretization is verified by convergence studies on two different computational domains. First, a cylindrical shell is considered where the central axis is excluded. Afterwards, the convergence studies are performed on a full cylindrical pipe. The reason for excluding the centerline is threefold. First, it is thus possible to ensure that the equations on the shell have been correctly implemented. Second, it is possible to determine the impact of the central axis on the condition numbers of the spatial operator. Thus, we could discover that the discretized system is much better conditioned for the cylindrical shell than in the full cylindrical domain. The reason for that is that the coefficients of the helically symmetric Navier-Stokes equations are singular at $r = 0$ when the centerline axis is included. Third, the introduction of a metric function is not necessary since the coefficients in the PDE are non-singular on the cylindrical shell.

In this restricted domain, we employ the manufactured solution (6.47) to compute errors measured by the difference between the numerical and exact solution in the L^2-norm. We use the mixed-order formulation, where the polynomial degree for the velocities is k and for the pressure $k' = k - 1$ and the equal-order formulation where the degrees for both are equal, i.e. $k = k'$. For the latter case we add an additional penalty term for the pressure jumps in the continuity equation (6.35a) to ensure stability. For the mixed-order formulation, the expected convergence rates of $k + 1$ for the velocity and k for the pressure are perfectly obtained. For the equal-order formulation, only for the velocities the expected convergence rates are obtained. We further show the results of the temporal convergence studies, where we consider the errors of the numerical solution against the unsteady manufactured solution (6.44) in the L^2-norm. As a second test case, we use the exact solution (5.19) of the helically invariant Navier-Stokes equations. For both test cases the expected convergence rates for a BDF scheme of third order are perfectly obtained.

Based on the assumption that all physical quantities are unique at the centerline combined with periodicity conditions for the helical coordinates, we first present a reduction of the DG space. This results in a change of the DG basis. We show that the values of the condition numbers as well as the growth rates decrease by the introduction of a penalty scaling. It remains an open question if other penalty functions exist which further decrease the condition number of the spatial operator. Finally, as before on the cylindrical shell, we present convergence studies where we measure the numerical error in a $B-$norm referring to the metric function $f(r) = B(r)^2$. For the mixed order formulation, we obtain the expected convergence rates of $k+1$ for the velocity and k for the pressure. For the equal-order formulation, the convergence rate $k+1$ is obtained only for the velocity. The temporal convergence studies show that the semi-explicit method is also applied correctly on the full cylindrical domain since the convergence rates are perfectly obtained in the present case.

In addition, results of two direct numerical simulations are presented in chapter 9. In simulation (I) the generation of vortices can be observed. For simulation (II) a shearing has been employed, from which Kelvin-Helmholtz instabilities are obtained. Finally, for simulation (I) energy spectra at different times are compared. It can be seen that the energy decreases for all wavenumbers except for one small range $6 \leq k_h \leq 10$. Moreover, it is shown that the energy spectra differ from the $k_h^{-5/3}$-scaling of Kolmogorov (see e.g. Pope and Pope, 2000).

10.3 Outlook

All three milestones of this dissertation, i.e. the new CL's for the Euler and Navier-Stokes equations in time-dependent helical coordinates, the exact solutions, and the numerical code can be used in different fields of future research. In particular, the newly developed code may be applied in turbulence research where numerical simulations of dimensional reduced flows are of highest interest. It is well-known that in two-dimensional turbulence physical mechanisms are significantly different to those in three dimensions. In the latter, energy is transferred from the large eddies to smaller ones and a stretching of the vortices appears, whereas in two dimensions the vortex stretching vanishes and the energy is transferred in opposite direction. As introduced at the beginning of this thesis in chapter 1, helically reduced flows are placed between two and three dimensions and to date it is not known in which direction energy is transferred. Using the present numerical discretization, simulations with high Reynolds numbers will give an answer to the energy transport in helically symmetric flows and to many other questions concerning the behavior of two and three dimensional turbulence.

The time-dependent coordinates offer the possibility to enforce a stretching of helical vortices, just by the assumption of a certain function for the helical parameter $\alpha(t)$. Techniques that are used in this thesis can also be applied to the system of Euler- and Navier-Stokes equations in the time-dependent helical coordinates to derive further exact solutions. Another step of future research can be the extension of the DG code for the time-dependent helical coordinate system.

Concerning the newly discovered exact solutions, both types derived in the present work are given by explicit closed-form expressions, suitable for further analysis and algebraic manipulation. For example, one can study the dynamics of points where the maximum of vorticity or its specific component(s) is achieved, referred to as the *vortex core* (e.g. Ali and Abid, 2014; Selçuk et al., 2017), as well as their other local and global characteristics. In particular, for the exact solution (5.21), the dimensionless vorticity component in the invariant direction is given by

$$\hat{\omega}^{\eta} = \frac{\hat{A}\hat{B}\hat{r}\hat{\xi}}{4\left(\hat{t}+\hat{t}_0\right)^2}\, e^{-\frac{\hat{r}^2}{4\left(\hat{t}+\hat{t}_0\right)}}\,. \tag{10.1}$$

If the vortex core is defined as the maximal value of $|\omega^{\eta}|$ as a function of the cylindrical radius $\hat{r}$, one readily finds that the radial position of the vortex core is described by an increasing function

$$\hat{r}^{\eta}_{max}(t) = \frac{1}{2a}\sqrt{4a^2\left(\hat{t}+\hat{t}_0\right)+2\left(\sqrt{4a^4\left(\hat{t}+\hat{t}_0\right)^2+12a^2\left(\hat{t}+\hat{t}_0\right)+1}-1\right)}\,. \tag{10.2}$$

Another possible direction of future research is to study the confluent Heun-type solutions (5.47) in more detail. Further physical solutions can possibly be found through equivalence transformations, other parameter choices and linear combinations of various modes that may describe specific situations of interest.

Bibliography

Ali, M. and Abid, M. (2014). Self-similar behaviour of a rotor wake vortex core. *Journal of Fluid Mechanics*, 740.

Anco, S. and B., G. (2002). Direct construction method for conservation laws of partial differential equations part ii: General treatment. *European Journal of Applied Mathematics*, 13(05):567–585.

Anco, S. and Bluman, G. (2002). Symmetry and integration methods for differential equations. *Applied Mathematical Sciences*, 154.

Andreev, V. K., Kaptsov, O., Pukhnachev, V. V., and Rodionov, A. (1998). *Applications of group-theoretical methods in hydrodynamics*, volume 450. Springer Science & Business Media.

Arnold, D. N. (1982a). An interior penalty finite element method with discontinuous elements. *SIAM J. Numer. Anal.*, 19(4):742.

Arnold, D. N. (1982b). An interior penalty finite element method with discontinuous elements. *SIAM journal on numerical analysis*, 19(4):742–760.

Arnold, D. N., Brezzi, F., Cockburn, B., and Marini, D. (2000). Discontinuous galerkin methods for elliptic problems. In *Discontinuous Galerkin Methods*, pages 89–101. Springer.

Arscott, F. M. (1995). *Heun's Differential Equations*. Clarendon Press.

Babuška, I. (1973). The finite element method with lagrangian multipliers. *Numerische Mathematik*, 20(3):179–192.

Barbosa, E. and Daube, O. (2005). A finite difference method for 3d incompressible flows in cylindrical coordinates. *Computers & fluids*, 34(8):950–971.

Bassi, F. and Rebay, S. (1997). A high-order accurate discontinuous finite element method for the numerical solution of the compressible navier–stokes equations. *Journal of computational physics*, 131(2):267–279.

Bassi, F., Rebay, S., Mariotti, G., Pedinotti, S., and Savini, M. (1997). A high-order accurate discontinuous finite element method for inviscid and viscous turbomachinery flows. In *Proceedings of the 2nd European Conference on Turbomachinery Fluid Dynamics and Thermodynamics*, pages 99–109. Technologisch Instituut, Antwerpen, Belgium.

Baumann, C. E. and Oden, J. T. (1998). A discontinuous hp finite element method for the solution of the euler equation of gas dynamics. In *Proceedings of the 10th International Conference on Finite Element in Fluids*.

Bluman, G., Cheviakov, A., and Anco, S. (2010). *Applications of symmetry methods to partial differential equations*. Springer.

Bogoyavlenskij, O. (2000a). Helically symmetric astrophysical jets. *Phys. Rev. E*, 62:8616–8627.

Bogoyavlenskij, O. I. (2000b). Exact helically symmetric plasma equilibria. *Letters in Mathematical Physics*, 51(4):235–247.

Bogoyavlenskij, O. I. (2000c). Helically symmetric astrophysical jets. *Physical Review E*, 62(6):8616.

Bogoyavlenskij, O. I. (2003a). Exact unsteady solutions to the navier–stokes and viscous mhd equations. *Physics Letters A*, 307(5-6):281–286.

Bogoyavlenskij, O. I. (2003b). Infinite families of exact periodic solutions to the navier-stokes equations. *Moscow Mathematical Journal*, 3(2):263–272.

Bottasso, C. L., Micheletti, S., and Sacco, R. (2002). The discontinuous petrov–galerkin method for elliptic problems. *Computer Methods in Applied Mechanics and Engineering*, 191(31):3391–3409.

Bragg, S. L. and Hawthorne, W. R. (1950). Some exact solutions of the flow through annular cascade actuator discs. *J. Aeronaut. Sci.*, 17:243–249.

Brezzi, F. and Fortin, M. (2012). *Mixed and hybrid finite element methods*, volume 15. Springer Science & Business Media.

Cantwell, B. (2002). *Introduction to Symmetry Analysis Paperback with CD-ROM*, volume 29. Cambridge University Press.

Cheviakov, A. (2007). Gem software package for computation of symmetries and conservation laws of differential equations. *Computer physics communications*, 176(1):48–61.

Cheviakov, A. and Bogoyavlenskij, O. (2004). Exact anisotropic mhd equilibria. *Journal of Physics A: Mathematical and General*, 37(30):7593.

Cheviakov, A. F. and Oberlack, M. (2014). Generalized Ertel's theorem and infinite hierarchies of conserved quantities for three-dimensional time-dependent Euler and Navier-Stokes equations. *J. Fluid Mech*, 760:368–386.

Clarkson, P. A. and Kruskal, M. D. (1989). New similarity reductions of the boussinesq equation. *Journal of Mathematical Physics*, 30(10):2201–2213.

Cockburn, B. (2003). Discontinuous galerkin methods. *ZAMM-Journal of Applied Mathematics and Mechanics/Zeitschrift für Angewandte Mathematik und Mechanik: Applied Mathematics and Mechanics*, 83(11):731–754.

Constantinescu, G. S. and Lele, S. (2002). A highly accurate technique for the treatment of flow equations at the polar axis in cylindrical coordinates using series expansions. *Journal of Computational Physics*, 183(1):165–186.

Delbende, I., Rossi, M., and Daube, O. (2012). Dns of flows with helical symmetry. *Theoretical and Computational Fluid Dynamics*, 26(1-4):141–160.

Demkowicz, L. and Gopalakrishnan, J. (2011). Analysis of the dpg method for the poisson equation. *SIAM Journal on Numerical Analysis*, 49(5):1788–1809.

Di Pietro, D. A. and Ern, A. (2011). *Mathematical aspects of discontinuous Galerkin methods*, volume 69. Springer Science & Business Media.

Dierkes, D. (2015). Time-dependent helical coordinates: derivation of the fundamental system and new conservation laws. Master's thesis, Technische Universität Darmstadt.

Dierkes, D. and Oberlack, M. (2017). Euler and navier–stokes equations in a new time-dependent helically symmetric system: derivation of the fundamental system and new conservation laws. *Journal of Fluid Mechanics*, 818:344–365.

Dierkes, D., Oberlack, M., and Cheviakov, A. (2020). New similarity reductions and exact solutions for helically symmetric viscous flows. *Physics of Fluids*, 32(5):053604.

Drazin, P. G. and Riley, N. (2006). *The Navier-Stokes equations: a classification of flows and exact solutions*. Number 334. Cambridge University Press.

Dritschel, D. (1991). Generalized helical beltrami flows in hydrodynamics and magnetohydrodynamics. *Journal of fluid mechanics*, 222:525–541.

El-Jaick, L. J. and Figueiredo, B. D. (2008). Solutions for confluent and double-confluent heun equations. *Journal of Mathematical Physics*, 49(8):083508.

Ellis, T., Demkowicz, L., and Chan, J. (2014). Locally conservative discontinuous petrov–galerkin finite elements for fluid problems. *Computers & Mathematics with Applications*, 68(11):1530–1549.

Ferrer, E. and Willden, R. (2011). A high order discontinuous galerkin finite element solver for the incompressible navier–stokes equations. *Computers & Fluids*, 46(1):224–230.

Geisenhofer, M., Kummer, F., and Müller, B. (2019). A discontinuous galerkin immersed boundary solver for compressible flows: Adaptive local time stepping for artificial viscosity–based shock-capturing on cut cells. *International Journal for Numerical Methods in Fluids*, 91(9):448–472.

Germano, M. (1982). On the effect of torsion on a helical pipe flow. *Journal of Fluid Mechanics*, 125:1–8.

Germano, M. (1989). The dean equations extended to a helical pipe flow. *Journal of Fluid Mechanics*, 203:289–305.

Grad, H. and Rubin, H. (1958). Hydromagnetic equilibria and force-free fields. *Journal of Nuclear Energy*, 7:284–285.

Griffin, M. D., Jones, E., and Anderson Jr, J. D. (1979). A computational fluid dynamic technique valid at the centerline for non-axisymmetric problems in cylindrical coordinates. *Journal of Computational Physics*, 30(3):352–360.

Hager, W. W. (1984). Condition estimates. *SIAM Journal on scientific and statistical computing*, 5(2):311–316.

Hortaçsu, M. (2013). heun functions and their uses in physics. In *Mathematical Physics*, pages 23–39. World Scientific.

Ibragimov, N. H. (1995). *CRC Handbook of Lie group analysis of differential equations*, volume 2. CRC press.

Ishkhanyan, A. and Grigoryan, A. (2014). Fifteen classes of solutions of the quantum two-state problem in terms of the confluent Heun function. *Journal of Physics A: Mathematical and Theoretical*, 47(46):465205.

Jamil, M. and Fetecau, C. (2010). Helical flows of maxwell fluid between coaxial cylinders with given shear stresses on the boundary. *Nonlinear Analysis: Real World Applications*, 11(5):4302–4311.

Johnson, J., Oberman, C., Kulsrud, R., and Frieman, E. (1958). Some stable hydromagnetic equilibria. *Physics of Fluids*, 1(4):281–296.

Kelbin, O. (2015). *Conservation laws of helical flows*. PhD thesis, Technische Universität.

Kelbin, O., Cheviakov, A. F., and Oberlack, M. (2013). New conservation laws of helically symmetric, plane and rotationally symmetric viscous and inviscid flows. *Journal of Fluid Mechanics*, 721:340–366.

Khorrami, M. R., Malik, M. R., and Ash, R. L. (1989). Application of spectral collocation techniques to the stability of swirling flows. *Journal of Computational Physics*, 81(1):206–229.

Kilmister, C. W. and Hydon, P. E. (2001). Symmetry Methods for Differential Equations: A Beginners Guide. *The Mathematical Gazette*, 85(504):556.

Klein, B., Kummer, F., Keil, M., and Oberlack, M. (2015). An extension of the simple based discontinuous galerkin solver to unsteady incompressible flows. *International Journal for Numerical Methods in Fluids*, 77(10):571–589.

Krause, D. and Kummer, F. (2017). An incompressible immersed boundary solver for moving body flows using a cut cell discontinuous galerkin method. *Computers & Fluids*, 153:118–129.

Kristensson, G. (2010). *Second Order Differential Equations: Special Functions and Their Classification*. Springer Science & Business Media.

Kummer, F. (2012). *The BoSSS Discontinuous Galerkin solver for incompressible fluid dynamics and an extension to singular equations.* PhD thesis, Technische Universität.

Kummer, F. (2017). Extended discontinuous galerkin methods for two-phase flows: the spatial discretization. *International Journal for Numerical Methods in Engineering*, 109(2):259–289.

Kummer, F., Emamy, N., Mousavi Belfeh Teymouri, R., and Oberlack, M. (2009). Report on the development of a generic discontinuous galerkin framework in .net. In *ParCFD 2009, 21st International Conference on Parallel Computational Fluid Dynamics, May 18–22, 2009, Moffett Field, California, USA*, pages 383–397.

Kummer, F. and Müller, B. (2018). Dg lecture notes. Lecture notes.

Li, B. Q. (2006). *Discontinuous finite elements in fluid dynamics and heat transfer*. Computational fluid and solid mechanics. Springer, London.

Lopez, J. and Shen, J. (1998). An efficient spectral-projection method for the navier–stokes equations in cylindrical geometries: I. axisymmetric cases. *Journal of Computational Physics*, 139(2):308–326.

Maplesoft (2017). *Maple User Manual*. Maplesoft, a division of Waterloo Maple Inc., Waterloo, Ontario.

Meleshko, S. and Pukhnachev, V. (1999). One class of partially invariant solutions of the navier-stokes equations. *Journal of applied mechanics and technical physics*, 40(2):208–216.

Mitchell, A., Morton, S., and Forsythe, J. (1997). Wind turbine wake aerodynamics. *Air Force Academy Colorado Springs, Dept. of Aeronautics, Report ADA425027*.

Motygin, O. V. (2015). On evaluation of the Heun functions. *arXiv:1506.03848*.

Müller, B. (2014). *Methods for higher order numerical simulations of complex inviscid fluids with immersed boundaries*. PhD thesis, Technische Universität.

Müller, B., Krämer-Eis, S., Kummer, F., and Oberlack, M. (2017). A high-order discontinuous galerkin method for compressible flows with immersed boundaries. *International Journal for Numerical Methods in Engineering*, 110(1):3–30.

Nair, R. D., Thomas, S. J., and Loft, R. D. (2005). A discontinuous galerkin global shallow water model. *Monthly weather review*, 133(4):876–888.

Oberlack, M. (2000). Symmetrie, invarianz und selbstähnlichkeit in der turbulenz (symmetry, invariance, and self-similarity in turbulence; habilitation). *RWTH Aachen, Aachen, 187pp*.

Pope, S. and Pope, S. B. (2000). *Turbulent Flows*. Cambridge University Press.

Pukhnachev, V. (2006). Symmetries in the Navier–Stokes equations. *Uspekhi Mekhaniki [Advances in Mechanics]*, 4(1):6–76.

Roberts, N. V., Bui-Thanh, T., and Demkowicz, L. (2014). The dpg method for the stokes problem. *Computers & Mathematics with Applications*, 67(4):966–995.

Ronveaux, A. (1995). *Heun's Differential Equations*. Oxford University Press.

Rosenhaus, V. and Shankar, R. (2019). Sub-symmetries and conservation laws. *Reports on Mathematical Physics*, 83(1):21–48.

Sarpkaya, T. (1971). On stationary and travelling vortex breakdowns. *Journal of Fluid Mechanics*, 45(03):545–559.

Schnack, D., Caramana, E., and Nebel, R. (1985). Three-dimensional magnetohydrodynamic studies of the reversed-field pinch. *Physics of Fluids*, 28(1):321–333.

Selçuk, C., Delbende, I., and Rossi, M. (2017). Helical vortices: Quasiequilibrium states and their time evolution. *Physical Review Fluids*, 2(8):084701.

Shafranov, V. D. (1958). Propagation of an electromagnetic field in a medium with spatial dispersion. *Soviet Physics JETP*, 7:1019–1029.

Shahbazi, K., Fischer, P. F., and Ethier, C. R. (2007). A high-order discontinuous galerkin method for the unsteady incompressible navier–stokes equations. *Journal of Computational Physics*, 222(1):391–407.

Stephani, H. (1994). *Differentialgleichungen: Symmetrien und Lösungsmethoden; mit 2 Tabellen*. Spektrum Akad. Verlag.

Taylor, G. (1923). Lxxv. on the decay of vortices in a viscous fluid. *The London, Edinburgh, and Dublin Philosophical Magazine and Journal of Science*, 46(274):671–674.

Tuttle, E. (1990). Laminar flow in twisted pipes. *Journal of Fluid Mechanics*, 219:545–570.

Utz, T. (2018). *Level set methods for high-order unfitted discontinuous Galerkin schemes*. PhD thesis, Technische Universität.

Utz, T., Kummer, F., and Oberlack, M. (2017). Interface-preserving level-set reinitialization for dg-fem. *International Journal for Numerical Methods in Fluids*, 84(4):183–198.

Vermeer, L., Sorensen, J., and Crespo, A. (2003). Wind turbine wake aerodynamics. *Progress in Aerospace Sciences*, 39(67):467 – 510.

Verzicco, R. and Orlandi, P. (1996). A finite-difference scheme for three-dimensional incompressible flows in cylindrical coordinates. *Journal of Computational Physics*, 123(2):402–414.

Wang, C. (1981). On the low-Reynolds-number flow in a helical pipe. *Journal of Fluid Mechanics*, 108:185–194.

Wihler, T. P. and Rivière, B. (2011). Discontinuous galerkin methods for second-order elliptic pde with low-regularity solutions. *Journal of scientific computing*, 46(2):151–165.

Wu, J.-Z., Ma, H.-Y., and Zhou, M.-D. (2007). *Vorticity and vortex dynamics*. Springer Science & Business Media.

Zabielski, L. and Mestel, A. (1998). Steady flow in a helically symmetric pipe. *Journal of Fluid Mechanics*, 370:297–320.

Zienkiewicz, O. and Taylor, R. (2002). Discontinuous galerkin methods: theory, computation and application (lecture notes in computational science and engineering), by b. cockburn, ge karniadakis and c.-w. shu (eds), springer, berlin, 2000. isbn 3-540-66787-3, gb£ 51.50. *International Journal for Numerical Methods in Engineering*, 53(7):1763–1764.

A Appendix: Derivation of the time-dependent helical coordinates

The present section is heavily based on the following publication of mine (Dierkes and Oberlack, 2017) as well as on results of my master's thesis (Dierkes, 2015).

Presently, a new time-dependent helical coordinate system for the Euler and Navier-Stokes equations is derived, using the method of group invariant reduction. Here, group invariance is meant in the sense of reduction of the spatial coordinates such as e.g. a reduction to plane flows.

The derivation is based on the helical symmetry which is a combination of the generalized Galilean invariance and the rotation group, given by (3.13). The corresponding infinitesimal generators for rotation and generalized Galilean invariance of the Euler and Navier-Stokes equations are given by (3.5h) and (3.5c), respectively

$$X_R = \frac{\partial}{\partial \varphi}, \tag{A.1a}$$

$$X_G = \alpha(t)\frac{\partial}{\partial z} + \dot{\alpha}(t)\frac{\partial}{\partial u^z} - z\ddot{\alpha}(t)\frac{\partial}{\partial p}. \tag{A.1b}$$

A new extended helical symmetry of the Euler and Navier-Stokes equations consists of a superposition of a rotation group X_R and the Generalized Galilean symmetry X_G. To maintain the nomenclature to earlier results on helical flows (see e.g. Kelbin et al., 2013), we choose the following linear combination of symmetries (A.1a) and (A.1b) to obtain

$$X = \frac{1}{b}X_R - X_G \tag{A.2}$$

$$= \frac{1}{b}\frac{\partial}{\partial \varphi} - \alpha(t)\frac{\partial}{\partial z} - \dot{\alpha}(t)\frac{\partial}{\partial u^z} + z\ddot{\alpha}(t)\frac{\partial}{\partial p}. \tag{A.3}$$

For the final aim of a helically symmetric coordinate system we need to define $\eta^*(r, \varphi, z, t)$ to be the variable, which should be eliminated from the system of equations such that the reduced system only contains two spatial variables.

Based on this idea, we derive a new set of variables, i.e. the reduced helical coordinates $(\tilde{r}, \xi)$, the helical velocities $(\tilde{u}^r, u^\eta, u^\xi)$ and the pressure $\tilde{p}$ summarized in the vector

$$\boldsymbol{\sigma} := (\xi, \tilde{r}, \tau, \tilde{u}^r, u^\eta, u^\xi, \tilde{p}). \tag{A.4}$$

For their derivation we employ the method of canonical coordinates (see e.g. Bluman et al., 2010), which results in two linear partial differential equations of first order, given by

$$X\eta^* = 1, \tag{A.5a}$$
$$X\boldsymbol{\sigma} = 0. \tag{A.5b}$$

Their solutions generate the new variables $(\eta, \boldsymbol{\sigma})$ and the symmetry (A.3) transforms into the symmetry

$$X = \frac{\partial}{\partial \eta^*}, \tag{A.6}$$

which is a translational symmetry in η^*.

Substituting (A.3) in (A.5a) leads to

$$X\eta^* = \frac{1}{b}\frac{\partial \eta^*}{\partial \varphi} - \alpha(t)\frac{\partial \eta^*}{\partial z} - \dot{\alpha}(t)\frac{\partial \eta^*}{\partial u^z} + z\ddot{\alpha}(t)\frac{\partial \eta^*}{\partial p} = 1, \tag{A.7}$$

which can be equivalently written in the form of a characteristic system

$$b\mathrm{d}\varphi = -\frac{\mathrm{d}z}{\alpha(t)} = -\frac{\mathrm{d}u^z}{\dot{\alpha}(t)} = \frac{\mathrm{d}p}{z\ddot{\alpha}(t)} = \frac{\mathrm{d}t}{0} = \frac{\mathrm{d}r}{0} = \frac{\mathrm{d}u^\varphi}{0} = \frac{\mathrm{d}u^r}{0} = \frac{\mathrm{d}\eta^*}{1}. \tag{A.8}$$

Solving the system (A.8), we obtain a general solution of equation (A.7) for the helical variable η^* given by

$$\eta^* = b\varphi + F\left(r, t, b\varphi + \frac{z}{\alpha}, p + \frac{1}{2}\frac{\ddot{\alpha}}{\alpha}z^2, u^\varphi, u^r, u^z + \dot{\alpha}b\varphi\right). \tag{A.9}$$

Similarly, substituting (A.3) in (A.5b) yields

$$X\boldsymbol{\sigma} = \frac{1}{b}\frac{\partial \boldsymbol{\sigma}}{\partial \varphi} - \alpha(t)\frac{\partial \boldsymbol{\sigma}}{\partial z} - \dot{\alpha}(t)\frac{\partial \boldsymbol{\sigma}}{\partial u^z} + z\ddot{\alpha}(t)\frac{\partial \boldsymbol{\sigma}}{\partial p} = 0, \tag{A.10}$$

and, written in the equivalent form of the characteristic system, we obtain

$$b\mathrm{d}\varphi = -\frac{\mathrm{d}z}{\alpha(t)} = -\frac{\mathrm{d}u^z}{\dot{\alpha}(t)} = \frac{\mathrm{d}p}{z\ddot{\alpha}(t)} = \frac{\mathrm{d}t}{0} = \frac{\mathrm{d}r}{0} = \frac{\mathrm{d}u^\varphi}{0} = \frac{\mathrm{d}u^r}{0} = \frac{\mathrm{d}\boldsymbol{\sigma}}{0}. \tag{A.11}$$

A general solution of (A.11) reads

$$\boldsymbol{\sigma} = \boldsymbol{F}\left(r, t, b\varphi + \frac{z}{\alpha}, p + \frac{1}{2}\frac{\ddot{\alpha}}{\alpha}z^2, u^\varphi, u^r, u^z + \dot{\alpha}b\varphi\right), \tag{A.12}$$

where $\boldsymbol{F} = (f^1, f^2, f^3, f^4, f^5, f^6, f^7)$ is a vector consisting of seven arbitrary functions depending on the arguments given in (A.12).

The specific new helical coordinates may now be manufactured from (A.9) and (A.12), respectively. In order to keep the complexity for the resulting Euler and Navier-Stokes equations in the helical coordinate system as low as possible, we choose the new independent coordinates as given in (3.14a)-(3.14d).

Analogous to the classical case the helical velocity components and the pressure are given by (3.14e)-(3.14h). They are a particular choice of the special solutions of (A.12).

B Appendix: Details of the exact solutions to the Navier-Stokes equations

B.1 Details of the derivation of the v-equation (5.13)

The substitution of the ansatz (5.6) into the Navier-Stokes equations (3.19) yields

$$\frac{1}{r}\left(ru^r\right)_r + \frac{1}{B}F^\xi = 0, \tag{B.1a}$$

$$\begin{aligned}&-\frac{B^2}{r}\left(\frac{b}{r}F^\xi + aF^\eta\right)^2\xi^2 - \frac{2B^2}{r}\left(\frac{b}{r}F^\xi + aF^\eta\right)\left(\frac{b}{r}G^\eta + aG^\xi\right)\xi + u^r_t + u^r u^r_r\\ &\quad - \frac{B^2}{r}\left(\frac{b}{r}G^\eta + aG^\xi\right)^2 + p_r - \nu\left[u^r_{rr} + \frac{1}{r}u^r_r - \frac{1}{r^2}\left(u^r + \frac{2Bb^2}{r}F^\xi + 2abBF^\eta\right)\right] = 0\end{aligned} \tag{B.1b}$$

$$\begin{aligned}&\left[F^\eta_t + u^r F^\eta_r + \frac{F^\xi F^\eta}{B} + \frac{u^r F^\eta a^2B^2}{r} - \nu B\left(\frac{F^\eta B''}{B^2} - \left(\frac{2ab}{r^2}F^\xi + \frac{\frac{b^2}{r^2}-a^2}{r}F^\eta\right)B'\right.\right.\\ &\qquad \left.\left. + \frac{2B'}{B^2}F^\eta_r - \frac{2abB}{r^2}F^\xi_r - \frac{B}{r}\left(\frac{b^2}{r^2}-a^2\right)F^\eta_r + \frac{1}{B}F^\eta_{rr} + \frac{B}{r^2}\left(\frac{b^2}{r^2}-a^2\right)F^\eta\right)\right]\xi\\ &\quad + G^\eta_t + u^r G^\eta_r + \frac{G^\xi F^\eta}{B} + \frac{a^2B^2}{r}u^r G^\eta - \nu B\left[\frac{B''}{B^2}G^\eta - \left(\frac{2ab}{r^2}G^\xi + \frac{\frac{b^2}{r^2}-a^2}{r}G^\eta\right)B'\right.\\ &\qquad \left. + \frac{2B'}{B^2}G^\eta_r - \frac{2abB}{r^2}G^\xi_r - \frac{B}{r}\left(\frac{b^2}{r^2}-a^2\right)G^\eta_r + \frac{1}{B}G^\eta_{rr} + \frac{B}{r^2}\left(\frac{b^2}{r^2}-a^2\right)G^\eta\right] = 0\end{aligned} \tag{B.1c}$$

$$\begin{aligned}&\left[F^\xi_t + u^r F^\xi_r + \frac{1}{B}\left(F^\xi\right)^2 + \frac{2abB^2}{r^2}u^r F^\eta + \frac{b^2B^2}{r^3}F^\xi u^r - \nu B\left(\frac{B''}{B^2}F^\xi + \left(\frac{2ab}{r^2}F^\eta - \frac{\frac{b^2}{r^2}-a^2}{r}F^\xi\right)B'\right.\right.\\ &\qquad \left.\left. + \frac{2B'}{B^2}F^\xi_r + \frac{2abB}{r^2}F^\eta_r - \frac{B}{r}\left(\frac{b^2}{r^2}-a^2\right)F^\xi_r + \frac{1}{B}F^\xi_{rr} - \frac{2abB}{r^3}F^\eta\right)\right]\xi\\ &\quad + G^\xi_t + u^r G^\xi_r + \frac{1}{B}G^\xi F^\xi + \frac{2abB^2}{r^2}u^r G^\eta + \frac{b^2B^2}{r^3}u^r G^\xi - \nu B\left[\frac{B''}{B^2}G^\xi + \left(\frac{2ab}{r^2}G^\eta - \frac{\frac{b^2}{r^2}-a^2}{r}G^\xi\right)B'\right.\\ &\qquad \left. + \frac{2B'}{B^2}G^\xi_r + \frac{2abB}{r^2}G^\eta_r - \frac{B}{r}\left(\frac{b^2}{r^2}-a^2\right)G^\xi_r + \frac{1}{B}G^\xi_{rr} - \frac{2abB}{r^3}G^\eta\right] = 0,\end{aligned} \tag{B.1d}$$

where (B.1a) is the continuity equation, (B.1b) is the r-momentum equation, (B.1c) is the η-momentum equation and (B.1d) is the ξ-momentum equation. In (B.1), the coefficients of the powers ξ^2, ξ^1, and ξ^0 must vanish independently. The condition of a vanishing coefficient of the ξ^2-term of (B.1b) leads to the relation (5.7)

$$F^{\eta} = -\frac{b}{ar} F^{\xi}.$$

Furthermore, the determining equations which arise from vanishing coefficients of the first-order terms ($O(\xi)$) of the ξ-momentum and η-momentum are equivalent. Using the vanishing coefficient of the $O(\xi^0)$-terms of the continuity equation, we obtain the condition (5.8), given by

$$F^{\xi} = -\frac{B}{r} \left(r u^r\right)_r,$$

and relating the unknown functions F^{ξ} and u^r. By substitution of this relation into the remaining helically invariant Navier-Stokes equations (3.19), one obtains a set of four determining PDEs for the unknowns $u^r, G^{\xi}, G^{\eta}, p$, which is given by (5.9). Its second PDE is a decoupled equation for u^r, from which the v-equation (5.13) follows after the substitution (5.12).

B.2 Derivation of the parameters in the Beltrami flow ansatz (5.33)

The derivation of the parameters $K_1 - K_8, R_1 - R_3$ and R_p in (5.33) proceeds as follows. Employing the solution (5.33) into (5.31a) yields

$$\begin{aligned} &\frac{e^{-\nu Q^2 t}}{B} \left(K_5 \lambda \sin(\lambda\xi) - K_6 \cos(\lambda\xi)\right) R_3 \\ &= \vartheta(r) e^{-\nu Q^2 t} \left(K_1 \cos(\lambda\xi) + K_2 \sin(\lambda\xi)\right) R_1, \end{aligned} \tag{B.2}$$

which may be simplified to

$$\left(\frac{K_5\lambda}{B} R_3 - K_2 \vartheta R_1\right) \sin(\lambda\xi) - \left(\frac{K_6\lambda}{B} R_3 + K_1 \vartheta R_1\right) \cos(\lambda\xi) = 0. \tag{B.3}$$

For vanishing coefficients of (B.3) we obtain

$$K_2 = \frac{K_5\lambda}{\vartheta B} \frac{R_3}{R_1}, \qquad K_1 = -\frac{K_6\lambda}{\vartheta B} \frac{R_3}{R_1}, \tag{B.4}$$

which leads to

$$\frac{K_2}{K_5} = -\frac{K_1}{K_6}. \tag{B.5}$$

Employing (5.33) into (5.31c) we obtain

$$\left(K_6\left(R_3' + \frac{a^2B^2}{r}R_3\right) - K_4\vartheta R_2\right)\sin(\lambda\xi) + \left(K_5\left(R_3' + \frac{a^2B^2}{r}R_3\right) - K_3\vartheta R_2\right)\cos(\lambda\xi) = 0. \tag{B.6}$$

As before, vanishing coefficients yield

$$K_3 = \frac{K_5}{\vartheta R_2}\left(R_3' + \frac{a^2B^2}{r}R_3\right), \qquad K_4 = \frac{K_6}{\vartheta R_2}\left(R_3' + \frac{a^2B^2}{r}R_3\right), \tag{B.7}$$

which is

$$\frac{K_3}{K_5} = -\frac{K_4}{K_6}. \tag{B.8}$$

Finally, employing (5.33) into (5.31b) leads to

$$\left(-\frac{K_1\lambda}{B}R_1 - \frac{K_4}{r}(rR_2)' - \frac{2K_6abB^2}{r^2}R_3 + \frac{K_4a^2B^2}{r}R_2 - K_6\vartheta R_3\right)\sin(\lambda\xi) + \left(-\frac{K_2\lambda}{B}R_1 - \frac{K_3}{r}(rR_2)' - \frac{2K_5abB^2}{r^2}R_3 + \frac{K_3a^2B^2}{r}R_2 - K_5\vartheta R_3\right)\cos(\lambda\xi) = 0. \tag{B.9}$$

For vanishing coefficients of (B.9) we obtain

$$K_5 = \frac{r^2}{(2abB^2 + \vartheta r^2)R_3}\left(-\frac{K_2\lambda}{B}R_1 - \frac{K_3}{r}(rR_2)' + \frac{K_3a^2B^2}{r}R_2\right), \tag{B.10a}$$

$$K_6 = \frac{r^2}{(2abB^2 + \vartheta r^2)R_3}\left(-\frac{K_1\lambda}{B}R_1 - \frac{K_4}{r}(rR_2)' + \frac{K_4a^2B^2}{r}R_2\right). \tag{B.10b}$$

Employing (5.33) into the continuity equation (5.29) leads to

$$\left(K_2R_1 + K_2rR_1' - K_3\lambda\frac{r}{B}R_2\right)\sin(\lambda\xi) + \left(K_1R_1 + K_1rR_1' - K_4\lambda\frac{r}{B}R_2\right)\cos(\lambda\xi) = 0. \tag{B.11}$$

The coefficients yield

$$K_1 = -K_4\lambda\frac{r}{B}\frac{R_2}{R_1 + rR_1'}, \qquad K_2 = K_3\lambda\frac{r}{B}\frac{R_2}{R_1 + rR_1'}, \tag{B.12}$$

which leads to

$$\frac{K_1}{K_4} = -\frac{K_2}{K_3}. \tag{B.13}$$

The condition (B.13) is a combination of (B.5) and (B.8). We now consider the system of linear ODE's, stemming from (B.4), (B.7), (B.10b) and (B.12) with nonlinear coefficients, given by

$$R_1 = -\frac{K_6}{K_1}\frac{\lambda}{\vartheta B}R_3, \tag{B.14a}$$

$$R_2 = \frac{K_6}{\vartheta K_4}\left(R_3' + \frac{a^2B^2}{r}R_3\right), \tag{B.14b}$$

$$R_3 = \frac{r^2}{K_6\left(2abB^2 + \vartheta r^2\right)}\left(-\frac{K_1\lambda}{B}R_1 - \frac{K_4}{r}\left(rR_2\right)' + \frac{K_4a^2B^2}{r}R_2\right), \tag{B.14c}$$

$$R_2 = \frac{K_2}{K_3}\frac{B}{\lambda r}\left(R_1 + rR_1'\right), \tag{B.14d}$$

which is a system for the unknowns R_1, R_2, R_3, ϑ. The constraints for the parameters $K_1, ..., K_6$ are given by (B.5) and (B.8). Employing (B.14a) and (B.14d) into (B.14b) and using the constraints (B.5), (B.8) leads to $\vartheta' = 0$ and hence $\vartheta = const$. The second order ODE (5.37) may be derived by employing (B.14a), (B.14d), (B.5) and (B.8) into (B.14c). As before for the Beltrami equations (5.28), we employ the ansatz (5.33) into the momentum equations (5.30). From the momentum equation in radial direction (5.30a) we obtain one additional constraint for the parameters, which is given by

$$\frac{K_7}{K_8} = -\frac{K_4}{K_3}. \tag{B.15}$$

The solution of the ODE (5.37) is related to that of the confluent Heun ODE (Ronveaux, 1995) with parameters (5.42), in which a, b are the helix pitch parameters (cf. (3.15a)), $n \in \mathbb{N}$ is the ξ-mode number, and $\vartheta =$ const. is the Beltrami parameter in (5.28). Here, we use the notation of the MAPLE-Software (Maplesoft, 2017) package for the Confluent Heun function.

Specifically, the general solution of the ODE (5.37) is given by (5.40). From the equations (B.14) we obtain the exact solutions (5.43) for $R_2(r)$ and $R_3(r)$. Substituting (5.33) and the derived solutions for $R_1(r), R_2(r), R_3(r)$ into the $\xi-$projection of momentum (5.30c) leads to the following equation for $R_p(r)$, given by

$$K_8\lambda r\left(a^2r^2 + b^2\right)^3 R_p(r) = 0, \tag{B.16}$$

which has the solution $R_p(r) = 0$. Hence, from (5.33e), it follows that the modified pressure P is zero, which in turn leads to the final solution for the pressure, given by (5.35).

C Appendix: Derivation of a new orthogonal helically invariant coordinate

Due to the singular behaviour of the helical coordinate $\tilde{\eta}$ at the origin $r = 0$, originally introduced by KCO, a new third coordinate is derived in the following. This coordinate is needed to formulate well-defined periodicity conditions at the centerline axis $r = 0$, that are necessary for the implementation of periodic boundary conditions in the DG discretization of the helically invariant Navier-Stokes equations.

We use the two helical coordinates introduced in KCO

$$\tilde{r} = r, \qquad \xi = az + b\varphi \tag{C.1}$$

and attend to find a third coordinate η in the invariant direction. From (C.1) one may determine the Jacobian matrix

$$\boldsymbol{J} = \begin{bmatrix} \frac{\partial \tilde{r}}{\partial r} & \frac{\partial \tilde{r}}{\partial \varphi} & \frac{\partial \tilde{r}}{\partial z} \\ \frac{\partial \xi}{\partial r} & \frac{\partial \xi}{\partial \varphi} & \frac{\partial \xi}{\partial z} \\ \frac{\partial \eta}{\partial r} & \frac{\partial \eta}{\partial \varphi} & \frac{\partial \eta}{\partial z} \end{bmatrix} = \begin{bmatrix} 1 & 0 & 0 \\ 0 & a & b \\ \frac{\partial \eta}{\partial r} & \frac{\partial \eta}{\partial \varphi} & \frac{\partial \eta}{\partial z} \end{bmatrix}. \tag{C.2}$$

The inverse relation reads

$$\boldsymbol{J}^{-1} = \begin{bmatrix} \frac{\partial r}{\partial \tilde{r}} & \frac{\partial r}{\partial \xi} & \frac{\partial r}{\partial \eta} \\ \frac{\partial \varphi}{\partial \tilde{r}} & \frac{\partial \varphi}{\partial \xi} & \frac{\partial \varphi}{\partial \eta} \\ \frac{\partial z}{\partial \tilde{r}} & \frac{\partial z}{\partial \xi} & \frac{\partial z}{\partial \eta} \end{bmatrix}, \tag{C.3}$$

which can be obtained by inverting (C.2). We have

$$\boldsymbol{J}^{-1} = \frac{1}{b\frac{\partial \eta}{\partial z} - a\frac{\partial \eta}{\partial \varphi}} \begin{bmatrix} 1 & 0 & 0 \\ a\frac{\partial \eta}{\partial r} & \frac{\partial \eta}{\partial z} & -a \\ -b\frac{\partial \eta}{\partial r} & \frac{\partial \eta}{\partial \varphi} & b \end{bmatrix}. \tag{C.4}$$

Comparing (C.3) and (C.4) leads to

$$\begin{aligned} \frac{\partial \varphi}{\partial \xi} &= \frac{\frac{\partial \eta}{\partial z}}{b\frac{\partial \eta}{\partial z} - a\frac{\partial \eta}{\partial \varphi}}, & \frac{\partial \varphi}{\partial \eta} &= \frac{-a}{b\frac{\partial \eta}{\partial z} - a\frac{\partial \eta}{\partial \varphi}}, \\ \frac{\partial z}{\partial \xi} &= \frac{-\frac{\partial \eta}{\partial \varphi}}{b\frac{\partial \eta}{\partial z} - a\frac{\partial \eta}{\partial \varphi}}, & \frac{\partial z}{\partial \eta} &= \frac{b}{b\frac{\partial \eta}{\partial z} - a\frac{\partial \eta}{\partial \varphi}}. \end{aligned} \tag{C.5}$$

The derivatives are given by

$$\partial_\eta = \frac{\partial r}{\partial \eta}\partial_r + \frac{\partial \varphi}{\partial \eta}\partial_\varphi + \frac{\partial z}{\partial \eta}\partial_z, \tag{C.6a}$$

$$\partial_\xi = \frac{\partial r}{\partial \xi}\partial_r + \frac{\partial \varphi}{\partial \xi}\partial_\varphi + \frac{\partial z}{\partial \xi}\partial_z. \tag{C.6b}$$

For the helical and cylindrical coordinates we know that

$$\frac{\partial r}{\partial \eta} = 0, \qquad \frac{\partial r}{\partial \xi} = 0, \qquad \partial_\varphi = r\boldsymbol{e}_\varphi, \qquad \partial_z = \boldsymbol{e}_z. \tag{C.7}$$

For orthogonality of the coordinate lines ξ = const. and η = const. the condition $\partial_\xi \cdot \partial_\eta = 0$ must be fulfilled. That leads to a determining PDE for the coordinate η, given by

$$\partial_\xi \cdot \partial_\eta = \frac{\partial \varphi}{\partial \xi}\frac{\partial \varphi}{\partial \eta}r^2 + \frac{\partial z}{\partial \xi}\frac{\partial z}{\partial \eta} \tag{C.8a}$$

$$= \frac{-ar^2\frac{\partial \eta}{\partial z}}{\left(b\frac{\partial \eta}{\partial z} - a\frac{\partial \eta}{\partial \varphi}\right)^2} + \frac{-b\frac{\partial \eta}{\partial \varphi}}{\left(b\frac{\partial \eta}{\partial z} - a\frac{\partial \eta}{\partial \varphi}\right)^2} = 0. \tag{C.8b}$$

The solution of the PDE can be derived using the method of characteristics

$$\frac{\mathrm{d}z}{ar^2} = \frac{\mathrm{d}\varphi}{b}, \qquad d\eta = 0, \tag{C.9}$$

which leads to

$$\eta = F\left(r, \varphi, z\right), \tag{C.10a}$$

$$C_1 = -bz + ar^2\varphi. \tag{C.10b}$$

Finally, the coordinate η reads

$$\eta = F\left(C_1\right) = -bz + ar^2\varphi. \tag{C.11}$$

We further show that, even though the coordinate lines of constant ξ and η are orthogonal, the three unit vectors $\boldsymbol{e}_r, \boldsymbol{e}_\xi$ and $\boldsymbol{e}_\eta$ are not orthogonal.

The gradient operator in cylindrical coordinates is given by

$$\nabla S = \frac{\partial S}{\partial r}\boldsymbol{e}_r + \frac{1}{r}\frac{\partial S}{\partial \varphi}\boldsymbol{e}_\varphi + \frac{\partial S}{\partial z}\boldsymbol{e}_z\,, \tag{C.12}$$

where S is a scalar quantity. Using that, we obtain

$$\boldsymbol{e}_r = \frac{\nabla r}{\|\nabla r\|}, \qquad \boldsymbol{e}_\xi = \frac{\nabla \xi}{\|\nabla \xi\|} \tag{C.13}$$

for the unit vectors $\boldsymbol{e}_r$ and $\boldsymbol{e}_{\tilde{\xi}}$. The gradient of the coordinate η is given by

$$\nabla\eta = \frac{\partial\eta}{\partial r}\boldsymbol{e}_r + \frac{1}{r}\frac{\partial\eta}{\partial\varphi}\boldsymbol{e}_\varphi + \frac{\partial\eta}{\partial z}\boldsymbol{e}_z \tag{C.14a}$$

$$= 2ar\varphi\boldsymbol{e}_r + ar\boldsymbol{e}_\varphi - b\boldsymbol{e}_z. \tag{C.14b}$$

The absolut value reads

$$\|\nabla\eta\| = r\sqrt{4a^2\varphi^2 + \frac{1}{B^2}}, \tag{C.15}$$

from which the unit vector of the invariant coordinate is determined:

$$\boldsymbol{e}_\eta = \frac{\nabla\eta}{\|\nabla\eta\|} = \frac{1}{r\sqrt{4a^2\varphi^2 + \frac{1}{B^2}}}\begin{pmatrix} 2ar\varphi \\ ar \\ -b \end{pmatrix}. \tag{C.16}$$

For orthogonality of the unit vectors, the condition that $\boldsymbol{e}_r \times \boldsymbol{e}_\eta \overset{!}{=} \boldsymbol{e}_{\tilde{\xi}}$ must hold. However, the cross product of both unit vectors is given by

$$\boldsymbol{e}_r \times \boldsymbol{e}_\eta = \begin{pmatrix} 1 \\ 0 \\ 0 \end{pmatrix} \times \frac{1}{r\sqrt{4a^2\varphi^2 + \frac{1}{B^2}}}\begin{pmatrix} 2ar\varphi \\ ar \\ -b \end{pmatrix} \tag{C.17}$$

$$= \frac{1}{r\sqrt{4a^2\varphi^2 + \frac{1}{B^2}}}\begin{pmatrix} 0 \\ b \\ ar \end{pmatrix} \neq \boldsymbol{e}_{\tilde{\xi}}, \tag{C.18}$$

which is only in the case of $\varphi = 0$ equal to the unit vector $\boldsymbol{e}_{\tilde{\xi}}$.